ON THE MODELLING OF TROPOSPHERIC EFFECTS IN ULTRA-HIGH FREQUENCY RADIO POSITIONING

H. W. JANES

January 1986

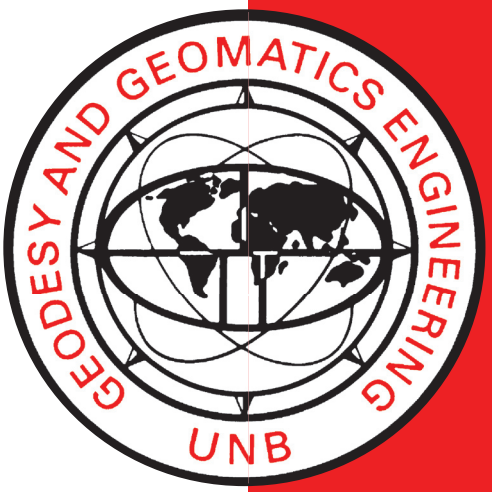

TECHNICAL REPORT
NO. 119

PREFACE

In order to make our extensive series of lecture notes more readily available, we have scanned the old master copies and produced electronic versions in Portable Document Format. The quality of the images varies depending on the quality of the originals. The images have not been converted to searchable text.

ON THE MODELLING OF TROPOSPHERIC EFFECTS

IN

ULTRA-HIGH FREQUENCY RADIO POSITIONING

Harold William Janes

This report is an unaltered printing of the author's
Master of Science in Engineering Thesis
submitted to this department in
December 1985

Department of Surveying Engineering
University of New Brunswick
P.O. Box 4400
Fredericton, N.B.
Canada
E3B 5A3

January 1986

ABSTRACT

Recent technological developments in Ultra-High Frequency (UHF) radio positioning offer the potential to extend metric range measurement accuracy beyond the standard radio horizon. At present, the principal obstacle to achieving this goal is our inability to reliably model, or otherwise account for, signal distortions produced by time and space variations in tropospheric refractive index. Trans-horizon propagation at UHF wavelengths is strongly influenced by small scale irregularities and layering in the refractivity structure of the troposphere which give rise to troposcatter and mode propagation mechanisms. Theoretical and empirical investigations in micrometeorology and turbulence theory over the past twenty years provide a basis for the qualitative understanding of wave propagation in a non-homogeneous and time varying troposphere. In this thesis we draw upon these fields to describe the sources and characteristics of tropospheric variability and its effect on the propagation of UHF radio waves and the accuracy of UHF radio positioning. In particular, we apply this foundation to an assessment of tropospheric effects in Atlantic Canadian waters, by correlating available surface and upper air meteorological data obtained at several stations in Nova Scotia with UHF ranging data collected in cooperation with the Canadian Hydrographic Service.

The meteorological data analysed indicate that surface heating effects and weather disturbances may combine to produce day-to-day variations in surface refractive index of the order of several parts in 10^5, and contribute to a strongly layered refractivity structure in the lower atmosphere. Up to 30% of the twice daily radiosonde ascents recorded during the summer months of 1982 were found to contain extreme refractivity layers within the first tropospheric kilometre. As a result, the average refractivity lapse over the first kilometre of the troposphere is in general poorly correlated with surface refractive index. In addition, significant differences in surface refractivity and the occurance and characteristics of atmospheric layering were encountered when comparing meteorological data recorded at coastal and offshore locations over distances of a few hundred kilometres. Seasonal variations in monthly mean surface refractivity of the order of 50 ppm were encountered.

The range measurement data analysed indicate that the stability of the troposcatter propagation mechanism used in extended range UHF radio positioning is strongly influenced by the degree of turbulent activity and the extent of non-standard layering encountered in the lower atmosphere. RMS range measurement stability over an 80 km troposcatter link was found to vary from 50-100 ppm during stable atmospheric conditions, to 200-400 ppm or more during periods of maximum turbulence and layering. The greatest periods of instability accompanied changes in prevailing weather conditions and appear related to enhanced scattering from elevated refractivity layers.

In the absence of corrective measures, these influences would appear to limit the accuracy of UHF trans-horizon ranging to approximately 100-500 ppm depending upon prevailing atmospheric conditions. Given careful consideration of tropospheric influences this limit could perhaps be reduced to 50-100 ppm. Possible alternatives include detailed observations of surface and upper air meteorology within the survey area, or the use of differential range monitoring coupled with space diversity and recursive filtering techniques. In either case, the effects of a non-homogeneous and time varying troposphere will likely continue to be a limiting factor in UHF system accuracy. In this regard, further study is required to establish appropriate corrective measures and to quantify the degree of improvement possible.

TABLE OF CONTENTS

TABLE OF CONTENTS (CONTINUED)

LIST OF TABLES

LIST OF TABLES (CONTINUED)

LIST OF FIGURES

LIST OF FIGURES (CONTINUED)

Page

LIST OF FIGURES (CONTINUED)

ACKNOWLEDGEMENTS

This research was partially funded by the Natural Sciences and Engineering Research Council of Canada under Strategic Grants entitled "Marine Geodesy" and "Marine Geodesy Applications" held by Dr. David E. Wells, and the Canadian Hydrographic Service through a research contract entitled "UHF Radiopositioning Performance Evaluation" held by Canadian Engineering Surveys Co. Ltd. of Edmonton, Alberta. The financial assistance provided by the Department of Surveying Engineering, University of New Brunswick is also gratefully acknowledged.

I wish to express my gratitude to my supervisor Dr. David E. Wells for his interest, guidance, generosity, and great patience during the completion of this work. The assistance of Dr. Richard Langley and Dr. James Tranquilla, both of whom provided many helpful comments and suggestions during the investigation and in reviewing the final manuscript, is also gratefully acknowledged. Thanks are also due to Mr. Mike Eaton of the Canadian Hydrographic Service, Atlantic Region, who provided the initial opportunity and encouragement for this study as well as the Syledis data used in chapter 5.

I reserve special thanks for my friends and fellow graduate students Nick Christou, Spiros Pagiatakis, Alistair Stuart, and Michael Pearce, for their enthusiasm and good humour, and for providing almost daily assistance in matters both technical and personal.

Finally, to my wife Nancy and my son Adam, I offer a very special note of gratitude for perseverence and sacrifice, without complaint, above and beyond the call.

1. INTRODUCTION

Recent technological developments in Ultra-High Frequency (UHF) radio positioning offer the potential to extend metric range measurement accuracy beyond the standard radio horizon. At present, the principal obstacle to achieving this goal is our inability to reliably model, or otherwise account for, signal distortions produced by time and space variations in tropospheric refractive index. These can be summarized as contributing two principal categories of range measurement error: phaselag uncertainty, arising from apparently random variations in the velocity and curvature of the propagating wave, and multipath interference, arising from reflection, refraction, and scattering within the tropospheric layer.

Theoretical and empirical investigations in micrometeorology and turbulence theory over the past twenty years provide a natural foundation for the study of wave propagation in a non-homogeneous and time varying troposphere. In this thesis we draw upon these fields to describe the sources and characteristics of tropospheric inhomogeneity and their effects on the propagation of UHF radio waves and the accuracy of UHF radio positioning. In particular, we apply this foundation to an assessment of tropospheric effects in Atlantic Canadian waters, by correlating

available surface and upper air meteorological data obtained at several stations in Nova Scotia with UHF ranging data collected in cooperation with the Canadian Hydrographic Service (CHS).

1.1) Background and Motivation.

For the most part, radio positioning involves the inference of range, range-difference, or range-rate information from measurements of the transit time of propagation of electromagnetic waves. Consequently, assumptions concerning the velocity and path of the advancing wavefronts must be made in order to scale time intervals into geometric distances. Whereas present day time and frequency standards permit transit time determination with a precision exceeding 1 part in 10^{10}, observed time delays may easily vary by several parts in 10^5 due to time and space changes in the electromagnetic properties of the earth's surface and atmosphere. For terrestrial radio positioning applications above 30 MHz, variability in the composition and distribution of tropospheric refractive index becomes the predominant limiting factor.

In recent years considerable attention in terrestrial radio positioning has been focused upon the Ultra-High Frequency (UHF) band, falling between 300 and 3000 MHz in the microwave spectrum. Within this band reduced atmospheric absorption and enhanced surface diffraction extend the useful range of space wave propagation to approximately twice the standard radio horizon. Thereafter, a variety of tropospheric mechanisms combine to further extend system operating range: (a)localized pockets and patches of non-uniform refractive index produce scattering, (b) abrupt horizontal layers of sharp refractivity decrease cause reflection, and (c) extended vertical gradients of refractive index give rise to ducted mode propagation. All of these mechanisms provide a means of extended range propagation at UHF wavelengths. Consequently, changes in the predominant mode of propagation as a function of prevailing meteorological conditions result in significant time and space variability in ranging characteristics.

1.2) Scope and Methodology.

In the following chapters we shall review the various sources of tropospheric refractivity variation and examine the models presently employed to describe their effects, proceeding from the largest scale to the smallest scale of influence.

In Chapter 2 the fundamental relationship between tropospheric refractivity and atmospheric temperature, pressure, and humidity is reviewed. The concept of a standard atmosphere is introduced, and its use as a starting point for various refractivity models based upon the assumption of a quasi-static, horizontally homogeneous atmosphere is discussed. A comparison of models used to approximate the height dependance of refractive index is presented and formulae for ray tracing in a spherically stratified atmosphere are developed. Finally, the concepts of effective earth radius and substandard and superstandard refraction are defined in terms of the vertical gradient of refractivity.

In Chapter 3 we review the meteorology of tropospheric layer formation and examine the mechanisms by which UHF radio waves may be trapped and propagate over long distances. The necessary conditions for the formation of ducting and reflection layers in the lower atmosphere are reviewed and a description of the fundamentals of mode propagation in layered media is presented.

In Chapter 4 we review the theory of troposcatter propagation. The meteorology of atmospheric turbulence is briefly examined and related to considerations of thermal stability in the lower troposphere. Various stochastic and spectral representations of the turbulent refractivity field are introduced. These provide the basis for a review of the eddy and layer scattering theories. The use of space diversity and time averaging techniques to improve short term ranging stability is discussed.

In Chapter 5 we examine the structure of the refractivity field in Atlantic Canadian waters and its effect on UHF range measurement accuracy by correlating meteorological data obtained at several sites in Nova Scotia with ranging data collected on three trans-horizon baselines in cooperation with the Canadian Hydrographic Service. The various natural phenomena contributing

to time and space variations in tropospheric refractivity are summarized according to spatial and temporal scale. A detailed assessment of the magnitude and characteristics of refractive index variation in Atlantic Canadian waters is presented. Various approaches to the modelling of these effects are contrasted based upon the time and space resolution of meteorological observations required to describe them.

Chapter 6 summarizes the principal findings of this study and their significance. Possible alternatives for the reduction of tropospheric effects in UHF radio positioning are examined and recommendations for further research are presented. Finally, Appendices I through IV contain tables and figures supporting in detail the refractivity analysis presented in Chapter 5.

2. STANDARD ATMOSPHERE REFRACTION MODELS.

In this section the properties of the standard atmosphere and reviewed and its use as the basis for various refractivity models is discussed. Formulae for ray tracing in a spherically stratified atmosphere are developed and the concepts of effective earth radius and substandard, standard, and superstandard refraction are introduced.

2.1) Definition of the Refractive Index.

The index of refraction n of a medium relates the speed of propagation c of an electromagnetic wave in free space to its speed v within the medium. Free space conditions are defined as those which exist in a vacuum infinitely removed from matter (Corson and Lorrain, 1970). Under such conditions the speed c is a constant with an established value of 299,792,458 m/s (Hudson, 1984), and is related to the permeability μ_0 and permittivity ϵ_0 of free space by the equation (Rao, 1977)

$$c = 1/\sqrt{\mu_0 \epsilon_0} \qquad (2.1)$$

in which

$\mu_0 = 4\pi \times 10^{-7}$ Henrys/metre.

$\epsilon_0 = 8.854 \times 10^{-12}$ Farads/metre.

The propagation speed v within a material (non-vacuum) medium will in general be less than the free space speed c due to the impeding effect of the medium on the wave. For ideal dielectric (non-conducting) media such as the troposphere the propagation speed v is given by (Rao, 1977)

$$v = 1/\sqrt{\mu\epsilon} \tag{2.2}$$

where μ and ϵ denote the permeability and permittivity of the medium respectively. The definitive relation for the refractive index can then be written as

$$n = \sqrt{\mu_r\epsilon_r} \tag{2.3}$$

wherein μ_r and ϵ_r are respectively the relative permeability and relative permittivity (or dielectric constant) of the medium. The relative permeability of dry air has a value of the order of $1 + 0.4 \times 10^{-6}$ (Smith and Weintraub, 1953) and for most purposes can be considered equal to unity, resulting in the approximate expression

$$n \approx \sqrt{\epsilon_r} \tag{2.4}$$

The free space speed c provides a convenient point of reference for electromagnetic distance measurement. Following Wells (1974) we shall define the geometric distance S as that distance which would be measured in free space by assuming the vacuum speed c. Hence

$$S = c\Delta t_v \tag{2.5}$$

We shall similarly define the electromagnetic distance D as that distance which would be measured within a material medium by assuming the vacuum speed c. Hence

$$D = c\Delta t_m \tag{2.6}$$

In reducing electromagnetic distances to geometric distances it is necessary to account for both the speed and curvature of the wave in the medium. In non-homogeneous and non-stationary media such as the atmosphere the refractive index will in general vary both with position and time. Under such conditions geometric distances are recoverable only if the refractive index variations over the propagation path and transmission time in question can be modelled. The

precision with which this can be done will ultimately determine the accuracy of the distance measurement.

To a first approximation the progress of an electromagnetic wave along a transmission path may be described in terms of the eikonal equation [1]

$$(\nabla\delta)^2 = (n(\mathbf{r}))^2 \tag{2.7}$$

wherein δ denotes an incremental element of the electromagnetic path length referred to the point of transmission, ∇ is the gradient operator, and the refractive index $n(\mathbf{r})$ is a spatial function of the position $\mathbf{r}(s)$ along the path. The electromagnetic distance between two points is then given by (Born and Wolf, 1965)

$$D(\mathbf{r}_1, \mathbf{r}_2) = \delta(\mathbf{r}_2) - \delta(\mathbf{r}_1) = \int_s n(\mathbf{r})\, ds \tag{2.8}$$

and the wave speed correction by (Saastamoinen, 1973)

$$\Delta D = \int_s (n(\mathbf{r})-1)\, ds \tag{2.9}$$

The geometry of the transmission path is governed by Fermat's Principle which states that the path followed by a wave travelling between two points in a material medium will be that path which renders the transit time of propagation a minimum. From equations 6 and 8 we can express the transit time as

$$\Delta t = 1/c \int_s n(\mathbf{r}) ds \rightarrow \text{minimum} \tag{2.10}$$

in which case an Euler differential equation of the form (Born and Wolf, 1965)

$$\frac{d}{ds}\left[n(\mathbf{r})\frac{d\mathbf{r}}{ds}\right] = \nabla n \tag{2.11}$$

provides the necessary and sufficient condition for the definite integral of equation 10 to be a minimum.

---

[1] The eikonal equation is the fundamental equation of geometric optics. It has as its basis the assumption that the radio wavelength is of negligable extent relative to the scale of the physical variations of the properties of the medium. A full development from Maxwells equations is provided in Born and Wolf (1965).

The relative permittivity ϵ_r of equation 4 provides a measure of the extent of polarization[2] induced in the troposphere by an applied electromagnetic field. The mean polarizability of the troposphere is composed of two effects: electronic or molecular polarization, arising from the displacement of the electron clouds of both polar and non-polar gas molecules relative to their respective nucleii, and dipolar polarization, arising from the distortion of the permanent dipole moments of polar gas molecules. For a non-polar gas the total polarizability per mole of gas molecules is described by the specific refractivity α and is related to the refractive index through the Lorentz-Lorenz formula (Corson and Lorrain, 1970)

$$\frac{n^2-1}{n^2+2} = \frac{\rho}{M}\alpha \qquad (2.12)$$

in which M denotes the molecular mass and ρ the density of the gas. Equation 12 describes explicitly the dependence of the refractive index upon the density of the medium and remains nearly constant in value over the range of frequencies encountered in the radio spectrum. Given the equation of state for an ideal gas (Menzel, 1960)

$$\rho = \frac{MP}{RT} \qquad (2.13)$$

in which P denotes the pressure and T the absolute temperature of the gas and R is the universal gas constant, we can relate the refractive index to atmospheric pressure and temperature by the equation

$$\frac{n^2-1}{n^2+2} = \frac{P\alpha}{RT} \qquad (2.14)$$

Empirical evidence suggests that n may vary from 1.0002 to 1.0004 under usual conditions (Bean and Dutton, 1966) and for this range of values we can invoke the following approximations with minimal loss of accuracy

$$n^2-1 \approx 2(n-1)$$

---

[2] Polarization phenomena in material media are discussed at length in Corson and Lorrain (1970) and Rao (1977).

$$n^2+2 \approx 3$$

which when substituted into equation 14 yield

$$n-1 \approx \frac{3\alpha}{2R}\frac{P}{T} = K_1\frac{P}{T} \tag{2.15}$$

wherein K_1 is a constant.

A similar procedure may be employed to account for the polarization effects induced in the polar molecules. In this case the refractive index obeys the Debye relation (Corson and Lorrain, 1970)

$$\frac{n^2-1}{n^2+2} = \frac{\rho}{M}\left[\alpha + \frac{\beta}{T}\right] \tag{2.16}$$

in which α accounts for the electronic polarization effect as before, and β the added influence of dipolar polarization. Again, by suitable approximation we obtain

$$n-1 = K_2\frac{P}{T}\left[\alpha + \frac{\beta}{T}\right] \tag{2.17}$$

in which K_2, α, and β are assumed constant.

If, for a mixture of polar and non-polar gases we assume non-interaction and the validity of Dalton's law of partial pressures we may sum the constituent gases to obtain a single expression for the refractive index of the medium of the form

$$n-1 = \sum_i K_i\frac{P_i}{T} + \sum_j K_j\frac{P_j}{T}\left[\alpha_j + \frac{\beta_j}{T}\right] \tag{2.18}$$

in which the first and second terms represent the contribution of the various non-polar and polar constituents respectively.

For the tropospheric case the non-polar gases include nitrogen (78%), oxygen (21%), argon (0.93%), carbon dioxide (0.03%), and lesser amounts of neon, helium, krypton, hydrogen, and other gases (List, 1971). These are of more or less uniform concentration throughout the troposphere and are considered together under the term "dry gases". The only polar constituent of note is water vapour, termed the "wet" component, which may comprise some 3-4% of the tropospheric volume near the surface but is of highly variable concentration with respect to time

and position. The water vapour content is the most critical parameter to be observed in the determination of the radio refractive index due to the strong dipolar polarization effect at radio frequencies. By way of comparison, the refractive index changes by approximately 4.4 ppm for every 1 mb change in water vapour concentration, by 1.4 ppm for every 1 °C change in temperature, and by 0.4 ppm for every 1 mb change in dry air pressure.

The refractive index is related to the refractivity N by the equation

$$N = (n-1) \times 10^6 \tag{2.19}$$

By updating the constants of equation 18 we obtain the familiar form relating the tropospheric radio refractivity to atmospheric pressure, temperature, and water vapour pressure, namely

$$N = K_1 \frac{P_d}{T} + K_2 \frac{e}{T} + K_3 \frac{e}{T^2} \tag{2.20}$$

Various empirical determinations of the above coefficients have been made over the years, principally on the basis of cavity resonator measurements. The most prominant of these are contrasted in Table 1. Laurila (1968,1976) has compared the accuracy of the Essen-Froome (1951), Essen (1953), and Smith-Weintraub (1953) determinations for typical value ranges and found equivalence within 0.5 N units. The determination by Thayer (1974) is based upon a synthesis of available measurement made at both optical and radio frequencies and has a stated accuracy of the order of 0.2 N units in moist air. All four determinations yield results sufficiently accurate for radio positioning considerations. Consequently, we shall retain the Smith-Weintraub (1953) formula in keeping with conventional radio-meteorological practice. The Smith-Weintraub formula is usually expressed in the form

$$N = \frac{77.6}{T}\left[P + 4810\frac{e}{T}\right] \tag{2.21}$$

wherein $P = P_d + e$ is the total atmospheric pressure.

Table 2.1

Constants in the Formula for the Radio Refractive Index of Air.

Source	Year	K_1 (K/mb)	K_2 (K/mb)	K_3 (K^2/mb)
Essen-Froome	1951	77.64	64.68	3.718×10^5
Essen	1953	77.62	64.68	3.718×10^5
Smith-Weintraub	1953	77.61	71.6	3.747×10^5
Thayer	1974	77.60	64.8	3.776×10^5

2.2) Definition of the Standard Atmosphere.

The Smith-Weintraub formula allows for the determination of the tropospheric refractivity at any point where pressure, temperature, and water vapour pressure can be observed. It has a stated accuracy of about 0.5 N units (Thayer, 1974) and is valid for temperature ranges of -50 to +40 °C, atmospheric pressures of from 200 to 1100 mb, water vapour partial pressures of from 0 to 30 mb, and frequencies up to 30 GHz (Smith and Weintraub, 1953). For modelling purposes the formula is usually expressed as the sum of the "wet" and "dry" terms:

$$N_d = 77.6\, P/T \tag{2.22}$$

$$N_w = 77.6\,(\,4810\, e/T^2) \tag{2.23}$$

Herein median conditions for the dry component of the refractivity shall be defined by the U.S. Standard Atmosphere as described in Dubin, Sissenwine, and Wexler (1962) and Minzner et al. (1976). The U.S. Standard Atmosphere is defined in terms of an idealized, laterally homogeneous and neutral atmosphere which is stationary with respect to the earth and devoid of moisture, and which conforms to the equation of state for an ideal gas (Menzel, 1960)

$$\rho = \frac{PM}{RT} \tag{2.24}$$

and the hydrostatic equation (Menzel, 1960)

$$\frac{dP}{dh} = -\rho g \tag{2.25}$$

such that the atmospheric pressure and temperature at any given altitude h are related by the expression (Dubin et al., 1962)

$$P_H = P_0 \exp\left[-\frac{M}{R}\int_0^h \frac{g}{T}\,dh\right] \tag{2.26}$$

In the above ρ denotes density, M the molecular mass of dry air, R the ideal gas constant, g the acceleration due to gravity, and h the altitude.

The U.S. Standard Atmosphere approximates median temperate (mid-latitude) climatic conditions and is based upon extensive long-term meteorological observation. The adopted primary constants for the tropospheric layer are summarized in Appendix I as excerpted from Dubin et al. (1962). As depicted in Figures I.1 and I.2 the tropospheric layer is characterized by a linear temperature and an exponential pressure lapse.

2.3) Dry Component Models.

The standard atmosphere serves as a fundamental reference for a number of empirical models used in radio positioning to approximate the vertical gradient of the dry component of the refractivity. In each case the integral of equation 26 is treated numerically by dividing the troposphere into a series of concentric spherical shells of varying thicknesses in which the gravitational term can be considered constant and the temperature profile is assigned a specific functional form. There are two principal approaches to performing the integration by layers. In the first the temperature lapse is assumed to be linear within each layer in keeping with Figure I.1. The integration is then accomplished within each layer with only slight approximation being required. The second approach treats the temperature as a constant within each layer in which case the integral vanishes and the profile is evaluated as a series of discontinuous segments.

The linear gradient approach is used whenever the layer thickness is too large to justify the assumption of constant temperature. It serves as the basis for the Hopfield (1969) quartic

refractivity model widely used to account for tropospheric refraction effects in satellite ranging applications (Saastamoinen, 1973; Wells, 1974; Hopfield, 1976; Black and Eisner, 1983). The constant temperature approach has the disadvantage of requiring a greater number of layers to accurately approximate the true atmosphere. However, it does have the advantage of simplicity and can be accurately employed for altitudes up to a few thousand metres. Consequently, it serves as the basis for the exponential (Bean and Thayer, 1959), parabolic (Bremmer, 1949), and equivalent earth radius (Schelling et al., 1933) refractivity models which are extensively used in terrestrial radio wave propagation modelling (Bean et al., 1966; Segal and Barrington, 1976; Hall, 1979; Meeks, 1982).

If from Figure I.1 we assume a constant temperature lapse defined by the expression

$$\alpha = -(dT/dH) \times 10^3 \tag{2.27}$$

then the normalized temperature variation within each layer may be expressed as

$$\Delta T_h = (T_o - \alpha h)/T_o \tag{2.28}$$

wherein h denotes the layer thickness in kilometres and α is in units of °C per kilometre. Assuming a constant value for gravity within each layer and substituting equation 28 into equation 26 and integrating yields (Dubin et al., 1962)

$$P_H = P_o \left[\frac{T_o - \alpha h}{T_o}\right]^{gM/R\alpha} \tag{2.29}$$

in which case the pressure is no longer an exponential function of height. Substituting equations 29 and 28 into equation 22 for the dry refractivity component and simplifying we arrive at the Hopfield (1969) model

$$N_H = N_o \left[\frac{T_o - \alpha h}{T_o}\right]^{gM/R\alpha - 1} \tag{2.30}$$

usually written in the form

$$N_H = N_o \left[\frac{h_d - h}{h_d}\right]^{\mu} \tag{2.31}$$

wherein $\mu = (gM/R\alpha) - 1$ is the order, and $h_d = (T_o/\alpha)$ is the scale height at which T = 0 K.

Median values for the order and scale height have been determined by fitting observed profiles obtained from radiosonde ascents to equation 31 using a least squares procedure. In general μ may vary from a value of 5.8 at a temperature lapse rate of 5°K/km to a value of 3.9 at a lapse rate of 7°K/km. Consequently Hopfield (1969) found that an integer value of $\mu=4$, corresponding to an average lapse rate of 6.8°K/km, provided the most reasonable approximation to observed data. Similarly, the value of the scale height which provided the closest approximation to observed data was found to be given by the expression (Hopfield, 1971, 1972)

$$h_d = 40.136 + 0.14872T_0 \tag{2.32}$$

where h_d is in kilometres and T_0 is the surface temperature in degrees celsius.

An alternative approach is to assume a constant temperature for each layer. In this case the integral of equation 26 vanishes and we have (Dubin et al., 1962)

$$P_H = P_0 \exp\left[\frac{-gM}{RT} h\right] \tag{2.33}$$

which serves as the basis for the Bean and Thayer (1959) exponential refractivity model

$$N_H = N_0 \exp(-h/H_d) \tag{2.34}$$

in which H_d is again an empirically determined scale height given in kilometres. Extensive tabulations of the variation in the exponential scale height as a function of climate and season have been compiled in the radio refractivity atlases of Bean et al. (1966) and Segal and Barrington (1977). Values typically range from 9 to 11 km.

A parabolic approximation to the dry refractivity profile can be derived from the exponential series expansion of equation 34, written as

$$N_H = N_0 (1 + Bh + Ch^2) \tag{2.35}$$

wherein third order terms and higher have been neglected. The coefficients $B=-1/H_d$ and $C=1/2H_d^2$ are again empirically determined by curve fitting least squares adjustment of observed profile data. Further truncation of the exponential series leads to the linear refractivity model

$$N_H = N_0 (1 + Bh) \tag{2.36}$$

which is inherent in the equivalent earth radius approach introduced by Schelling et al. (1933).

The above four refractivity models are contrasted in Figure 1 for the standard pressure and temperature profile data of Appendix I. It is evident that the quartic model of Hopfield is in essential agreement with the standard dry refractivity profile within 1 N unit over the entire tropospheric layer, that is, up to the tropopause at an altitude of approximately 11 km. The exponential and parabolic models provide a similar degree of agreement up to altitudes of 5 and 4 km respectively, and the linear refractivity model only provides acceptable agreement within the first kilometre of the atmosphere.

2.4) Wet Component Models.

The equation of state for an ideal gas implies that its volume can be made infinitesimally small by varying either temperature or pressure, and neglects the presence of inter-molecular atomic forces. Neither of these assumptions holds particularly well for moist air. The equation of state for moist air is more properly written in the form of the van der Waals equation (Menzel, 1960)

$$P + \frac{a}{v^2} = \frac{mRT}{M(v-b)} \tag{2.37}$$

wherein the inverse squared term a/v^2 accounts for the forces of intermolecular attraction, the term $(v-b)$ accounts for the finite volume of the water vapour molecules, and a and b are empirically determined constants. In accounting for the presence of water vapour frequent use is made of the virtual temperature (Menzel, 1960):

$$T_v = \frac{T}{(1-M_w/M_d)\, e/P} = \frac{T}{(1-0.379e/P)} \tag{2.38}$$

such that the equation of state for moist air may be written in the approximate form (Fleagle and Bussinger, 1980)

$$P = \rho \frac{R}{M}\left[\frac{T}{(1-0.379e/P)}\right] \tag{2.39}$$

which is similar in form to van der Waals equation. As used here the virtual temperature is the temperature of dry air having the same pressure and density as moist air. The neglect of the

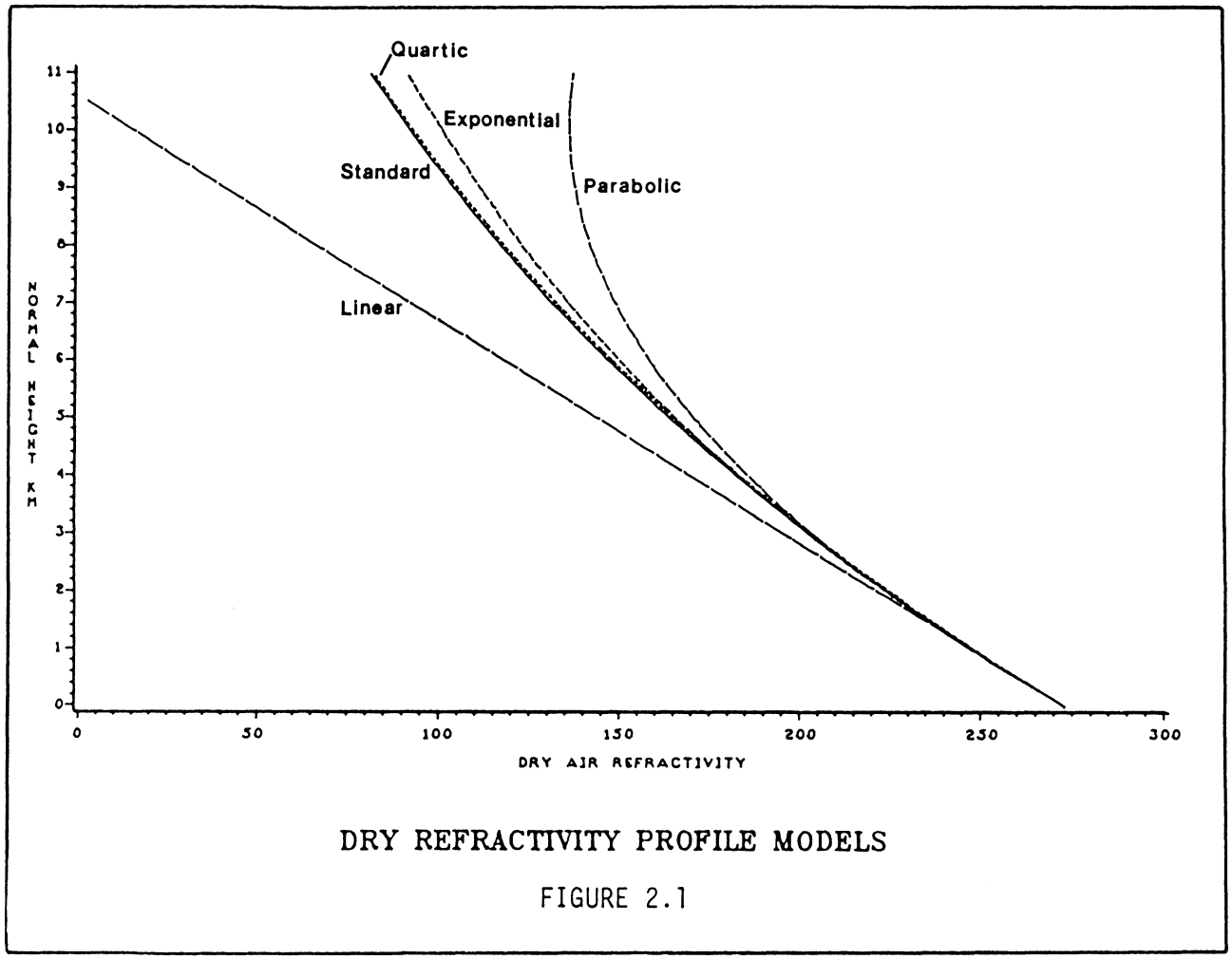

DRY REFRACTIVITY PROFILE MODELS

FIGURE 2.1

virtual temperature term inherent in the assumption of ideal gas behaviour gives rise to an error in atmospheric pressure of from 0.2-1.5% over the temperature range 0-40°C at 100% relative humidity.

The saturated water vapour pressure e_s is defined as the partial pressure of water vapour in equilibrium with liquid water. Given the absolute temperature T, the saturated vapour pressure may be computed from the empirical Goff-Gratch formula (Wells, 1974)

$$e_s = e_{stm}(T_s/T)^{5.02808}\, e^{(-A(T))} \tag{2.40}$$

wherein T_s is the steam point temperature (373.16K), e_{stm} is the saturated vapour pressure at T_s (1013.246 mb), and

$$A(T) = A_1(T) + A_2(T) + A_3(T)$$

wherein

$$A_1(T) = 18.19728\,(T_s/T-1)$$

$$A_2(T) = 0.0187265(\,1-e^{(-8.03945(Ts/T-1))}\,) \tag{2.41}$$

$$A_3(T) = 3.1813 \times 10^{-7}(\,e^{(26.1205(1-T/Ts))}-1)$$

Alternatively, tabulated values of e_s based upon the Goff-Gratch formulation may be found in the Smithsonian Meteorological Tables (List, 1970) or similar compilations.

The strict dependence of e_s on temperature is depicted in Figure 2. Over the temperature range depicted e_s increases by nearly three orders of magnitude. Consequently the contribution of water vapour to the refractivity is largely negligible below -20 °C but contributes some 30% of the total at temperatures approaching 30 °C.

Water vapour pressure is commonly determined indirectly by means of psychrometric (wet bulb temperature) or hygrometric (relative humidity) observations. For psychrometric observations e may be determined from the empirical formula (List, 1970)

$$e = e_{sw} - 4.5 \times 10^{-4}\,(1+1.68 \times 10^{-3}T_w)(T-T_w)P \tag{2.42}$$

wherein e_{sw} denotes the saturated water vapour pressure at the wet bulb temperature T_w. For hygrometric observations e may be determined from (List, 1970)

$$e = (Ue_s)/100 \tag{2.43}$$

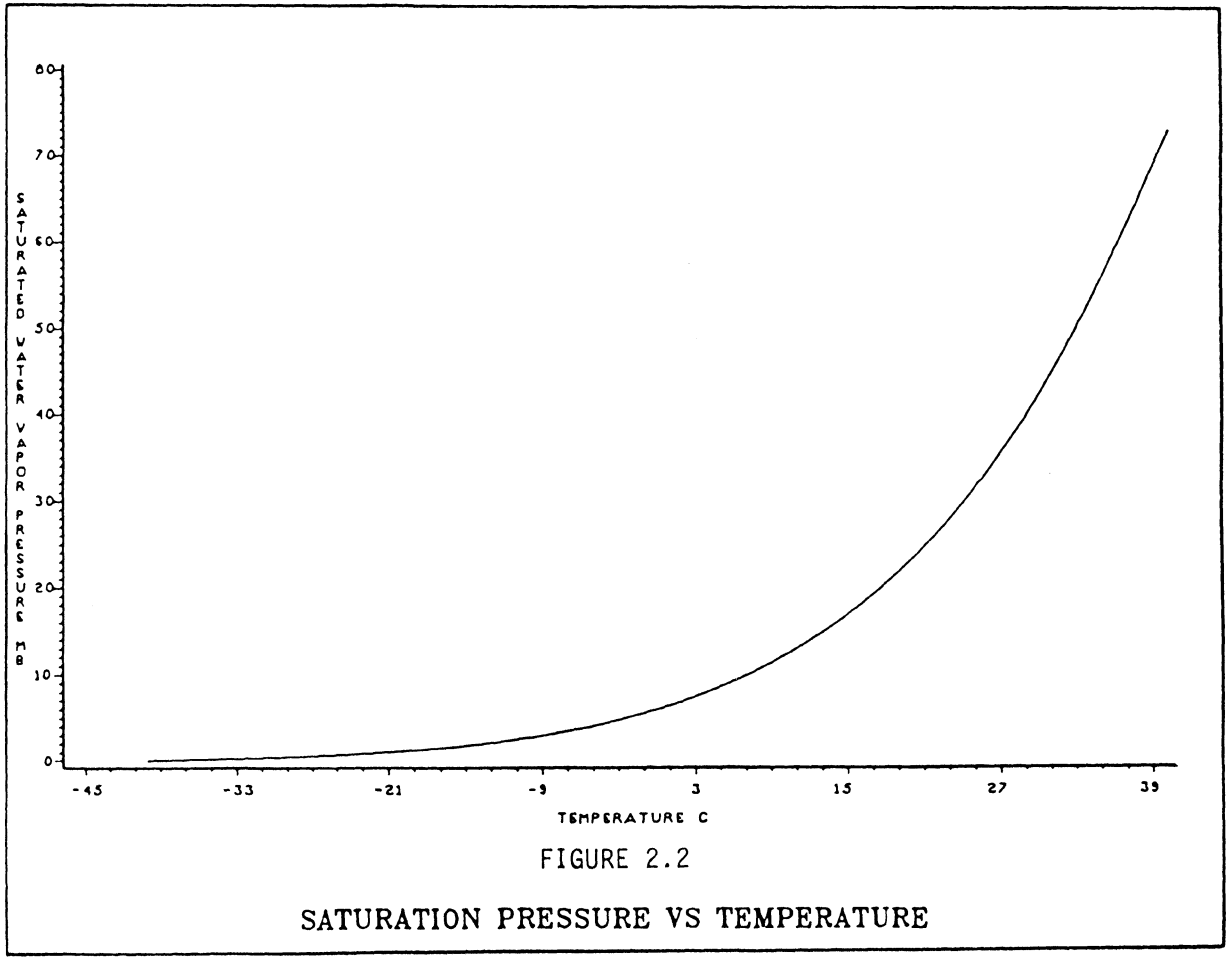

FIGURE 2.2

SATURATION PRESSURE VS TEMPERATURE

wherein e_s is evaluated at the dry bulb temperature T and U is the relative humidity in percent.

Although the assumption of ideal gas behaviour is less valid for moist air and the water vapour content of the atmosphere is highly variable, experimental evidence suggests that a similar treatment of the wet refractivity lapse can be an adequate approximation. Consequently quartic, exponential, and linear models of the wet refractivity profile have been widely adopted (Bean and Dutton, 1966; Hopfield, 1971, 1972; Segal and Barrington, 1977; Hall, 1979). In terms of the quartic model Hopfield (1971) has shown that wet term scale heights of the order of 9-11 Km can provide a reasonably close approximation to observed data. The radio refractivity atlases of Bean et al. (1966) and Segal and Barrington (1977) include extensive statistics on the distribution of the exponential wet-term scale height as a function of climate and season. Their results similarly indicate that an exponential model with scale heights of the order of 1.5-2.5 Km can provide a reasonable approximation to observed profile data. However the wet refractivity term is generally an order of magnitude less predictable than its dry air counterpart and remains a significant source of model uncertainty, especially at the low elevation angles common in terrestrial radio navigation.

Figure 3 depicts the variation of the wet and dry components of the refractivity as a function of height within the troposphere assuming a well mixed standard atmosphere with a constant, height invariant relative humidity. This is equivalent to adopting an exponential lapse rate for the partial pressure of water vapour. The contribution of the wet term may vary from some 10-30% of the total refractivity at the surface but is generally less than 1% of the total at the height of the tropopause.

2.5) Equivalent Earth Radius Approach to Tropospheric Refraction.

In treating tropospheric refraction, horizontal refractivity gradients are often neglected, being in general an order of magnitude less severe than those in the vertical direction. As a consequence ray curvature may be evaluated in terms of of a spherically stratified but horizontally homogeneous atmosphere. The following development follows that of Kerr (1951)

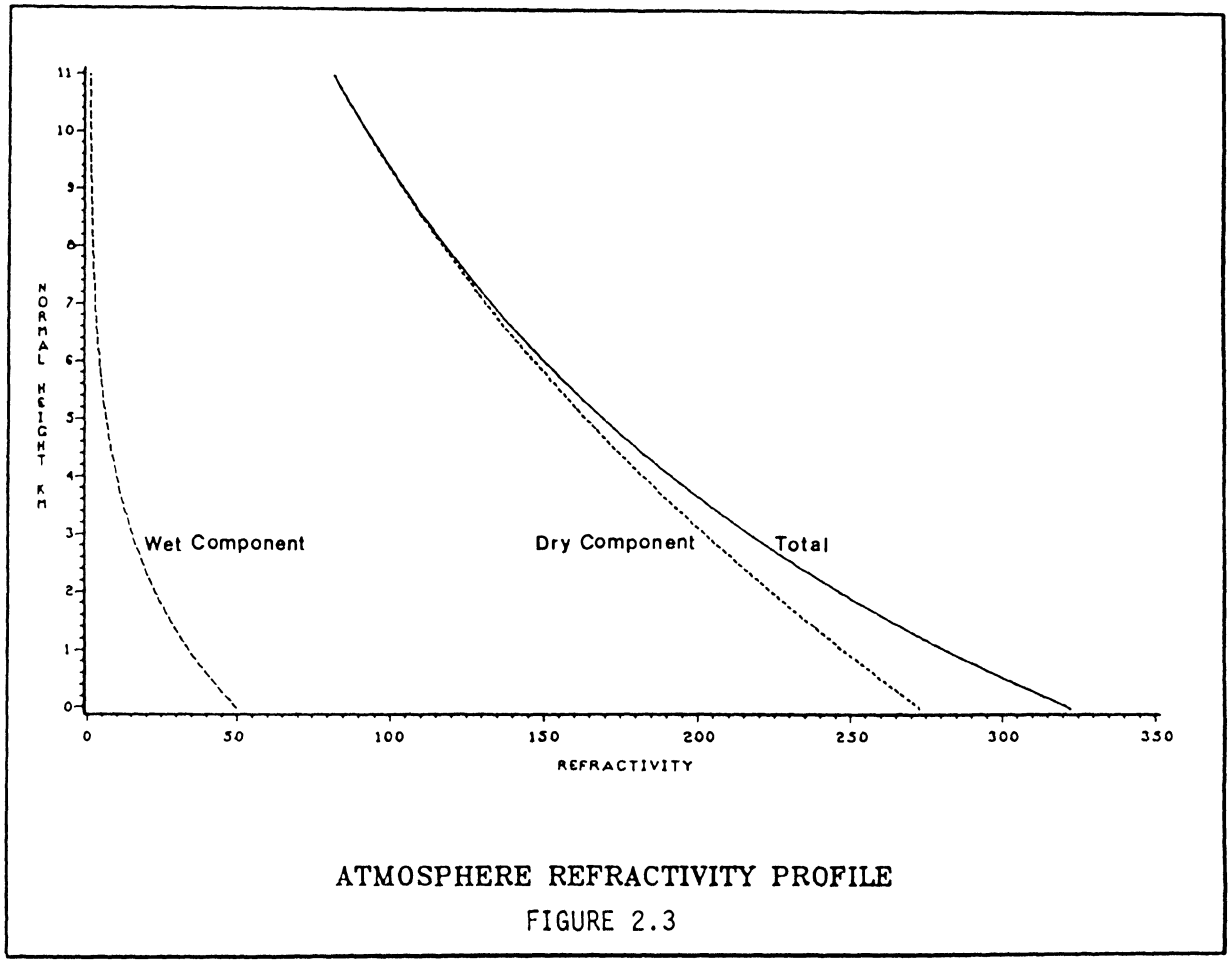

ATMOSPHERE REFRACTIVITY PROFILE

FIGURE 2.3

and Bean and Dutton (1966). The geometry of the curvature problem is depicted in Figure 4. Assuming a spherical coordinate system $S(\phi,\lambda,r)$ and given a position vector $\mathbf{p}(s)$ of a typical point on the ray referred to the point of transmission, the Euler differential form for the ray path can be written

$$\frac{d}{ds}\left[n(\mathbf{p})\frac{d\mathbf{p}}{ds}\right] = \frac{dn}{ds} \tag{2.44}$$

wherein $d\mathbf{p}/ds$ defines the unit vector tangent to the ray path at the point in question.

Let the vector $\mathbf{r}$ define the position of a point on the ray relative to the origin. Recognizing that $\mathbf{r}$ and dn/dh are both in the radial direction and hence parallel the vector product of $\mathbf{r}$ by equation 44 yields

$$\frac{d}{ds}\left[\mathbf{r} \times n\frac{d\mathbf{p}}{ds}\right] = 0 \tag{2.45}$$

which can be written

$$\frac{d}{ds}\left(rn\sin\beta\right) = 0 \tag{2.46}$$

wherein β is the angle between the radial (zenith) direction and the direction of propagation. Thus $nr\sin\beta$ is a constant for any given ray. This is the generalization of Snell's law to the case of a spherically stratified atmosphere, more commonly written (Reed and Russell, 1953)

$$n_h (R+h)\sin\beta = n_o R \sin\beta_o \tag{2.47}$$

wherein R denotes the average earth radius (6371 km) and h the altitude.

It follows then that for spherically stratified media ray curvature is restricted to planes containing the geocentre and point of transmission. Equation 44 can be re-written in the radial plane as

$$\frac{d}{dr}\left[n(r)\frac{d\mathbf{p}}{dr}\right] = \frac{dn}{dr} \tag{2.48}$$

Recognizing from the geometry of Figure 4 that $d\mathbf{p}=d\rho\tau$, and $dr/d\rho=\cos\psi$, where ρ is the radius of curvature of the ray, we obtain the rate of bending due to refraction

$$\frac{d\tau}{ds} = \frac{1}{n}\frac{dn}{dr}\cos\psi \tag{2.49}$$

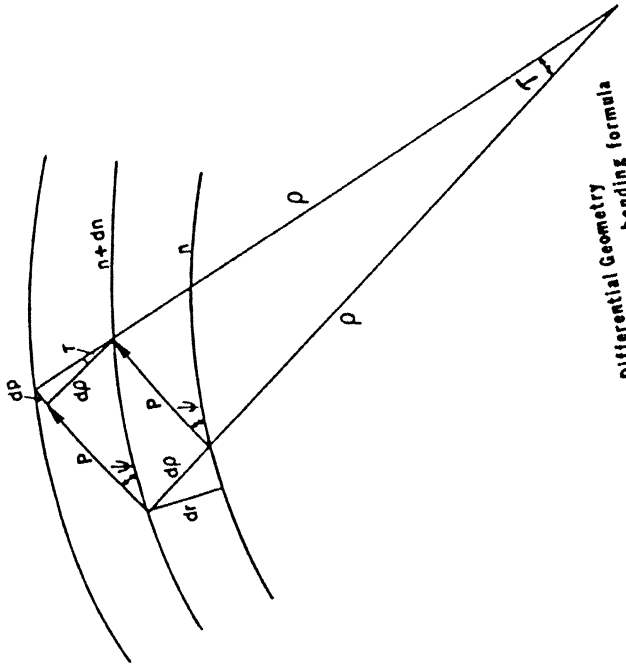
dρ
dφ
τ
P
ψ
n+dn
n
ρ
ρ
dr
Differential Geometry
used in derivation of ray bending formula

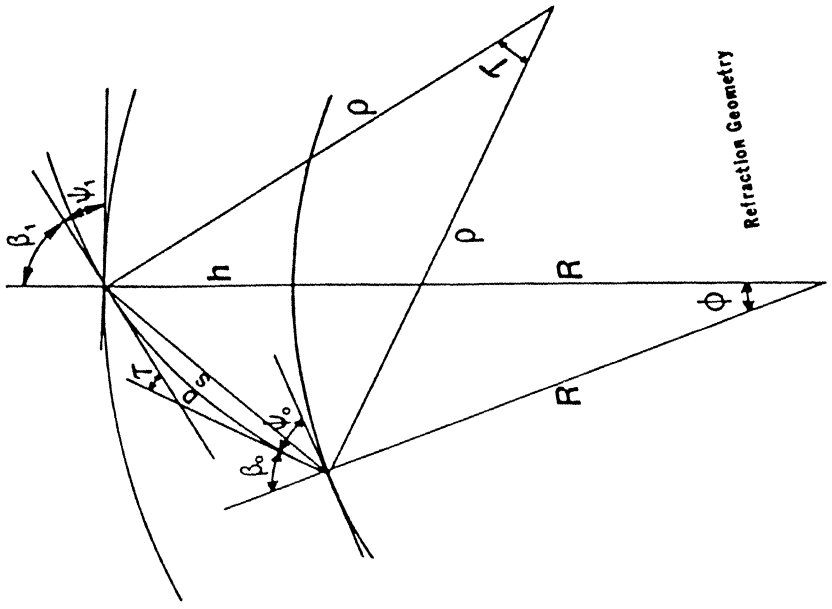
β₁
ψ₁
h
ρ
ρ
r
R
R
φ
τ
ds
ψ₀
β₀
Refraction Geometry

FIGURE 2.4

wherein ψ is the elevation angle relative to a surface of constant refractive index.

The total angular refraction of the ray is defined by the bending angle

$$\tau = -\int \frac{d\tau}{ds}\, ds \tag{2.50}$$

again, from geometry we have $ds/dr = 1/\sin\psi$, yielding finally

$$\tau = -\int \frac{\cot\psi}{n}\, dn \tag{2.51}$$

in which the negative sign is chosen so as to denote positive bending for a path that is concave downward. Obviously there is no bending in the zenith direction $\psi = 90^{o}$.

Equation 51 for the ray bending is well known (Kerr, 1951; Bean and Dutton, 1966; Livingston, 1970; Hopfield, 1976) but difficult to evaluate due to the height dependence of the refractivity. Various approximate solutions have been put forward based upon numerical integration techniques in which the atmosphere is represented by a series of spherical strata having some prescribed functional form of $n(r)$. These include the ray tracing formula of Schulkin (1952), Bean and Cahoon (1957), Thayer (1967), Saastamoinen (1973), and Hopfield (1976). Such approximations are generally quite reasonable when applied to high elevation angles but become increasingly inadequate at lower angles where the effects of horizontal refractivity gradients and wet component refractivity variations become more critical.

The classical method of accounting for the curvature of the ray path in terrestrial applications is to assume a linear refractivity gradient over the first few kilometres of the atmosphere. Assuming horizontally projected rays such that $\cos\psi \approx 1$, and recognizing that $n \approx 1$, the curvature of the radio wave can be approximated by

$$\rho^{-1} = \frac{d\tau}{ds} \approx -\frac{dn}{dh} \tag{2.52}$$

Equation 52 states that rays travelling in a nearly horizontal direction will have a curvature approximately equal to the vertical gradient of the refractive index. Consequently the refractivity gradient in the first 100 m and first kilometre of the atmosphere have become

parameters of considerable interest in terrestrial radio wave propagation. Again, the refractivity atlases of Bean et al. (1966) and Segal and Barrington (1976) contain extensive statistics on the climatic and seasonal variations of the refractive index gradient.

The curvature of the ray relative to that of the earth may be expressed as

$$1/R - 1/\rho = 1/k_e R = 1/R_e \tag{2.53}$$

wherein R_e is known as the effective earth radius and k_e as the effective earth radius factor. From equation 53 we have (Kerr, 1951)

$$k_e = \frac{\rho}{\rho - R} = \frac{1}{1 + k'} \tag{2.54}$$

in which the coefficient of refraction k' is given by (Rueger, 1980)

$$k' = R/\rho = -(dn/dh)R \tag{2.55}$$

The concept of the effective earth radius was first advanced by Schelling et al. (1933) and remains widely applied for the planning and evaluation of terrestrial radio links at low altitudes and for distances out to a few hundred kilometres (Bean et al., 1966; Segal and Barrington, 1977; Clark et al., 1978; Hall, 1979; Rueger, 1980). It provides a convenient geometric transformation whereby the curved propagation of rays in the actual atmosphere is transformed to rectilinear ray propagation over a fictitious earth of effective radius R_e.

Under standard atmospheric conditions the refractivity gradient within the first few kilometres has a value of approximately -40 N/km, in which case we can set $k' \approx 1/4$, $k_e \approx 4/3$, and $\rho \approx 4R$. Consequently it has become customary practice in dealing with radio wave propagation at low altitudes to define standard refraction in terms of a "4/3 Earth Radius" atmospheric model in which the radius of curvature of propagating rays is approximately four times that of the earth.

For distances of up to 200 Km the ray path may be considered approximately circular such that the geometric distance S and electromagnetic distance D are related by

$$S = 2\rho \sin(\tau/2) = 2\rho \sin(D/2\rho) \tag{2.56}$$

expanding $\sin(D/2\rho)$ and substituting $R=\rho k'$ yields the curvature correction (Rueger, 1980)

$$\Delta D_c = -k'^2 \frac{D^3}{24R^2} \tag{2.57}$$

For homogeneous media the speed correction as given by equation 9 reduces to

$$\Delta D_v = (n-1)\, S \tag{2.58}$$

in which case the reduction of electromagnetic distances to geometric distances is accomplished by

$$S = D - \left(\frac{n-1}{n}\right)D - k' \frac{D^3}{24R^2} \tag{2.59}$$

wherein the second term accounts for the curvature and is generally less than 1 ppm for refractivity gradients more positive than -150 N/km, and can hence be neglected for most practical radio navigation purposes.

The curvature of the ray path also determines the extent of direct wave propagation and hence the limits of the interference, diffraction, and troposcatter propagation zones. Bowditch (1981) defines the radio horizon line as the locus of points at which horizontally projected rays from a transmitter become tangent to the surface, taking into account the effects of ray curvature due to refraction. The distance to the radio horizon D_r is in general a function of transmitter height h_T and ray curvature. Reed and Russell (1953) offer the formula

$$D_r^2 = 2Rk_e h_T \tag{2.60}$$

which assumes a smooth spherical earth. The geometric horizon is then simply the radio horizon in the absence of refraction, that is, for an effective earth radius factor $k_e = 1$. The radio horizon distance D_g and geometric horizon distance D_r are then related by

$$D_r = \sqrt{k_e D_g} \tag{2.61}$$

By convention sub-standard refraction is said to occur when

$$dn/dh > -0.041 \times 10^{-6}\ m^{-1} \tag{2.62}$$

in which case propagating rays are bent downward less than the standard amount. Similarly super-standard refraction occurs when

$$dn/dh < -0.041 \times 10^{-6}\ m^{-1} \tag{2.63}$$

such that the rays follow the earth more closely than under standard conditions. Ducting is said to occur when

$$dn/dh < -0.157 \times 10^{-6}\ m^{-1} \tag{2.64}$$

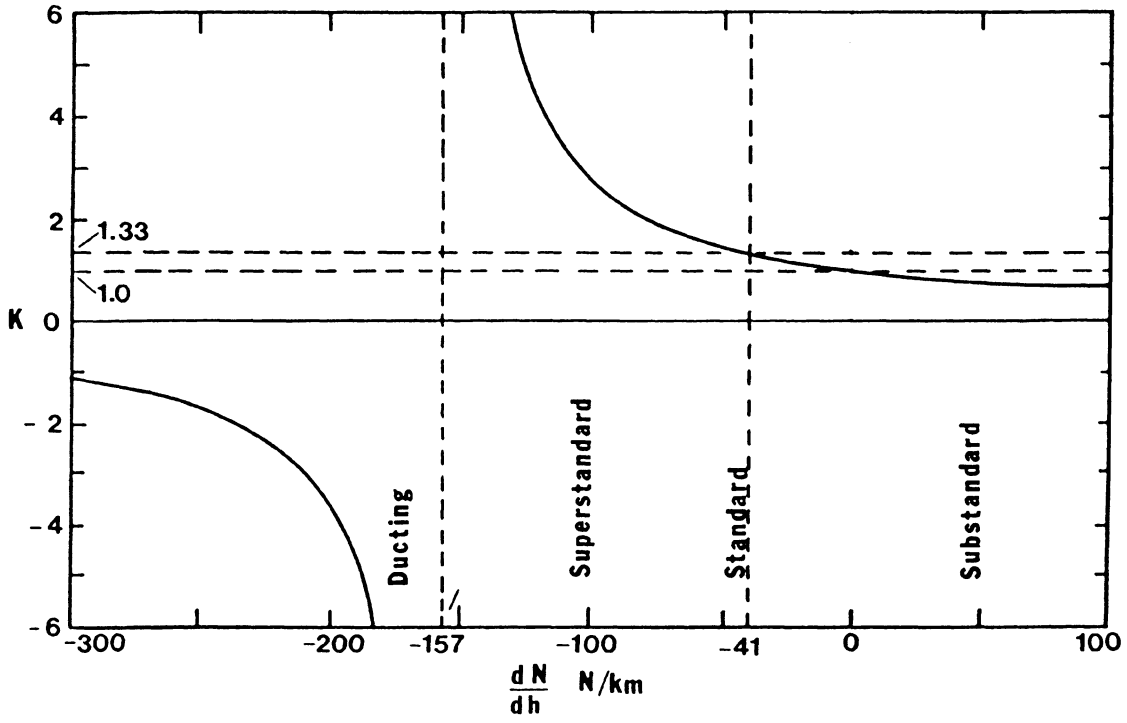

Refraction Zones as a Function of the Effective Earth Radius Factor K and of the Refractivity Gradient dN/dh

FIGURE 2.5

in which case the ray curvature meets or exceeds that of the earth. Under ducting conditions the effective earth radius factor and the radio horizon distance both tend to infinity. Figure 5 (Hall, 1983) depicts the sub-standard, super-standard, and ducting refraction zones as a function of k_e and dn/dh.

3. TROPOSPHERIC DUCTING AND LAYER REFLECTION.

Layering in the lower atmosphere has long been recognized as an important parameter in trans-horizon propagation at frequencies above 30 MHz (Saxton, 1951; Bullington, 1957). Two mechanisms have been suggested as being principally responsible for the guiding of short radio waves by atmospheric layers. The first, termed "ducting", attributes trapping to the strong refractive bending which takes place within layers exhibiting extreme refractivity gradients over a vertical extent which is large relative to the radio wavelength. The second, termed "layer reflection", attributes trapping to the partial reflection of radio energy from abrupt changes in the refractive index over layers of small vertical extent but large horizontal dimension. Both are generally treated together as forms of guided wave propagation.

Empirical evidence suggests that both mechanisms tend to co-exist, and are present more or less continuously to varying degrees in a stratified atmosphere characterized by a wide and dynamically changing range of layer sizes and structures (Birnbaum and Bussey,1955; Saxton et al.,1964; Lane,1965; Lane,1968; Hall and Comer,1970). Consequently, propagation in layered media has been an area of active investigation (Budden,1961; Wait,1962; Brekhovskikh,1980). However, marked stratification of the type which leads to greatly enhanced field strengths well

beyond the standard radio horizon is commonly viewed as an abnormal condition not sufficiently reliable for long range communication. Rather, atmospheric layering is usually accompanied by anomalous propagation velocity and multipath phase delay effects of a type which can give rise to serious range measurement error (Thompson,1975; Cartwright and Tattersall,1977). As such the detection of such conditions can be of great importance in precise radio navigation. In this section we review the meteorology of tropospheric layer formation and examine the mechanisms by which UHF radio waves may be trapped and propagated over long distances.

3.1) Layer Formation Processes in the Troposphere.

The physical phenomena which give rise to the formation of tropospheric trapping layers are discussed at length from a radio meteorological viewpoint in a number of texts including Kerr (1951), Bean and Dutton (1966), Livingston (1970), and Hall (1979). In general, layer formation is characterized by a combination of temperature inversion and increased humidity lapse in the lower atmosphere. Under more standard conditions in a well mixed atmosphere turbulence acts to inhibit the layering process such that temperature and humidity decrease in a uniform manner with altitude as discussed in the previous section. However, where stable and quiet atmospheric conditions persist for extended periods extensive stratification involving several layers can be built up and maintained. In this regard the effect of temperature inversions is doubly important in that (a) they can be widespread in area and persist for long periods, and (b) they act to suppress turbulence such that zones of abnormal humidity can develop. The resulting layers typically show great variability in height, thickness, and horizontal extent and consequently may act to influence propagation in various ways.

Within the first hundred metres of the atmosphere the layer formation process is generally linked to surface heating effects. In the absence of turbulent mixing the solar radiation cycle frequently gives rise to alternating horizontal bands of high and low humidity accompanied by temperature inversion immediately above the surface. In particular, strong evaporation ducts may be formed by the concentration of water vapour near the surface during periods of prolonged

solar heating. The trapping properties of evaporation ducts are well known and have been reported by various authors (Jeske and Brocks,1966; Joseph and Smith,1972; Richter and Hitney,1980). Refractivity deficits of 30-50 N units over layer thicknesses of several tens of metres are not uncommon in temperate and tropical marine climates. Conversely, nocturnal surface cooling can lead to temperature inversion conditions conducive to trapping. Example of surface inversion ducts are cited in Kerr (1951), Birnbaum and Bussey (1955), Hall and Comer (1969), and Cartwright and Tattersall (1977). Refractivity changes of a 30-50 N units over vertical extents of several tens of metres again seem typical. Finally, advection, the lateral motion of one air mass over another due to the differential heating of two dissimilar surfaces can give rise to the formation of strong horizontal boundary layers, and has long been recognized as a principal cause of duct formation in coastal regions (Kerr, 1951). Advection layering may be strengthened by wind shear, the variation with height of the horizontal component of wind velocity. Very abrupt refractivity deficits of 10 - 50 N units over layer thicknesses of under ten metres have been reported by Saxton et al. (1964), and Lane (1965, 1968).

At higher elevations the effects of subsidence must be considered in addition to advection and wind shear. Subsidence is the slow settlement and spreading of cool, dry air from great elevations and is often associated with stable high pressure anticyclonic conditions. Subsidence layering typically takes place at elevations of from 500 m to 2000 m and is characterized by marked temperature inversion and humidity lapse. Empirical evidence provided by vertical incidence radar and airborne refractometry suggests that subsidence layers are among the most abrupt, sometimes reaching 20 - 30 N units over vertical ranges of only a few metres, and may extend in the horizontal for several tens of kilometres or more. Examples are cited in Saxton et al. (1964), Lane (1965), and Hall and Comer (1970).

Figures 1 and 2 depict two examples of extreme refractive index changes in surface and elevated layer structures. Figure 1 depicts the refractivity profile over the first 70 m of the troposphere as determined from phsychrometric observations taken on a 100 m tower installation at Suffolk, England in July, 1975 and reported in Cartwright and Tattersall (1977). The

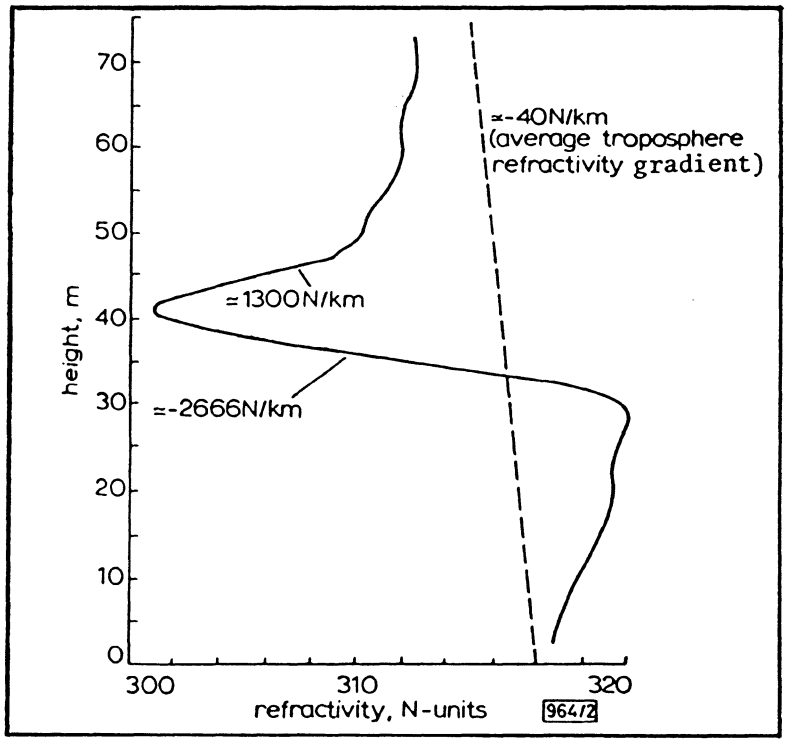

Refractivity in a Nocturnal Surface Inversion

(Cartwright and Tattersall,1979)

Figure 3.1

observed behaviour is attributed to a strong temperature inversion layer formed by nocturnal surface cooling. A variation of some 20 N units over a layer height of just under 10 m is evident. Figure 2 depicts the refractivity profile associated with the presence of a strong subsidence layer at a height of 1.2 Km as determined from airborne refractometer ascents at Hampshire, England in August, 1961 and reported by Lane (1965). In this case an abrupt change in refractivity of 20-30 N units was encountered in a vertical extent of under 5 metres.

Extensive statistics on the frequency of occurrence, altitude, and thickness of both surface and elevated ducting layers over most of the globe are provided in Bean et al. (1966). A more detailed treatment of similar information for Canada is given in Segal and Barrington (1977). Collectively these works indicate that surface based layers of 50-70 m in height are not uncommon in polar and temperate regions at certain times of the year, and are a frequent occurrence in tropical waters all year round. Elevated layers of 100-300 m thickness at heights of 1-3 Km are also a common occurrence.

3.2) Tropospheric Ducting.

In discussing propagation in the presence of atmospheric ducts it is often useful to introduce the concept of a modified refractive index m, related to the refractive index n by the equation (Bremmer, 1949)

$$m(h) = \frac{h+R}{R}\, n(h) \approx n(h) + \frac{h}{R} \qquad (3.1)$$

The modified refractivity M, can then be defined as

$$M = (m-1) \times 10^6 = N + 0.157h \qquad (3.2)$$

wherein N is the refractivity, h is the height, and R=6371 km is the adopted average earth radius.

The modified index is simply an extension to the effective earth radius concept as put forward by Schelling et al. (1933) and described in the previous section. It provides a convenient transformation whereby a spherically stratified atmosphere may be replaced to a first approximation by a plane stratified system. Differentiating equation 2 with respect to height yields

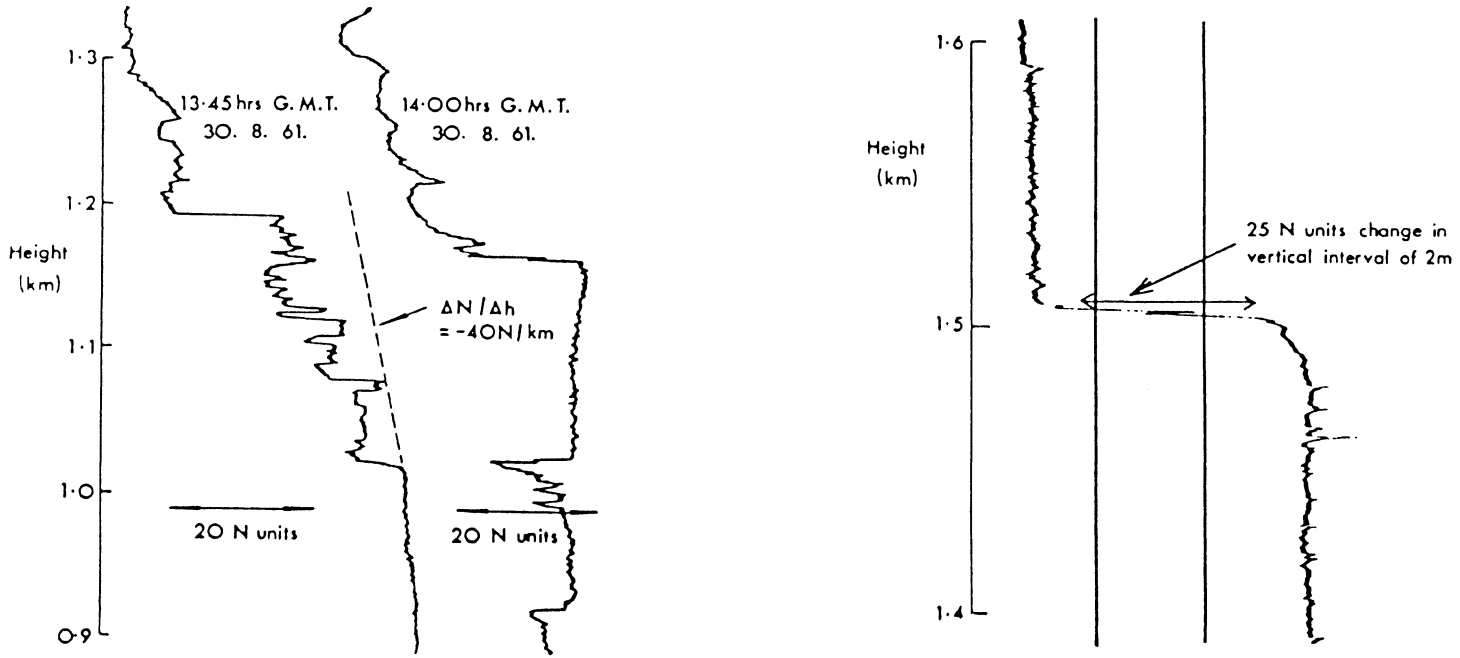

Refractivity Profile in a Subsidence Inversion

(Lane, 1965)

Figure 3.2

$$\frac{dM}{dh} = \frac{dN}{dh} + 0.157\ m^{-1} \qquad (3.3)$$

Clearly dM/dh will be negative, and the ray curvature will exceed the curvature of the earth, for refractivity gradients less than -157 N/Km. The existence of a trapping layer therefore requires a region in which $dM/dh < 0$. Three basic layer categories can be distinguished. Idealized depictions of the refractivity and modified refractivity profiles for each of these are presented in Figure 3. If the modified refractivity gradient is negative at the surface then the associated layer is termed a surface-based duct (Figure 3b). If the gradient is positive at the surface but at some altitude the value of the modified refractivity is less than the surface value then the layer is termed an elevated surface-based duct (Figure 3c). Finally, if the profile contains a segment of negative gradient but the minimum value of the modified refractivity occurs at the surface then the layer is termed an elevated duct (Figure 3d). In all cases the point at which the gradient becomes positive locates the height at which a horizontal ray will remain concentric to the earth and fixes the upper boundary of the duct.

Radio wave propagation in the presence of a tropospheric duct is in many ways analgous to that in a waveguide[1] and may be similarly treated by extending the mode theory of waveguide propagation. The guiding of radio waves in layered media by the mode theory approach has been the subject of recurring investigation since the 1940's, and extensive treatments of both the wave and ray theory aspects are given in Booker and Walkinshaw (1946), Bremmer (1949), Kerr (1951), Budden (1961), Wait (1962), and Brekhovskikh (1980). According to the mode theory the field radiated from a transmitter can be viewed as the sum of a number of elementary waves or modes formed by the superposition of uniform plane waves reflected from the walls of the guide at oblique angles of incidence. Each mode is composed of two component crossing waves the superposition of which gives rise to a standing wave distribution transverse to the axis of the guide. The mode denotes the number of standing wavelengths existing between the walls of the guide. The necessary condition for a self consistent or resonant mode is that the total change of

[1] For a discussion of waveguide systems see Jordan and Balmain (1966), Corson and Lorrain (1970), or Rao (1977).

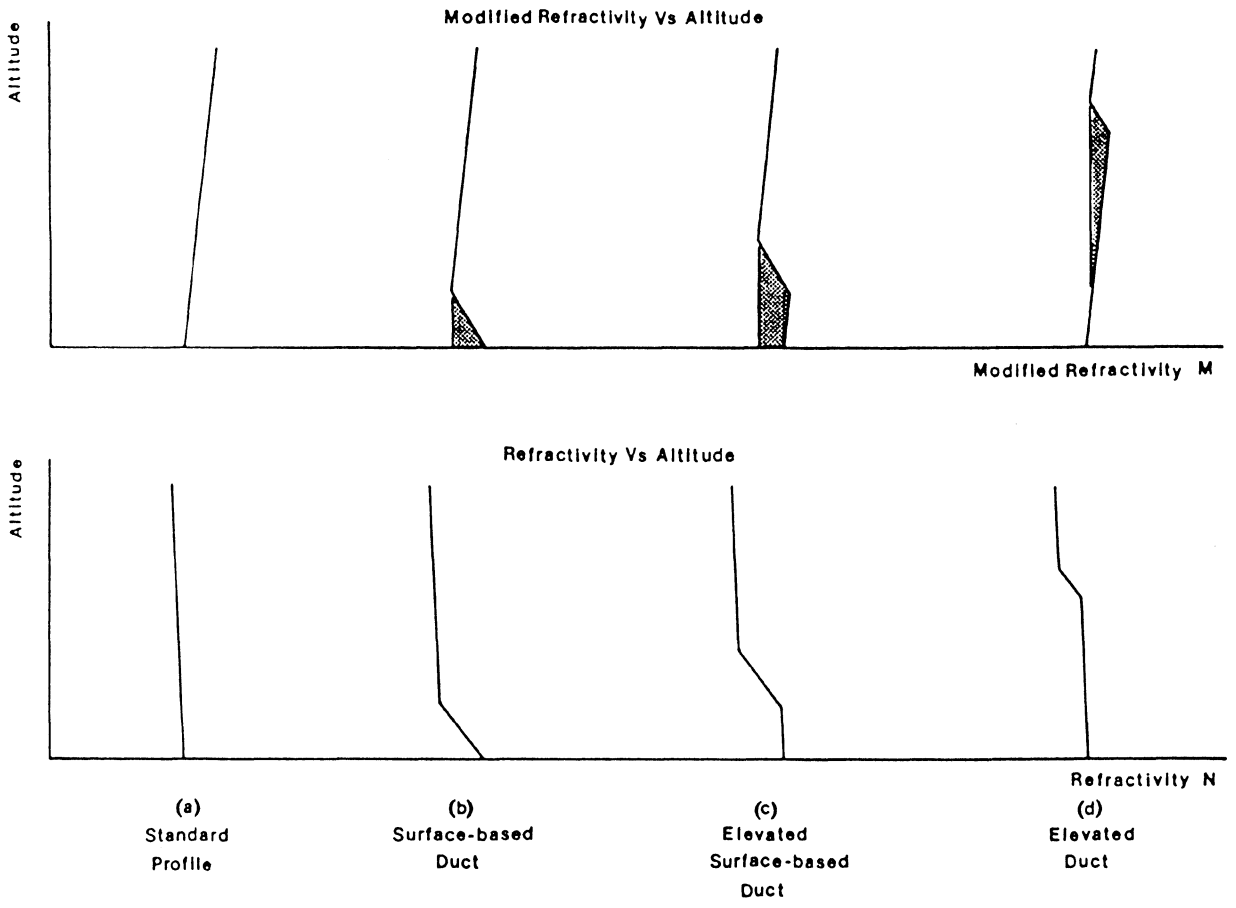

Figure 3.3
Refractivity Profiles and Duct Classification

phase transverse to the guide due to the double passage of the wave across the guide and back, plus the phase changes incurred upon reflection at the guide boundaries, must be an integer number of 2π radians. This requires that (Wait, 1962)

$$R_1(\beta)R_2(\beta)\, e^{(-2jkh\cos\beta)} = e^{(-2j\pi q)} \tag{3.4}$$

wherein β denotes the angle of incidence, h is the height of the guide, q is the order of the mode, and $k=\omega/v$ is the phase constant. Equation 4 is termed the fundamental equation of mode theory. The presence of the exponential term on the left-hand side accounts for the double passage of the wave across the guide, and the factors $R_1(\beta)$ and $R_2(\beta)$ are reflection coefficients[2] of the form (Kerr, 1950)

$$R(\beta) = R\, e^{(-j\,\delta\phi_r)} \tag{3.5}$$

wherein the modulus R is the ratio of the amplitudes of the reflected to the incident waves, and $\delta\phi_r$ is the phase shift incurred upon reflection.

Guided waves exhibit properties markedly different from those propagating in homogeneous media. By way of illustration let us consider the case of a uniform plane wave propagating between two perfectly reflecting (conducting) plates according to the cartesian coordinate geometry of Figure 4A. For such cases it can be shown that the incident wave is totally reflected such that R=1 and $\delta\phi_r = -\pi$, in which case the resonance condition 4 reduces to

$$kh\cos\beta = \pi q \tag{3.6}$$

or

$$\cos\beta = q\lambda/2h \tag{3.7}$$

wherein we have made use of the relation $k=2\pi/\lambda$. Thus the angle of incidence at resonance varies inversely with the wavelength and the order of the mode, and directly with the width of the guide. For $q\lambda \ll 2h$, $\beta \equiv 90^\circ$ and the waves are incident at glancing angles. As the wavelength or the order of the mode increase the waves begin to bounce more obliquely until at the cut-off wavelength

---

[2] Reflection coefficients are treated in detail in a number of texts on electromagnetic waves including Stratton (1941), Kerr (1951), Corson and Lorrain (1970), and Rao (1977).

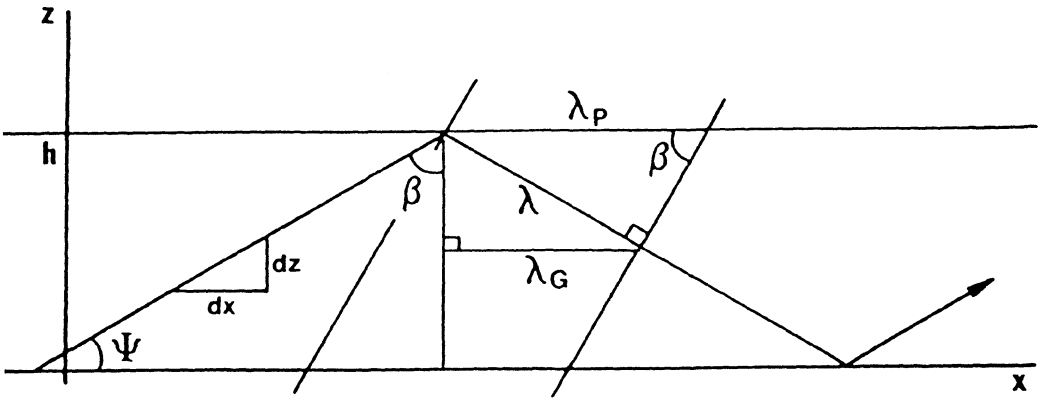

(a) Waveguide

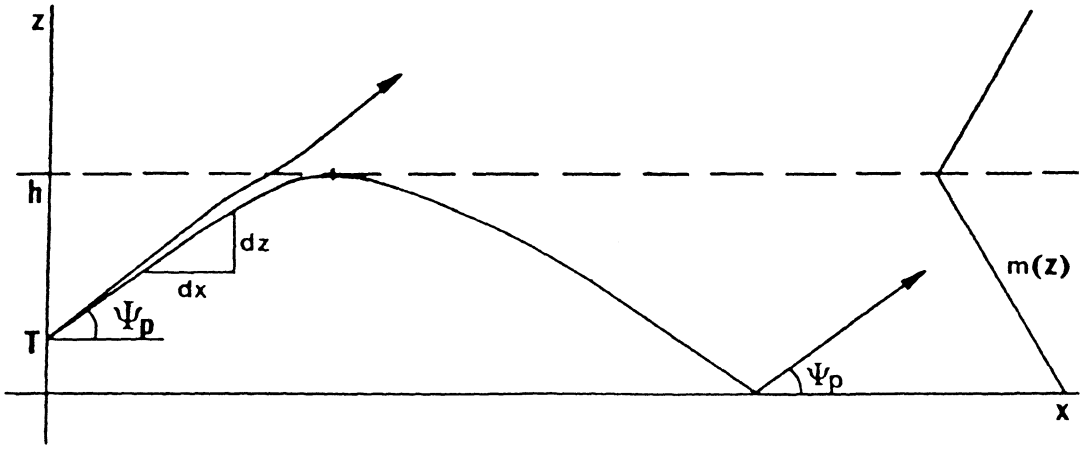

(b) Tropospheric Duct

Figure 3.4

Single Mode Propagation in a Waveguide and a Tropospheric Duct

$$\lambda_c = 2h/q \tag{3.8}$$

the waves simply bounce back and forth transverse to the guide axis and no energy is propagated down the guide. Hence a resonant mode will propagate only when the wavelength is less than the cut-off wavelength for that particular mode. This requires that the guide be at least q number of one-half wavelengths in width, where m is the order of the mode.

It may also be shown that guided wave propagation is in general dispersive and that phase and group velocities may be defined that are a function of the wavelength and order of the mode. Combining equations 7 and 8 we have

$$\cos\beta = \lambda/\lambda_c \tag{3.9}$$

Referring to Figure 4A we can define the phase velocity $v_p > v$ for a mode of order q as (Jordan and Balmain, 1966)

$$v_p = \omega/(k \sin\beta) = v/\sqrt{1-(\lambda/\lambda_c)^2} \tag{3.10}$$

In this sense the phase velocity is viewed as the apparent velocity of the wave along the guide axis. The fact that the phase velocity exceeds the actual wave velocity can be understood from geometry when one considers that the wave front will appear to travel the distance $\lambda_p > \lambda$ in the same interval of time. However, due to the zigzag path travelled by the wave its actual progress down the guide will be

$$v_g = v\sin\beta = v\sqrt{1-(\lambda/\lambda_c)^2} \tag{3.11}$$

wherein $v_g < v$ is termed the guide or group velocity. A comparison of equations 10 and 11 yields the condition

$$v_p v_g = v^2 = 1/\mu\epsilon \tag{3.12}$$

In the case of single mode propagation in a tropospheric duct a similar situation exists with slight modifications: (1) The refractive index and the angle of incidence are no longer constants but are continuously varying functions of height, and (2) The tropospheric boundary surfaces are never abrupt, smooth, or perfectly reflecting.

Whereas in the case of a waveguide all modes are perfectly reflected and confined to the guide, in the case of a tropospheric duct all modes to some extent penetrate or leak through the

ducting layer, and most are imperfectly reflected at the surface of the earth. As a result only the lower order modes propagate to any significant distance. These modes, corresponding to cases of glancing incidence, may be represented by rays that proceed by a series of reflections just as in the case of a waveguide. The following development follows that of Kerr (1951).

Consider the ray geometry associated with single mode propagation in an atmospheric duct as represented in Figure 3b. The curvature of the ray path conforms to Snell's law, which by assuming the modified refractive index m, may be written in the form

$$m(z)\cos\psi(z) = C \tag{3.13}$$

wherein $\psi(z)$ is the elevation angle (complement of the angle of incidence), $m(z)$ is the modified refractive index, and C is a constant. Alternatively we can write Snells law in the form

$$m(z)\sin\psi(z) = \pm\sqrt{m^2(z)-C^2} \tag{3.14}$$

where the sign of the radical accounts for the possibility of both positive and negative elevation angles. Combining these two forms of Snells law it is obvious that

$$\tan\psi(z) = \pm\frac{\sqrt{m^2(z)-C^2}}{C} = \frac{dz}{dx} \tag{3.15}$$

where x and z are the coordinates of a typical point on the ray. Since dx is always positive the radical will be assigned the same sign as dz. For small elevation angles and refractive indices near unity we can employ the approximations

$$m^2(z) - C^2 \approx 2[m(z) - C] \tag{3.16}$$

$$\psi(z) \approx \tan\psi(z) = dz/dx \tag{3.17}$$

$$m(z)\cos\psi(z) \approx m(z) - \frac{\psi^2(z)}{2} \tag{3.18}$$

such that equation 15 becomes approximately

$$\psi(z) \approx \pm\sqrt{2}\sqrt{m(z)-m(z_t)+\frac{\psi(z_t)^2}{2}} \tag{3.19}$$

wherein z_t denotes the transmitter height. A projected ray will have a turning point $\psi(z_h)=0^o$, where h is the duct height, for all initial elevation angles $\psi(z_t)$ less than the value ψ_p given by

$$\psi_p = \pm\sqrt{2\,[m(z_h)-m(z_t)]} \tag{3.20}$$

Hence the critical angle ψ_p, known as the angle of penetration, effectively divides the family of rays into two groups; those which are trapped within the duct and are guided, and those which penetrate the ducting layer. The turning points of the trapped rays define a caustic surface at which there is a phase change of 90°. This phase change, termed the phase anomaly, is characteristic of points at which neighbouring rays intersect and is well known in optics in relation to ray convergence at a focal plane.[3] We shall assume glancing incidence such that a phase change of -180° occurs upon reflection at the earths surface. With these changes the fundamental resonance condition 4 becomes

$$\int_{z_o}^{z_h} m(z) \sin\psi \, dz = (q-¼)\lambda/2 \qquad (3.21)$$

wherein z_h is the maximum height which defines the turning point $\cos\psi=1$ of the trapped rays. Setting z_0 equal to the elevation of the base of the duct, and employing equations 13 and 14 we have

$$\int_{z_o}^{z_h} \sqrt{m^2(z_0)-m^2(z_h)} \, dz = (m-¼)\lambda/2 \qquad (3.22)$$

and since $m(z_0)$ and $m(z_h)$ are nearly unity this can be reduced to the approximate form

$$\sqrt{2}\int_{z_o}^{z_h} \sqrt{m(z_0)-m(z_h)} \, dz = (m-¼)\lambda/2 \qquad (3.23)$$

By assuming a linear lapse rate for the modified index change over the width of the duct such that

$$m(z_0)-m(z_h)= \alpha_m h \qquad (3.24)$$

wherein α_m is the lapse rate and $h=z_h-z_0$ is the duct width, we obtain the following approximate expression for the longest wavelength trapped

$$\lambda_{max} = \frac{4}{3}\sqrt{2}\, h\,[\alpha_m h]^{½} \qquad (3.25)$$

This result has been used by various authors including Bremmer (1949), Kerr (1951), Wait(1962), Bean and Dutton (1966), and Segal and Barrington (1977).

Figure 5 depicts the maximum trapped wavelength as a function of duct width and the lapse rate of the modified index according to equation 25. The wavelength of UHF systems is typically of

---

[3] See for example Born and Wolf (1965).

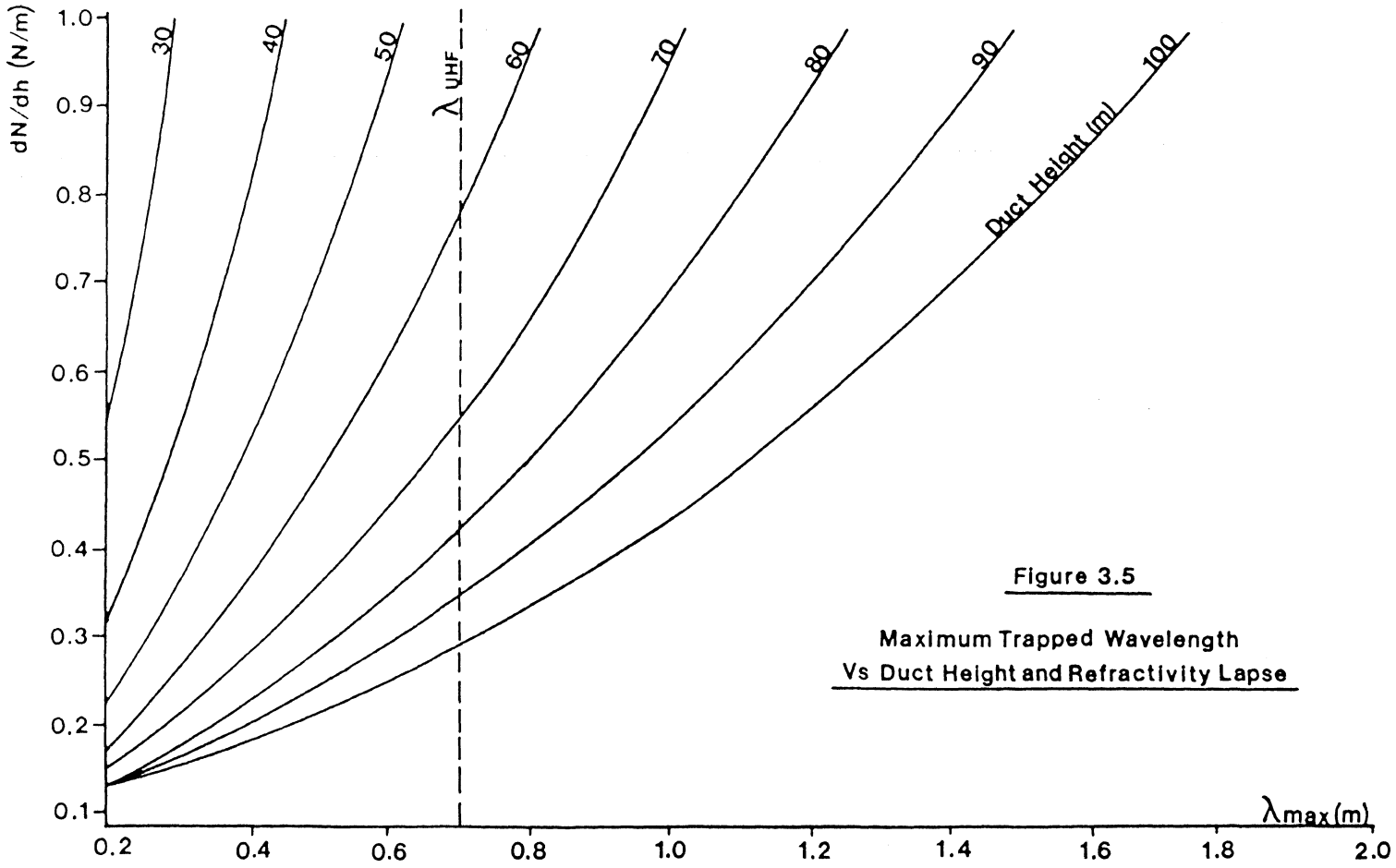

Figure 3.5

Maximum Trapped Wavelength
Vs Duct Height and Refractivity Lapse

the order of 0.7 metres. It is evident that the duct height is the critical parameter to be observed, and that complete trapping is predicted for UHF frequencies only for duct heights of the order of 75 metres or more. Typical duct thicknesses are such that complete trapping seldom occurs below microwave frequencies. However, the values of λ_{max} presented here do not represent strict cut-off conditions, and although energy at these wavelengths and shorter will be strongly guided, significant signal enhancement can occur at wavelengths several times those cited.

3.3) Layer Reflection.

Whether a refractivity gradient more negative than -157 N/Km will give rise to guided wave propagation through refraction or reflection depends largely upon the vertical extent of the layer relative to the radio wavelength. Refractivity gradients which have inadequate depth to trap by refractive bending may be more than adequate to reflect energy incident at glancing angles. For this reason reflection tends to be the predominant phenomenon at VHF and UHF wavelengths while refraction is predominant at higher frequencies.

The modulus of the reflection coefficient for an abrupt plane boundary separating two air masses may be written in the Fresnel form (Wait, 1962)

$$R(\psi) = \frac{\sin\psi - [2\delta m + (\delta m)^2 + \sin^2\psi]^{1/2}}{\sin\psi + [2\delta m + (\delta m)^2 + \sin^2\psi]^{1/2}} \qquad (3.26)$$

wherein δm denotes the change in the modified index across the boundary layer. Assuming that $1 >> \sin^2\psi >> \delta m$ yields the approximate form (Wait, 1962)

$$R(\psi) \approx \frac{-\delta m}{2\sin^2\psi} \approx \frac{-\delta m}{2\psi^2} \qquad (3.27)$$

which is valid for values of ψ of up to a few degrees and for both vertical and horizontal polarization (Wait, 1962).

In general the refractivity change will not be abrupt but will occur gradually and continuously over a finite height interval. In this case the reflectivity of the layer will depend upon:

1) The magnitude of the refractivity change δm.

2) The vertical extent of the layer.

3) The form the refractivity profile takes within the layer.

4) The grazing angle of the incident energy.

The method of calculating the reflection coefficient under such conditions is illustrated schematically in Figure 6 for a boundary layer subdivided into differential strata. The incremental reflection coefficient $dR(\psi)$, arising from the refractivity change $d(\delta m)/dz$ within each stratum is then given by (Wait, 1962)

$$dR(\psi) = \frac{1}{2\psi^2} \frac{d(\delta m)}{dz} e^{-j2k\sin\psi z} \tag{3.28}$$

wherein the exponential term has been incorporated to account for the two way path of the ray. The total reflection coefficient is then obtained by integrating over the extent of the layer, yielding

$$R(\psi) = \frac{1}{2\psi^2} \int_{z_o}^{z_h} \frac{d(\delta m)}{dz} e^{-2jk\sin\psi z}\, dz \tag{3.29}$$

This function has been evaluated for several layer forms by various authors including Saxton (1951), Friis et al. (1957), Du Castel et al. (1962), Beckmann and Spizzichino (1963), Wait and Jackson (1964), Hall (1968A), and Thayer (1970). In any case, there is almost certainly no unique form likely to be representative of all possible layer structures. Hence, herein we shall adopt the linear form of Figure 6 as a simple and representative analytical model, in which case equation 29 takes the form (Hall, 1968A)

$$R(\psi) = \frac{\alpha_m h}{2\psi^2} \left[\frac{\sin\chi}{\chi}\right] \tag{3.30}$$

wherein $\delta m = \alpha_m h$ denotes the refractivity change across the layer, and

$$\chi = k\sin\psi h = 2\pi\sin\psi\ h/\lambda \tag{3.31}$$

is termed the effective width of the layer (Wait and Jackson, 1964).

It is apparent that in the limit as h/λ becomes very small the reflection coefficient of equation 30 reduces to equation 27, the Fresnel value appropriate to a sharp discontinuity. Conversely, when h/λ is large the coefficient is greatly reduced in magnitude. This characteristic

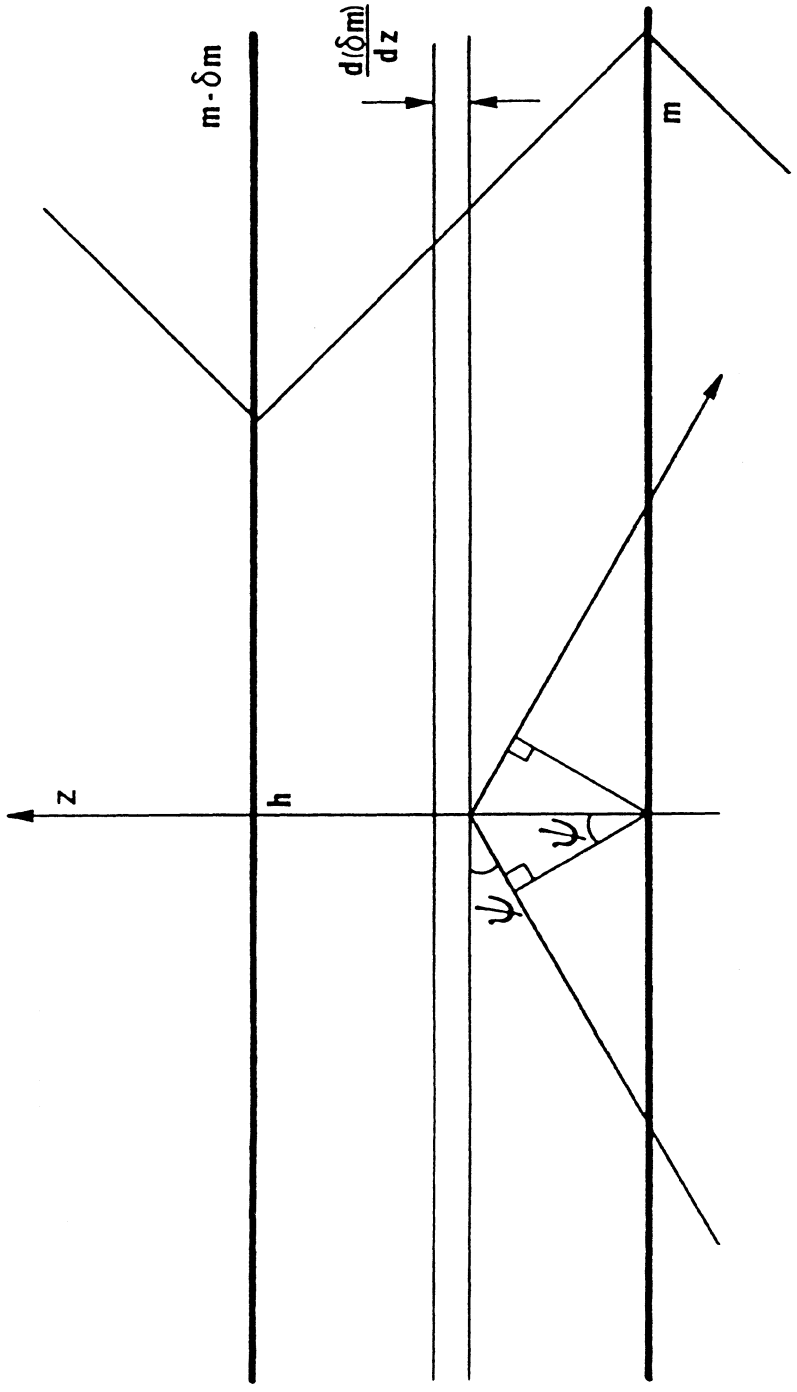

Figure 3.6
Incremental Reflection at a Tropospheric Boundary Layer

suggests an expression for the reflection coefficient in a stratified troposphere of the general form (Hall,1979)

$$R(\psi) = R_F(\psi)F_R \qquad (3.32)$$

wherein $R_F(\psi)$ is the Fresnel reflection coefficient for an abrupt boundary as given by equation 27, and F_R is a form factor which accounts for the shape and the gradualness of the layer.

The reflection coefficient will in general vary inversely to the square of the grazing angle ψ and the ratio h/λ. Consequently reflections from tropospheric layers are not of much consequence above UHF frequencies, but can provide a significant trapping mechanism for VHF and UHF wavelengths. As with other aspects of radio meteorology, agreement between theory and practice is limited by the lack of data concerning the refractivity distribution along the transmission path. However, reasonable confirmation of the validity of tropospheric reflection as a trapping mechanism has been demonstrated by various authors by correlating field strength variations with meteorological data gathered by radiosonde and refractometer observations at the centre of trans-horizon VHF and UHF radio links. These include the studies of Crawford et al (1959), Lane and Sollum (1965), Hall (1968A,B), Hall and Comer (1970), and Thayer (1970).

Our development of layer propagation theory is far from complete. In recent years activity has centred upon the formulation of full wave solutions to the trapping problem. Contributions in this regard include those of Wait and Spies (1969), Chang(1971), Pappert and Goodhart (1977), Cho and Wait (1978),Dougherty and Hart (1979),Richter and Hitney (1980), and Baumgartner et al. (1983). Such full-wave solutions provide a much better description of the field behaviour in the presence of trapping layers and , in particular, the enhanced field strengths observed above and below ducts due to leakage of energy out of trapping layers, and the trapping of energy within layers originating from transmitters external to the duct. However, while wave theory provides a more rigorous basis for analysis, only limited success has been achieved to date in layer propagation modelling as a whole, principally due to the complexity involved in predicting variations in the height, thickness, profile, and surface characteristics of

trapping layers. A number of these shortcoming and others are discussed in Jeske and Brocks (1966) and Almond and Clark (1983).

4. SCATTERING BY TROPOSPHERIC IRREGULARITIES.

In this section we consider the effect of the small scale irregularities in the tropospheric refractive index created by turbulence. For this purpose it is convenient to consider the refractivity distribution as being comprised of two components: (1) a median or signal component chiefly a deterministic function of altitude as described in the preceeding chapters and which varies slowly in time and space, and (2) a smaller stochastic or noise component super-imposed upon the median which arises from the localized and instantaneous fluctuations in atmospheric pressure, temperature, and humidity as generated by turbulent mixing processes in the atmosphere. The principal effect of the stochastic refractivity variations are twofold in that they act to scatter radio energy and to produce random fluctuations in the phase and amplitude of the received signal as a function of time and space.

Empirical evidence has established that tropospheric scattering comprises the principal source of trans-horizon radio field strength at frequencies above 30 MHz (Saxton et al., 1951; Bullington et al., 1955; Crawford et al., 1959; Chisholm et al., 1962; Saxton et al., 1964). Two principal mechanisms have been suggested to explain the troposcatter field:

1.) In the eddy theory small blobs or eddies of irregular refractive index are viewed as elementary electric dipoles which are polarized by the incident field and reradiate energy in all directions. The contribution of all such eddies within the common volume occupied by the transmitting and receiving antennas mutually interfere in the manner of an irregular three-dimensional diffraction grating such that the redirected energy is concentrated in the forward direction with the principal maximum depending upon the spacing of the irregularities and the angle of incidence of the original signal. The eddy theory was initially proposed by Booker and Gordon (1950), and has been adopted in modified forms by various authors including Megaw (1950), Saxton(1951), Villars and Weisskopf (1954); Staras (1955), Silverman (1956), Wheelon (1959), Chernov (1960), and Tatarskii (1961).

2.) The layer theory relates the scattered field to diffuse reflection from an array of small and irregularly shaped layers of small horizontal extent randomly distributed throughout the common volume. The analogy with three-dimensional diffraction gratings can again be drawn. The proponents of this theory include Saxton (1951), Friis et al. (1959), Du Castel et al. (1962), and Beckmann and Spizzichino (1963).

Empirical evidence confirms that both mechanisms tend to coexist and that both are intimately related to the intensity and structure of atmospheric turbulence. In the remainder of this chapter we shall briefly review the meteorology of turbulence in the troposphere, the statistical characterizations of the resulting refractive index irregularities, and the theories of scattering by eddies and irregular layers.

4.1) The Meteorology of Atmospheric Turbulence.

The mechanics of atmospheric turbulence are treated in detail in Sutton (1953), Lumley and Panofsky (1964), Monin and Yaglom (1971), and Panofsky and Dutton (1984). For our purposes it will be sufficient to adopt a simpler and more qualitative approach following that of Dutton and Panofsky (1970).

Turbulence may be defined in simple terms as any type of fluid motion which appears as strongly rotational, three-dimensional, and random. Two sources of turbulent activity in the atmosphere can be distinguished. Mechanical turbulence occurs at the boundaries of neighbouring air masses and at the surface of the earth when relative motion gives rise to shear stresses. Convective turbulence occurs when irregularities in the vertical temperature profile promote thermally unstable and bouyant air masses. The principal distinguishing characteristic of turbulent activity is its apparent randomness, as opposed to laminar flow in which each element of fluid volume follows (within certain limits) the same predictable path as its predecessors.

Many of the characteristics of atmospheric turbulence can be illustrated in terms of a simplified energy budget of the form (Dutton and Panofsky, 1970)

$$\frac{dE}{dt} = M + B - D + Q \qquad (4.1)$$

wherein E is the mean kinetic energy of the turbulence per unit mass, t is time, M is the rate of production of mechanical turbulent energy by shear forces, B is the rate of production of convective turbulent energy by bouyant forces, Q is a transport term, and D is the rate of the frictional dissipation of turbulent energy into heat.

The term M is proportional to the square of vertical wind shear, the rate of change of horizontal wind velocity with height, and is almost always positive. Both change in wind speed and direction enter into this term. The term B depends upon the vertical temperature gradient and has to do with the balance between the bouyant and gravitational forces acting upon an air mass. When a parcel of air is displaced vertically from its surroundings it undergoes a decrease in temperature in keeping with the change in ambient pressure according to the ideal gas law. If heat exchange effects are considered negligable the temperature decrease is termed the adiabatic temperature lapse rate, and is typically 1°C per 100m. At the adiabatic rate bouyant and gravitational forces remain in balance as the parcel ascends, leading to a condition of neutral equilibrium in which the density of the parcel is always the same as its surroundings. For lapse rates less than the adiabatic rate the ascending parcel will have a density greater than its surroundings in which case gravitational forces will exceed bouyant forces , the parcel will tend to

return to its initial level, and a condition of stable equilibrium is said to exist. Conversely, at lapse rates greater than the adiabatic rate the density of the displaced parcel will be less than its surroundings and bouyant forces will tend to displace it further, leading to a state of unstable equilibrium.

Under conditions of unstable equilibrium the term B is positive and the resulting bouyancy gives rise to convective turbulence. Positive conditions may occur between air masses of different thermal characteristics or at the surface due to prolonged solar heating. Often mechanical mixing serves as the catalyst which initiates the displacement process. Whenever the term B is negative , as is the case under temperature inversion, it acts as an energy sink which reduces the action of mechanical turbulence. Hence, those conditions which are favourable to the formation of stable atmospheric layers conducive to ducting and layer reflection are exactly the opposite of those favourable to strong turbulent activity and scattering.

In general M and B initiate large scale turbulent eddies which decay by transferring energy into smaller and smaller eddies until the energy is finally dissipated into heat by friction and viscosity. The rate of energy dissipation D is thus always positive. Because the coefficient of viscosity of air is small dissipation occurs at the small end of the eddy size scale. The final term in our simplified energy budget is the transport term Q which allows for the possibility that energy created in one location may be transferred and dissipated in another location.

In order for turbulence to occur in thermally stable air the rate of energy production by mechanical processes must exceed the rate of energy drainage by stratification. A quantitative measure of this energy balance is given by the flux Richardson number (Dutton and Panofsky, 1970)

$$R_f = -B/M \qquad (4.2)$$

Assuming the transport term to be negligible the energy budget can be rewritten in terms of R_f as

$$\frac{dE}{dt} = M(1 - R_f) - D \qquad (4.3)$$

When R_f is negative both B and M are energy inputs and vigorous turbulence will result. When R_f is positive thermal stability and stratification inhibit the growth of turbulence. If R_f is

zero turbulence is strictly mechanical. The critical Richardson number R_c provides an indication of the upper limit beyond which turbulence will not generally persist. For such a case $dE/dt = 0$ and we have

$$R_c = 1 - D/M \tag{4.4}$$

The computation of the flux Richardson number is generally impractical for systems as large and complex as the troposphere. Alternatively the gradient form R_i of the Richardson number is used as an approximation (Dutton and Panofsky, 1970)

$$R_i = \frac{g}{\Theta} \frac{\partial \Theta}{\partial z} \left[\frac{\partial \mathbf{u}}{\partial z}^2 + \frac{\partial \mathbf{v}}{\partial z}^2 \right]^{-1/2} \tag{4.5}$$

wherein Θ is termed the potential temperature, g is the gravitational acceleration, and **u** and **v** are wind velocity vectors in two orthogonal horizontal directions.

The potential temperature Θ is defined as that temperature a parcel of air would have if brought adiabatically to a standard sea level pressure of 1000 mb. Hence, if Θ increases with height the air is in stable equilibrium, if it decreases with height the air is thermally unstable and convective turbulence may develop. In neutrally stable air the adiabatic lapse rate prevails and Θ is a constant with respect to height. Θ is given by the expression (Fleagle and Bussinger, 1980)

$$\Theta = T(P_o/P)^{R/Cp} \tag{4.6}$$

wherein R is the gas constant and C_p is the specific heat at constant pressure.

The flux and gradient forms of the Richardson number are related by (Panofsky and Dutton, 1984)

$$R_f = (K_h/K_m) R_i \tag{4.7}$$

where K_m is the eddy viscosity and K_h is the eddy conductivity of the layer. K_h provides a measure of the rate of heat transfer by conduction, K_m by mechanical mixing.

Mechanical turbulence enters into the denominator of equation 5 and depends essentially upon the square of the wind shear which arises from changes in the wind speed or direction as a function of height. Convective turbulence enters through the gradient of the potential temperature

term in the numerator. Hence, large values of wind shear and temperature deficit across a layer give rise to small and negative Richardson numbers and pronounced turbulence. Conversely, positive gradients in Θ, such as occur in inversion layers, give rise to positive values of R_i, in which case the negative bouyancy forces associated with stable stratification tend to inhibit turbulence.

For the gradient case the critical Richardson number varies from 0.25 to 1.0 depending upon height and terrain. Numerous radiosonde, vertical incidence radar, and refractometer studies have established the general conditions under which strong turbulence might be expected to flourish. Typical studies are those of Crain et al. (1953), Birnbaum and Bussey (1955), Wheelon (1957A), Planck (1959), Gossard (1960A,1960B), Straiton et al. (1962), Bull (1966), Bean et al. (1967), and Lane (1968). The conclusions of these studies can be summarized as follows:

1.) Turbulence is frequently associated with regions of strong vertical wind shear and temperature deficit. These two factors are often closely related.

2.) Turbulence is strongest within the first few hundred metres of the surface due to the combined effects of surface shear and solar heating.

3.) Turbulence is frequently more intense over irregular terrain due to increased surface shear, and in coastal regions where advection breezes promote mixing of dissimilar air masses.

4.) In middle latitudes turbulence is most frequent and most intense in summer months, because the higher surface temperatures found in these months promotes strong thermal instabilities in the lower atmosphere.

5.) Turbulence is always associated with weather fronts since they mark the separation of air masses of different characteristic wind velocities and temperatures.

6.) Temperature inversions are energy sinks for turbulent activity and tend to stabilize air flow.

4.2) Characterization of Refractive Index Irregularities.

The direct effect of turbulent mixing in the troposphere is to create apparently random temporal and spatial variations in the value of the refractive index. The usual appraoch is to express the total variation as the sum of a mean and stochastic component (Booker and Gordon, 1950; Villars and Weisskopf, 1954; Silverman, 1957)

$$N(\mathbf{r},t) = \bar{N}(\mathbf{r},t) + N'(\mathbf{r},t) \tag{4.8}$$

wherein the total refractivity $N(\mathbf{r},t)$ is a function of the three dimensional position vector $\mathbf{r}$ and the time t. The function $\bar{N}(\mathbf{r},t)$ is treated as a deterministic function of altitude which varies slowly in space and time as described in preceeding chapters. The stochastic function $N'(\mathbf{r},t)$ is considered a stationary random field which is normally distributed and spatially homogeneous and isotropic[1]. Based upon these assumptions we can relate the following statistical properties of the random field $N'(\mathbf{r},t)$ (Silverman, 1957; Wheelon, 1959):

1.) The mean value $\bar{N'}$ of the field is a constant equal to zero, given by the expected value :

$$\bar{N'} = E[N'(\mathbf{r},t)] = 0 \tag{4.9}$$

2.) The variance $\sigma^2_{N'}$ describing the mean square fluctuation at any point of the field is also a constant, expressed as the expectation :

$$\sigma^2_{N'} = C(0,0) = E[N'(\mathbf{r},t)N'(\mathbf{r},t)] \tag{4.10}$$

wherein $C(0,0)$ denotes the autocovariance function at zero time and space lag.

3.) The autocovariance function $C(\boldsymbol{\delta},\tau)$ of the field depends only on the time and space separation of two points in the field and is independent of absolute position, time, or direction such that

$$C(\boldsymbol{\delta},\tau) = C(\mathbf{r},t;\mathbf{r}+\boldsymbol{\delta},t+\tau) = E[N'(\mathbf{r},t)N'(\mathbf{r}+\boldsymbol{\delta},t+\tau)] \tag{4.11}$$

Alternatively we can express the autocovariance function as

$$C(\boldsymbol{\delta},\tau) = \sigma^2_{N'}\,\rho(\boldsymbol{\delta},\tau) \tag{4.12}$$

where $\rho(\boldsymbol{\delta},\tau)$ is the correlation coefficient of the field.

---

[1]For a detailed discussion of random field statistics see VanMarcke (1984).

4.) The field $N'(\mathbf{r},t)$ is completely described in statistical terms by its ensemble mean and autocovariance function . Assuming ergodicity holds these may be computed on the basis of sampling over any representative realization of the field.

The first three of these properties arise from the assumptions of stationarity, homogeneity, and isotropy ; the fourth from the assumption of a gaussian distribution. The underlying turbulent velocity fluctuations are assumed to have the same statistical properties as the refractivity field they create. It is generally further assumed that the temporal variations in the refractivity field are negligable over the time interval associated with the propagation time of an electromagnetic wave. In this case the spatial autocovariance function $C(\boldsymbol{\delta})$ provides one possible means of characterizing the random fluctuations in refractive index. The integral scale length or correlation distance (Megaw, 1957; Monin and Yaglom, 1971)

$$\ell = [C(0)]^{-1}\int_0^{\infty} C(\boldsymbol{\delta})\, d\delta \tag{4.13}$$

defines the separation distance at which correlation between two points in the field becomes insignificant.

Alternatively, spatial spectra can be used to describe the size and intensity of the irregularities. The autocovariance function $C(\boldsymbol{\delta})$ and the power spectral density or spectrum of irregularities $S(\mathbf{k})$ are related by the three dimensional form of the Weiner-Kinchine relations[2]

$$S(\mathbf{k}) = \frac{1}{8\pi^3}\int_V C(\boldsymbol{\delta})\cdot e^{-j\mathbf{k}\cdot\boldsymbol{\delta}}\, d^3\boldsymbol{\delta} \tag{4.14}$$

$$C(\boldsymbol{\delta}) = \int_V S(\mathbf{k})\cdot e^{j\mathbf{k}\cdot\boldsymbol{\delta}}\, d^3\mathbf{k} \tag{4.15}$$

where $d^3\boldsymbol{\delta} = (\delta_x\delta_y\delta_z)$ is an element of volume and $\mathbf{k}=2\pi/\boldsymbol{\delta}$ is the spatial wavenumber. Obviously $C(\boldsymbol{\delta})$ and $S(\mathbf{k})$ form Fourier transform pairs. Assuming $N'(\boldsymbol{\delta})$ to be an isotropic real

---

[2] A variety of forms for the power spectral density are used in turbulence theory and random fields. The various forms of the Weiner-Kinchine relations cited here are fully developed and explained in Monin and Yaglom (1971), Panofsky and Dutton (1984), and VanMarcke (1984).

scalar field, $C(\delta)$, $\delta=|\boldsymbol{\delta}|$ is necessarily an even and real positive function. In this case $S(k)$ must also be real and positive for all $k=|\mathbf{k}| > 0$. It can then be shown that equivalent one dimensional forms are

$$S(k) = \frac{1}{2\pi} \int_{-\infty}^{\infty} C(\delta) \cos(k\delta)\, d\delta \tag{4.16}$$

$$C(\delta) = \int_{-\infty}^{\infty} S(k) \cos(k\delta)\, dk \tag{4.17}$$

Alternatively, adopting a spherical reference frame $\mathbf{r}(\phi,\lambda,\delta)$ centred within the volume results in the following equivalent spherical forms for isotropic fields

$$S(k) = \frac{1}{2\pi^2} \int_{0}^{\infty} \frac{\sin(k\delta)\, C(\delta)\, \delta^2}{k\delta}\, d\delta \tag{4.18}$$

$$C(\delta) = 4\pi \int_{0}^{\infty} \frac{\sin(k\delta)\, S(k)\, k^2}{k\delta}\, dk \tag{4.19}$$

The above Weiner-Kinchine forms appear in a number of papers dealing with troposcatter propagation (Villars and Weiskopf, 1954; Staras, 1955; Silverman, 1956; Megaw, 1957; Wheelon, 1959; Chernov, 1960; Tatarskii, 1961). In particular we note from equation 15 that the variance

$$\sigma^2_{N'} = C(0) = \int_{-\infty}^{\infty} S(k)\, dk \tag{4.20}$$

relates the mean square refractivity fluctuation at a point to the one dimensional spectral density $S(k)$ and indicates the relative contribution of the various spatial wavenumbers to the overall variance.

The earliest models of the stochastic refractivity field were expressed in terms of their correlation functions. Spectra were then computed in a secondary fashion using a suitable form of the Weiner-Kinchine relations. Generally these models were selected more for their computational convenience than for their relationship to any underlying model of atmospheric

turbulence. Among the more prominent correlation models are the Exponential model (Booker and Gordon, 1950)

$$\rho(\delta) = e^{(-\delta/\ell)} \tag{4.21}$$

The Gaussian model (Wheelon, 1955)

$$\rho(\delta) = \exp(-\delta^2/\ell^2) \tag{4.22}$$

and the Bessel model (Norton, 1957)

$$\rho(\delta) = (\delta/\ell) K_v(\delta/\ell) \tag{4.23}$$

wherein $K_v(a)$ is the modified Bessel function of the third kind and second order (Abramowitz and Stegun, 1965).

Alternatively, the use of spectra makes direct contact with the theories of turbulent mixing as described in Monin and Yaglom (1971) or Panofsky and Dutton (1984). Such theories predict three distinct bands within the spectrum of a fully developed turbulent process as depicted in Figure 1 (Wheelon, 1959). The input or eddy formation band contains the largest scale irregularities and is of principal importance in layer reflection theories of scattering. Eddies within this band are typically non-isotropic and non-homogeneous and have scale lengths $\ell_0 = 2\pi/k_0$ of the order of a few hundred metres in the horizontal and a few tens of metres in the vertical. Since the creation of turbulent eddies from laminar flow is as yet poorly understood present models of turbulence do not represent this band well. At the other end of the spectrum the dissipation band is characterized by a sharp drop in turbulent activity due to the destructive action of viscosity and diffusion. In the troposphere the scale length $\ell_d = 2\pi/k_d$ is of the order of a few centimetres. The intermediate or inertial band $k_0 < k < k_d$ is characterized by the redistribution of turbulent energy toward higher and higher wavenumbers and represents the repeated subdivision of the turbulent field into smaller and smaller eddies. Consequently the eddies within this band are more nearly spherical, isotropic, and homogeneous and provide the basis for the various eddy theories of tropospheric scattering.

Much of modern turbulence theory is based upon the Obukhoff-Kolmogorov universal equilibrium theory of homogeneous turbulence as described in Monin and Yaglom (1971) and

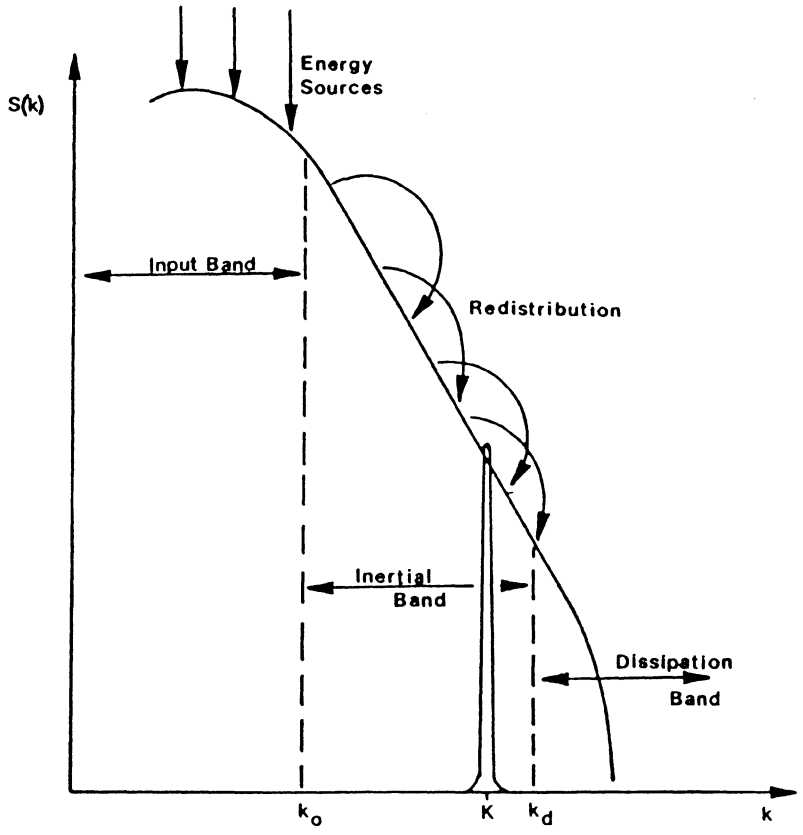

Figure 4.1
Idealized Spectrum of Refractive Index Irregularities

(Wheelon, 1959)

Panofsky and Dutton (1984). One of the principal assertions of this theory is that there exists a range of wavenumbers (scale sizes) within the inertial band for which the turbulent irregularities can be considered locally homogeneous and isotropic. The difference in the refractivity values $N'(\mathbf{r}_1)$ and $N'(\mathbf{r}_2)$ at any two closely spaced points $\mathbf{r}_1$ and $\mathbf{r}_2$ within the field is then chiefly due to those irregularities with dimensions $\ell = 2\pi/k$ which do not exceed the separation distance $\delta = |\mathbf{r}_1 - \mathbf{r}_2|$. Assuming isotropy holds, the field of first differences can then be defined as (Monin and Yaglom, 1971)

$$N'(\delta) = N'(\mathbf{r}+\delta) - N'(\mathbf{r}) \qquad (4.24)$$

and local variations in refractivity can be described in terms of the structure function (Monin and Yaglom, 1971)

$$D_N(\delta) = E[\, N'(\delta)^2] \qquad (4.25)$$

Roughly speaking $D_N(\delta)$ is a covariance which characterizes the range of refractivity variation arising from those irregularities with dimensions less than or equivalent to δ. Such a field is said to be locally homogeneous or homogeneous in increments (VanMarcke, 1984). A principal result of the equilibrium theory of locally homogeneous turbulence is that the structure function and power spectrum obey relationships of the form (Monin and Yaglom, 1975)

$$D_N(\delta) = C_N^2\, \delta^{2/3} \qquad (4.26)$$

$$S_N(k) \equiv C_N^2\, k^{-5/3} \qquad (4.27)$$

That is, the intensity of the refractivity fluctuations decrease as the 5/3 power of their size. C_N^2 is termed the structure constant and is essentially a measure of the variance of the fluctuations with scale lengths less than or equivalent to the separation distance δ.

In actuality the slope of the refractivity spectrum often varies considerably over its total range. Crain et al. (1953), Birnbaum and Bussey (1955), Planck (1959), Gossard (1960A,1960B), Straiton et al. (1962), Bull (1966), Bean et al. (1967), and Lane and Paltridge (1968) have found that the 5/3 law holds reasonably well under well-mixed adiabatic conditions at all altitudes and for scale lengths of up to a few tens of metres. However these same studies indicate a considerable variation in the slope of the spectrum at smaller wavenumbers

(larger scale lengths) depending upon altitude, the source of turbulent energy, and the degree of atmospheric stratification. A typical example of the degree of variation as a function of altitude under well-mixed conditions is depicted in Figure 2 as excerpted from Gossard (1960B). As a general rule fluctuation intensity decreases and scale size increases as a function of altitude within a well-mixed adiabatic atmosphere. A typical range of variation is of the order of a 5.0-0.5 N units over scale lengths of 10-200 metres depending upon height. Most of this variation arises from humidity fluctuations. However, the modulus of thespectral slope is frequently much larger than 5/3 for scale lengths greater than a few tens of metres near the surface and in or near regions of extreme temperature lapse (thermally unstable layers), indicating large scale irregularities of great intensity often exist within these regions. Conversely, fluctuation intensity has been found to decrease sharply within thermally stable inversion layers. Consequently the slope of the spectrum shows considerable variability at small wavenumber values in a manner closely linked with atmospheric stability.

There are two commonly used approaches to modelling the variability of the small wavenumber end of the spectrum based upon different models of turbulent behaviour. The turbulent mixing approach assumes that mechanical mixing feeds fluctuations into the spectrum over an input range of eddy sizes $k<k_0$. The subsequent redistribution of energy toward higher wavenumbers is then assumed to proceed by the breakup of eddies due to convective mixing. This approach is outlined in Silverman (1956) who proposes a spectrum of the form

$$S(k) = \sigma'^2_{N'} (k_0^{2/3}/k^{11/3}) \qquad k > k_0 \tag{4.28}$$

wherein

$$\sigma'^2_{N'} = k_0^{-2} (d\bar{N}/dh)^2 \tag{4.29}$$

Alternatively, the mixing in gradient approach considers only the breakup of established refractivity gradients and layers by the action of convection. No external sources are considered. As described by Villars and Weisskopf (1955) and Wheelon (1957B) this approach suggests a spectrum of the form

$$S(k) = (d\bar{N}/dh)^2 k^{-5} \qquad k > k_0 \tag{4.30}$$

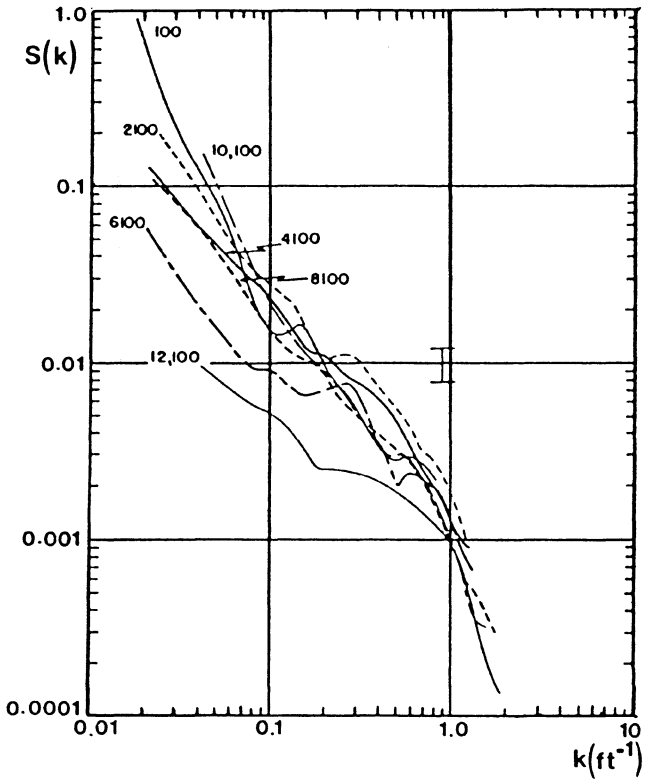

Figure 4.2

Typical Refractivity Spectra Vs Altitude

(Gossard ,1960)

Both of these forms relate the intensity of refractivity fluctuation to the mean refractivity gradient, an intuitively appealing result and one which has been verified in a general way by correlating observed field strength behaviour with median gradients on trans-horizon troposcatter paths (Bean and Meaney, 1955; Dennis, 1962; Boitias and Battesti, 1983). Consequently most methods of predicting troposcatter field strength are based in part upon this parameter (Norton et al., 1955A; Rice et al., 1966; Larson, 1968).

4.3) Scatter Propagation.

Very extensive literature is available on the theory of trans-horizon troposcatter propagation. In particular, detailed treatments of the problem are presented in Chernov (1960), Tatarskii (1961), and Monin and Yaglom (1971). In addition, a variety of technical papers dealing with various aspects of trans-horizon troposcatter propagation have been published over the past thirty years. The reader's attention is drawn to volume 43(10) of the Proceedings of the Institute of Radio Engineers (1955), and to the Institute of Electrical Engineers (UK) Conference Publication 48 (1968), both of which deal specifically with troposcatter phenomena and provide a wealth of information. Accounts of a more basic and descriptive nature can be found in Matthews (1965), Picquenard (1974), and Hall (1979). In the following we shall similarly restrict our attention to a brief description, drawing directly upon the more detailed treatments in the references cited.

We shall consider the troposphere as a nonconducting medium ($\sigma=0$) whose relative permeability μ_r is unity and whose relative permittivity $\epsilon_r=n^2$ is composed of a deterministic and stochastic component such that

$$\epsilon_r(\mathbf{r},t) = \overline{\epsilon_r}(\mathbf{r},t) + \epsilon'_r(\mathbf{r},t) \qquad (4.31)$$

where $\epsilon'_r(\mathbf{r},t) = n^2(\mathbf{r},t) - \overline{n^2}(\mathbf{r},t)$ such that the approximation (Wheelon, 1957)

$$\epsilon'_r \approx 2n' = 2N'10^6 \qquad (4.32)$$

provides the necessary connection with the previous use of refractive index spectra. The above approximation is exact for random fluctuations in refractive index of the order of 30 ppm or less.

As before, the term $\overline{\epsilon_r}(\mathbf{r},t)$ is treated as a slowly varying deterministic function of height, and the term $\epsilon'_r(\mathbf{r},t)$ is described in terms of a stationary, gaussian, homogeneous, and isotropic random field having zero mean and constant variance. The description of electromagnetic wave propagation in such a medium rests upon Maxwell's equations and the constitutive relations which may be expressed for this purpose in the form (Corson and Lorrain, 1970)

$$\nabla\cdot\mathbf{D} = 0 \tag{4.33}$$

$$\nabla\cdot\mathbf{B} = 0 \tag{4.34}$$

$$\nabla\times\mathbf{E} = -\partial\mathbf{B}/\partial t \tag{4.35}$$

$$\nabla\times\mathbf{H} = \partial\mathbf{D}/\partial t \tag{4.36}$$

$$\mathbf{D} = \epsilon(\mathbf{r},t)\mathbf{E} \tag{4.37}$$

$$\mathbf{B} = \mu_0\mathbf{H} \tag{4.38}$$

In the above system **E** is the electric field intensity, **D** is the electric displacement field, **B** is the magnetic induction field, **H** is the magnetic field intensity, and $\epsilon=\epsilon_0\epsilon_r$ is the permittivity of the medium. Eliminating the magnetic field components from the curl equations 35 and 36 yields the relation (Wheelon, 1955)

$$\nabla^2\mathbf{E} - \frac{1}{c^2}\epsilon(\mathbf{r},t)\frac{\partial^2\mathbf{E}}{\partial t^2} = \nabla(\nabla\cdot\mathbf{E}) \tag{4.39}$$

wherein $c=\sqrt{\mu_0\epsilon_0}$ is the speed of light in vacuo. Over most practical distances the permittivity field $\epsilon(\mathbf{r},t)$ will remain virtually constant within the time of propagation. Denoting the propagation constant by $k=\omega/c$ where ω expresses the time variation of the electric field, we obtain

$$\{\nabla^2 + k^2[\overline{\epsilon(\mathbf{r})} + \epsilon'(\mathbf{r})]\}\mathbf{E} = \nabla(\nabla\cdot\mathbf{E}) \tag{4.40}$$

The effect of the turbulent refractive index irregularities are contained in the term $k^2[\epsilon'(\mathbf{r})]$. Wheelon (1955) has shown that the divergence term on the right hand side can be safely neglected at radio frequencies such that we obtain an approximate wave equation of the form (Wheelon, 1955)

$$\{\nabla^2 + k^2[\overline{\epsilon(\mathbf{r})} + \epsilon'(\mathbf{r})]\}\mathbf{E} = 0 \tag{4.41}$$

Equation 41 is a perturbation equation which cannot be solved exactly since $\epsilon'(\mathbf{r})$ is an unknown function of position. The Born approximation is widely used to approximate the solution in the absence of multiple scattering, that is, under the assumption that each element of the incident wave is scattered only once. Bugnolo (1960) has shown this to be a reasonable assumption at radio frequencies over distances of several hundred kilometres. To achieve a solution the wave equation is re-cast in the perturbation form (Wheelon, 1955)

$$\{\nabla^2 + k^2\overline{\epsilon(\mathbf{r})}\}E = -k^2\epsilon'(\mathbf{r})E \tag{4.42}$$

which is then solved in an iterative fashion by expansion in terms of Neumann series (Jones,1979). The first iteration in the series is the Born approximation corresponding to single scattering. The total field $E_T(\mathbf{r})$ is the sum of an unperturbed and scattered field and is given by (Wheelon, 1955; Tatarskii, 1961)

$$E_T(\mathbf{r}) = E_0 e^{-i\mathbf{k}_i\cdot\mathbf{r}} - k^2\int_{v'} G(\mathbf{r},\mathbf{r}')\epsilon'(\mathbf{r}')E_0 e^{-i\mathbf{k}_i\cdot\mathbf{r}'}\, d^3\mathbf{r}' \tag{4.43}$$

The first term on the right represents the unperturbed field. The second term is the scattered field arising from the irregularities in the volume element $dv'=d^3\mathbf{r}'=(dr'_x dr'_y dr'_z)$. These can be interpreted as an array of elementary dipoles of dimension $r'=|\mathbf{r}'|$ polarized by the incident field and reradiating field energy in all directions. We choose the origin within the volume v'. Then $G(\mathbf{r},\mathbf{r}')$ is the Green's function (Jones, 1979)

$$G(\mathbf{r},\mathbf{r}') = \frac{-1}{4\pi}\left[\frac{e^{ik|\mathbf{r}-\mathbf{r}'|}}{|\mathbf{r}-\mathbf{r}'|}\right] \tag{4.44}$$

A typical scattering geometry is depicted in Figure 3. For trans-horizon scattering the unperturbed component is absent due to earth screening and the entire field arises from the scattering term. We assume that the scattering element is midway between the transmitting and receiving stations such that the distances $r_i=|\mathbf{r}_i|$ and $r_s=|\mathbf{r}_s|$ are approximately equal and large in comparison with the dimensions r' of the scattering element . It can then be assumed that the incident wave $E_i(\mathbf{r}_i)=E_0 e^{-i\mathbf{k}_i\cdot\mathbf{r}_i}$ is a uniform plane wave having constant amplitude over the volume. This corresponds to the Fraunhofer approximation for diffraction of a plane incident wave

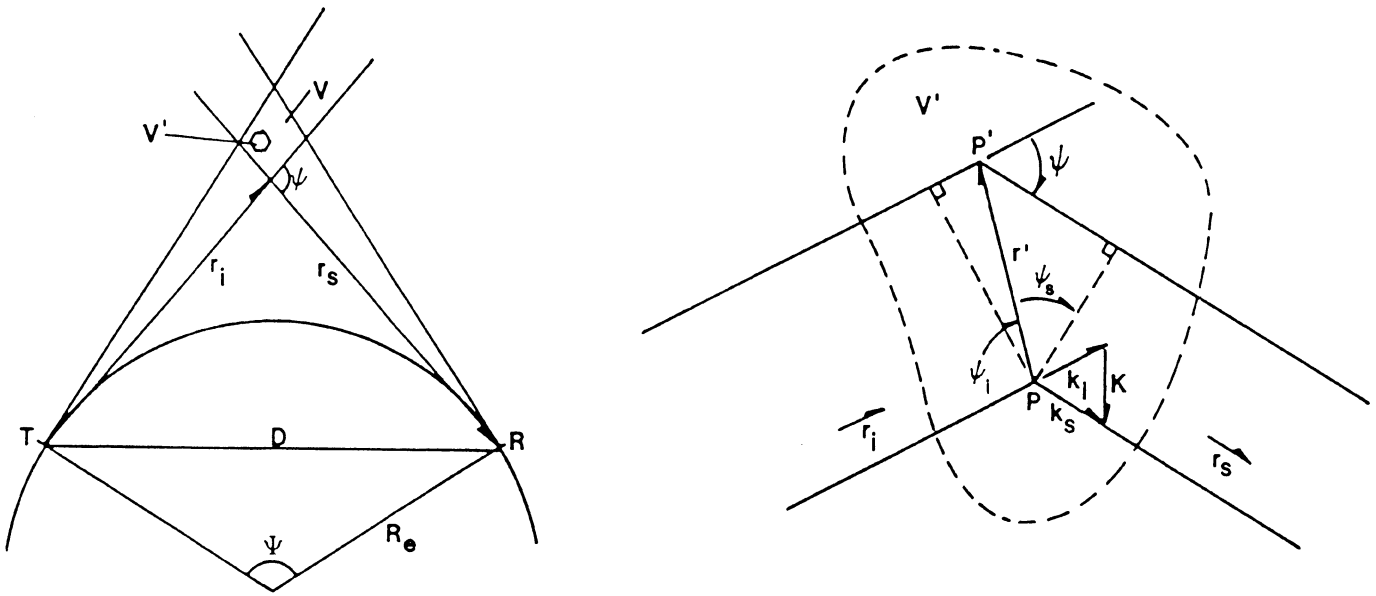

Figure 4.3

Geometry for Scatter Propagation Beyond the Horizon

(Picquenard, 1974)

by a distant aperture (Born and Wolf, 1965; Elmore and Heald, 1969). It can be shown that under such conditions the Green's function may take the approximate form (Wheelon, 1955; Tatarskii, 1961)

$$G(\mathbf{r},\mathbf{r}') \approx \frac{-1}{4\pi}\left[\frac{e^{ik|\mathbf{r}_s|}}{|\mathbf{r}_s|}\cdot e^{-i\mathbf{k}_s\cdot\mathbf{r}'}\right] \tag{4.45}$$

and that the expression for the scattered wave then becomes (Villars and Weisskopf, 1954; Wheelon, 1955; Tatarskii, 1961)

$$E_s(\mathbf{r}_s) = \frac{E_0\, e^{ikr_s}}{4\pi r_s}\, k^2 \int_{v'} \epsilon'(\mathbf{r}')\, e^{i\mathbf{K}\cdot\mathbf{r}'}\, d^3\mathbf{r}' \tag{4.46}$$

wherein $\mathbf{K}=\mathbf{k}_s-\mathbf{k}_i$ is termed the scattering difference vector. Since $\epsilon'(\mathbf{r}')$ is a statistical quantity so will be $E_s(\mathbf{r}_s)$. From the geometry of Figure 3 we note that the phase difference $\Delta\phi$ generated between two points P and P' separated by the scattering element dimension r' is given by

$$\Delta\phi = -\mathbf{k}_i\cdot\mathbf{r}' + \mathbf{k}_s\cdot\mathbf{r}' = \mathbf{K}\cdot\mathbf{r}' \tag{4.47}$$

By assuming $|\mathbf{k}_i|\approx|\mathbf{k}_s|=k$ and $\psi_i\approx\psi_s$, and by setting the scattering angle $\psi=\psi_i+\psi_s$ we obtain

$$|\mathbf{K}| = 2k\sin(\psi/2) \tag{4.48}$$

This is one form of the Bragg condition of crystal diffraction theory. It expresses the necessary spacing required for minimum interference of adjacent planes of diffracting elements in three dimensional gratings (Born and Wolf, 1965; Elmore and Heald, 1969).

The scattering cross section $\alpha(\psi,k)$ per unit volume, per unit incident power density, and per unit solid angle is defined by Villars and Weisskopf (1954) as the expected value

$$\alpha(\psi,k) = \frac{r_s^2}{V}\, E\left[\frac{|E_s|^2}{|E_i|^2}\right] \tag{4.49}$$

wherein the incident wave $E_i(r_i) = E_0 e^{-ikr_i}$. Combining this with expression 46 for the scattered wave and substituting into equation 49 yields

$$\alpha(\psi,k) = \frac{k^4}{16\pi^2}\int_{v_1'}\int_{v_2'} E[\epsilon'(\mathbf{r}_1)\epsilon'(\mathbf{r}_2)]\, e^{i\mathbf{K}\cdot\mathbf{r}_1}\, e^{i\mathbf{K}\cdot\mathbf{r}_2}\, d^3\mathbf{r}_1\, d^3\mathbf{r}_2 \tag{4.50}$$

By setting $\boldsymbol{\delta}=\mathbf{r}_2-\mathbf{r}_1$ and employing the spatial autocovariance function

$$C(\boldsymbol{\delta}) = E[\epsilon'(\mathbf{r}_1)\epsilon'(\mathbf{r}_2)] \tag{4.51}$$

we obtain the scattering cross section in terms of the spatial covariance function $C(\boldsymbol{\delta})$ as (Wheelon, 1959)

$$\alpha(\psi, k) = \frac{k^4}{16\pi^2} \int_V C(\boldsymbol{\delta})\, e^{i\mathbf{K}\cdot\boldsymbol{\delta}}\, d_3\boldsymbol{\delta} \tag{4.52}$$

Applying the Weiner-Kinchine relations gives the cross section in terms of the spatial spectrum of irregularities as (Wheelon, 1959)

$$\alpha(\psi, k) = \frac{k^4}{16\pi^2}\, S(|\mathbf{K}|) \tag{4.53}$$

From equation 53 we note that the scattering process acts like a narrow band filter on the spectrum of Figure 1 emphasizing the wavenumber $K=2k\sin(\psi/2)$. Thus only a small band of spectral components contribute to the scattering for a given frequency and angle of incidence. These irregularities form a spatial diffraction grating of fixed spacing determined by the scale of turbulence dimension ℓ where

$$\ell = 2\pi/K \approx 2\pi/k\psi = \lambda/\psi \tag{4.54}$$

For UHF frequencies in the 400-500 MHz range and scattering angles of the order of 1° the scale length of interest falls within the 30-50 metre range and therefore lies within the high wavenumber inertial band where the isotropic assumption holds reasonably well.

The scattering cross section formulation makes direct contact with the physical theories of turbulence through the spectrum of irregularities $S(K)$. It remains to integrate the cross section over the entire common volume defined by the patterns of the transmitting and receiving antennas. This leads to a general scattered power equation of the form (Wheelon, 1959)

$$\frac{P_R}{P_T} = \frac{\lambda^2}{16\pi^2} \int_V \frac{G_T G_R \alpha(\psi, k)}{D_R^2 D_T^2}\, d^3\mathbf{r} \tag{4.55}$$

wherein G_T and G_R are the antenna gains of the transmitting and receiving antennas respectively.

The tropospheric scatter mechanism described above is evidently a form of multipath propagation in which the received signal embodies a number of constituent elements which arrive

at the receiver by many slightly different and time varying electromagnetic paths. Since the electromagnetic length of each contributing wave path varies with turbulent motion, temporal phase and amplitude variations are set up by mutual phase interference at the receiver. These are known to be approximately Rayleigh distributed (Rice, 1953; Silverman, 1955) with periods inversely proportional to wavelength and ranging from one to several seconds for wavelengths of from 0.1 to 1.0 metres (Rice, 1953; Norton et al., 1955B; Vigants, 1971). The result is a characteristic second-to-second fluctuation in observed phase within the troposcatter zone, the intensity of which is directly related to changes in the degree of turbulent activity within the common volume. Consequently the most severe variations may be expected in the vicinity of weather fronts, in coastal zones due to the diurnal action of circulatory breezes, and in the presence of extreme temperature and refractivity gradients.

The phase stability characteristics of trans-horizon troposcatter links have been investigated by a variety of authors. In particular, detailed treatments of the phase correlation between two spaced antennas in terms of the exponential, Gaussian, and Bessel correlation models discussed earlier have been attempted by Rice (1953), Muchmore and Wheelon (1955), Staras (1955), Herbstreit and Thompson (1955), Wheelon (1957), Chernov (1960), Tartarskii (1961), Gjessing and Boresson (1968), and Monin and Yaglom (1971). Space diversity techniques are often employed to reduce the severity of short term phase fluctuations. The basic idea is that the signal simultaneously received at two spatially separated antenna will be incompletely correlated by an amount proportional to their separation. For the case of antennas separated in a direction normal to the transmission path the signal is assumed to be correlated over a distance roughly equivalent to the largest scale of turbulence contributing to the field. This reflects the notion that only those refractive index irregularities which are large relative to the antenna separation, or diversity distance, will contribute to the phase instability on both paths simultaneously.

In equation 54 we have defined the scale length of interest to be approximately $\ell=\lambda/\psi$. Noting from the geometry of Figure 2 that for small grazing angles $\psi\approx\sin\psi=D/R_e$ where R_e is the equivalent earth radius, we obtain for the diversity distance in the vertical

$$\Delta h_d \approx \lambda(R_e/D) \qquad (4.56)$$

The diversity distance Δh_d as defined above is independent of the form of the spatial correlation function of the refractive index irregularities and depends only upon their scale length and the glancing angle of the incident wave . Roughly speaking, the field of refractive index irregularities can be thought of as being similar to a three dimensional diffraction grating with diffraction centres spaced in planes according to the scale length ℓ defined by the Bragg condition. The diversity distance is then analgous to the spacing between the maxima and minima in the resulting diffraction patterns such that the maxima from one plane of diffraction centres falls upon the minima of its adjacent planes thus guaranteeing minimum mutual interference. For frequencies between 400 and 500 MHz and for distances of the order of 100 Km Δh_d is of the order of 50-60 wavelengths.

This simplified approach has been employed by a variety of investigators to reduce phase variation on trans-horizon circuits (Van Wamback and Ross, 1951; Gordon, 1955; Bullington et al.,1955; Crawford et al., 1959; and Chisholm et al., 1962). However, because the structure of the random field of refractive index irregularities is highly variable and as yet poorly understood no one simple correlation model can be expected to be representative of the full range of possible variations. Consequently, there is as yet poor agreement between theory and practice on this point.

A principal limitation of the eddy scattering theory outlined above is that it fails to adequately account for the scattering arising from irregularities in the low wavenumber end of the spectrum depicted in Figure 1. The larger irregularities within this region of the spectrum typically feature a flat layerlike shape with their thickness varying from a few metres to a few tens of metres in the vertical and their horizontal extent covering several hundred metres. Saxton

et al. (1964) and Hall and Comer (1970) indicate that these irregularities frequently develop from the breakup of larger inversion and ducting layers in the lower troposphere.

Numerous authors have suggested that diffuse reflection from these localized layers may contribute significantly to the energy scattered beyond the radio horizon at UHF wavelengths (Saxton, 1951; Friis et al., 1957; Du Castel et al., 1962; Beckmann and Spizzichino, 1963; Matthews and Dufu, 1968; Fehlhaber, 1968). This conclusion is supported by several refractometer and beam swinging experiments which indicate that large and intense refractive index irregularities are often concentrated in shallow vertical layers rather than being uniformly distributed throughout the scattering volume (Waterman, 1958; Crawford et al. 1959; Chisholm et al., 1962; Saxton et al., 1964; Lane and Paltridge, 1968; Barrow, 1968).

In scattering by layer reflection the most important parameters to be considered are the number of layers existing within the common volume, their dimensions relative to those of the first Fresnel zone, and their surface roughness relative to a wavelength. For reflection by a single layer it is usually assumed that the most important scattering region is enclosed within the first Fresnel zone. An understanding of this concept can be gained through Figure 4. We assume a reflecting layer of large extent lies midway between two antennas separated by the chord distance d. The beam patterns of the two antennas illuminate an elliptical region on the reflecting surface oriented such that its semi-major axis lies in the direction of propagation. The transmission path defined by the axis of the beam patterns passes through the origin O and is given by the length $r_t=r_i+r_s$. Moving radially outward on the surface from the origin introduces an increase in the total transmission path. The locii of points for which the path length increases by $\delta r=n\lambda/2$ where n is an integer value, defines a family of concentric ellipses upon the reflecting surface. The area of the fresnel zone defined by any two such neighbouring ellipses is a constant and the contribution of each successive zone to the total power redirected is a slowly decreasing function of distance from the origin. Since succesive zones result in contributions which are on average in phase opposition, these tend to cancel out leaving a total reflected power roughly equivalent to half that originating within the first Fresnel zone. For the geometry depicted in Figure 4 Beckmann

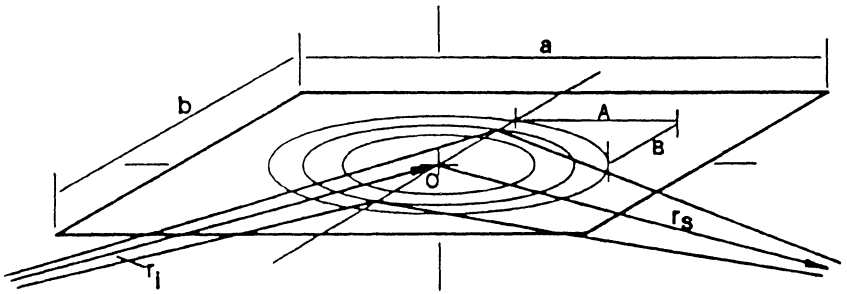

Fresnel Zones on a Reflecting Layer

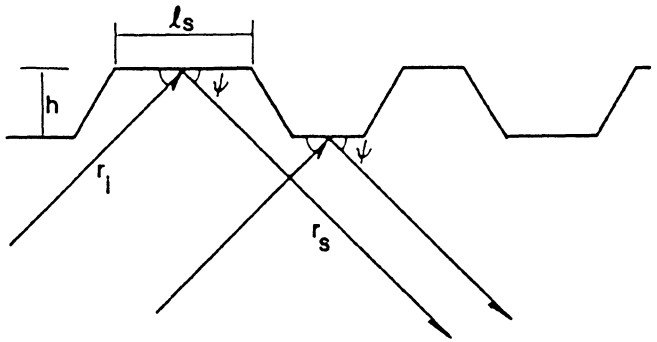

Rayleigh's Criterion

Figure 4.4

and Spizzichino (1963) have shown that the dimensions of the first zone are approximately given by

$$A = \sqrt{\lambda d} / \sin\psi \tag{4.57}$$

in the sense of propagation and by

$$B = \sqrt{\lambda d} \tag{4.58}$$

in the transverse direction.

Given a smooth reflecting layer with dimensions exceeding those of first Fresnel zone the ratio of the received to the transmitted power is of the form (Friis et al., 1957)

$$\frac{P_r}{P_t} = \frac{C}{4\pi r_t^2} R^2 \alpha(\psi) \tag{4.59}$$

wherein C is a constant depending upon antenna gain and wavelength. The first term is essentially the free space power loss due to spherical spreading. The second involves the square of the fresnel reflection coefficient of the layer determined as discussed in chapter 3. In the third $\alpha(\psi)$ is the scattering cross-section coefficient of the layer and is defined as the ratio of the effective area of the layer to the effective area of the first Fresnel zone as seen from the transmitter. From the geometry of Figure 4 we have

$$\alpha(\psi) = \frac{ab \sin\psi}{\pi\lambda d} \tag{4.60}$$

Both the Fresnel reflection coefficient R and the scattering coefficient α are dependant upon the angle of incidence ψ. If there are N contributing layers within the common volume the total redirected power is given by the integral (Friis et al., 1957)

$$\frac{P_r}{P_t} = \frac{CN^2}{4\pi r_t^2} \int_V R^2 \alpha \, d^3r' \tag{4.61}$$

wherein it is assumed that the size and number of reflecting layers remain uniform throughout the common volume.

The reflection coefficient employed above must be modified to account for the roughness of the surface. A surface is said to be smooth and capable of supporting specular reflection if its

irregularities produce phase variations in neighbouring rays which are small in a wavelength. This is the essence of Rayleigh's criterion. Considering the geometry depicted in Figure 4 the phase difference between two neighbouring rays reflected from an irregular surface is given by

$$\Delta\phi = \frac{4\pi h \sin\psi}{\lambda} \qquad (4.62)$$

which obviously goes to zero only for small values of h/λ or small angles of incidence ψ.

In modelling scattering by rough surfaces the common approach is to approximate the surface by an array of discrete points which vary in height from the specular plane in a random manner according to some assumed statistical distribution. Random field statistics can then again be used to describe the spatial correlation between neighbouring points on the surface in much the same manner as developed above for the eddy theory of scattering. A detailed examination of the form of the reflection coefficient for such random rough surfaces obeying a variety of statistical distributions is given by Beckmann and Spizzichino (1963).

Relative motion of the contributing layers produces phase fluctuation effects similar to those predicted by the eddy theories. Given that the troposphere typically features a broad range or irregularities it can generally be assumed that both modes of troposcatter propagation contribute to varying degrees to the trans-horizon field on a more-or-less continual basis. Certainly, both interpretations are required to adequately account for observed behaviour.

5. ASSESSMENT OF TROPOSPHERIC EFFECTS IN ATLANTIC CANADIAN WATERS.

For the most part, radio positioning systems infer position from range, range difference, and range rate measurements based upon the transit time of propagation of electromagnetic radiation. Consequently, assumptions concerning the velocity and path of the advancing wavefront must be made in order to scale time interval measurements into geometric distances. These in turn require assumptions concerning the structure of the refractivity field existing along the transmission path during the time of propagation.

A variety of natural phenomena contribute to variations in refractive index. The principal variational influences may be considered as arising from climate, season, earth rotation, local topography and meteorology, and atmospheric turbulence. In treating these effects the refractive index is best modelled as a random function of time and space. The mean refractivity structure is described in terms of an empirically determined standard atmospheric model, which is assumed to vary slowly in time and space as a function of climate, season, and time of day. On average, the atmosphere is assumed to be well mixed, quasi-static, and horizontally homogeneous such that the refractive index varies strictly as a function of altitude.

Stochastic variations arise from the random disturbing influences of topography, weather systems, and turbulence. These are of a scale and complexity that presently defy conventional modelling approaches, and represent a fundamental limitation in the precision with which the refractivity field may be described. Consequently, geodetic research has in recent years focused upon the development of models based upon micrometeorological and turbulence theory considerations, which attempt to relate in statistical terms the amplitude, scale, and period of random fluctuation to parameters describing the degree of thermal stability and intensity of turbulence in the lower atmosphere. A concise review of recent advances in this area may be found in Brunner (1984). While these provide the basis for a better qualitative understanding of the complex behaviour of random fluctuations in refractivity, an extended period of empirical investigation is likely to be required before the development of practically applicable and effective models can be fully realized.

Range measurement errors arise as a result of the temporal and spatial changes that occur in the refractivity structure of the real atmosphere relative to that of the adopted standard. In addition, the methods of geometric optics commonly employed to describe ray propagation in the standard atmosphere are of limited validity when applied to mode propagation and scattering problems. Two principal categories of error result:

1.) Phaselag errors, which arise as a result of uncertainties in the effective speed and curvature of the propagating wave, and

2.) Multipath errors, which arise as a result of additional paths arising from the influences of ducting, reflection, and scattering in the lower atmosphere.

The overall structure of the refractivity field will vary as a function of climate. The effect of climate as determined by Bean et al (1966) is summarized in Figures 1 and 2 based upon a five year study of daily surface and upper air meteorological observations at 268 globally distributed stations. Figure 1 depicts the global distribution of the annual mean value of surface refractivity reduced to sea level. The principal effect of climate is to produce a latitude dependent variation in surface refractivity of the order of 80 N units, ranging from a low of the order of 300 N units in

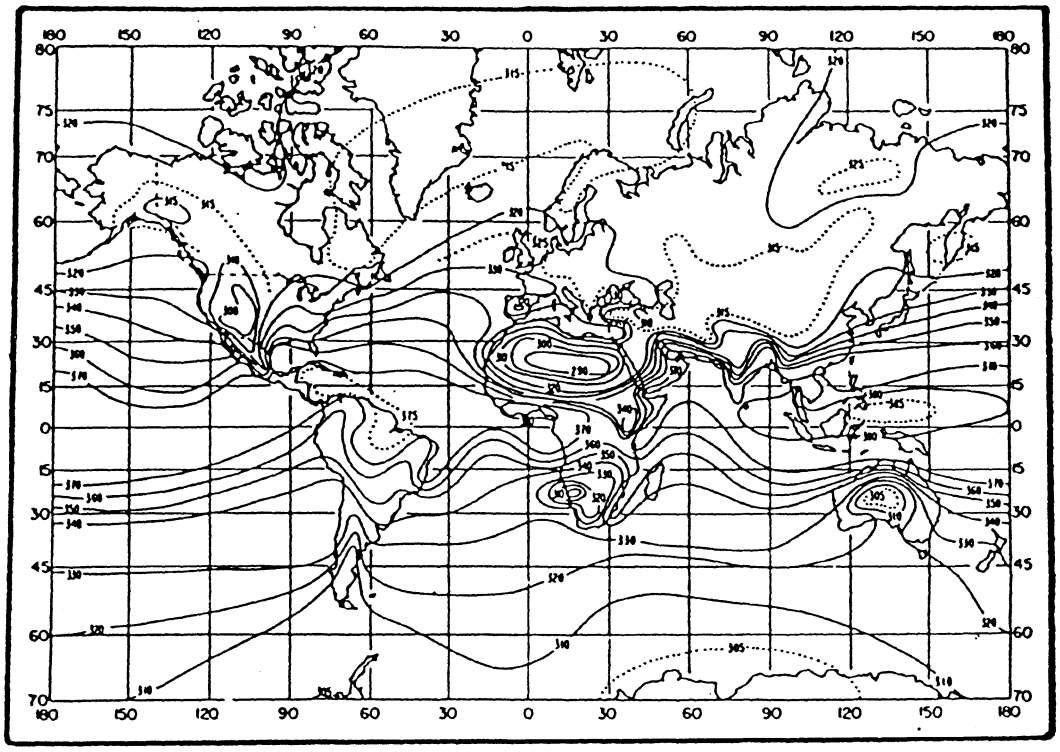

FIGURE 5.1

GLOBAL DISTRIBUTION OF ANNUAL MEAN SEA LEVEL REFRACTIVITY

(Bean, 1966)

polar regions to a high of 380 N units along the equator. Figure 2 presents a similar representation of annual mean gradient data based upon the same study. A latitude dependence is again evident, with the lapse rate ranging from a low of the order of 40 N/Km in polar regions to 60 N/Km along the equator. In both cases significant longitude dependent variations are limited to low latitudes, where important differences in water vapour concentration in the lower atmosphere frequently occur between arid inland regions and humid coastal areas.

From the above study, a surface refractivity of the order of 325 N units and a refractivity gradient of the order of 50 N/Km can be used to approximate regional standard atmospheric refractivity conditions in Atlantic Canadian waters. These values are however based upon a relatively sparse sampling of information at widely distributed stations. Considering the diversity of seasonal, weather, and topographic conditions that exist in the region, significant local variations from these standard values can therefore be expected.

The most critical phenomena to be considered are those which produce significant irregularities in refractive index relative to the scale and period of survey. Consequently, a knowledge of the magnitude, scale, period, and characteristic influence of each contributing constituent is necessary to evaluate model precision. In UHF radio positioning applications the survey area may extend 200 kilometres offshore and encompass several hundreds of kilometres of coastline. Typically, simultaneous range measurements are made to three or more shore-based reference stations, and significantly different trans-horizon transmission paths may be involved. The period of survey may extend from several days to a year or more.

Assuming a median range of the order of 100 kilometres, the 1-2 metre instrumental resolution typical in UHF radio positioning systems translates into a level of significant variation of the order of 10-20 ppm. At this level of significance, the principal spatial variations of interest can be considered as arising from topography and weather systems, while the principal temporal variations arise from seasonal, diurnal, weather, and turbulence effects.

At best, meteorological observations are limited by the practical considerations of time, cost, and accessibility to surface observations of temperature, pressure, and humidity at the

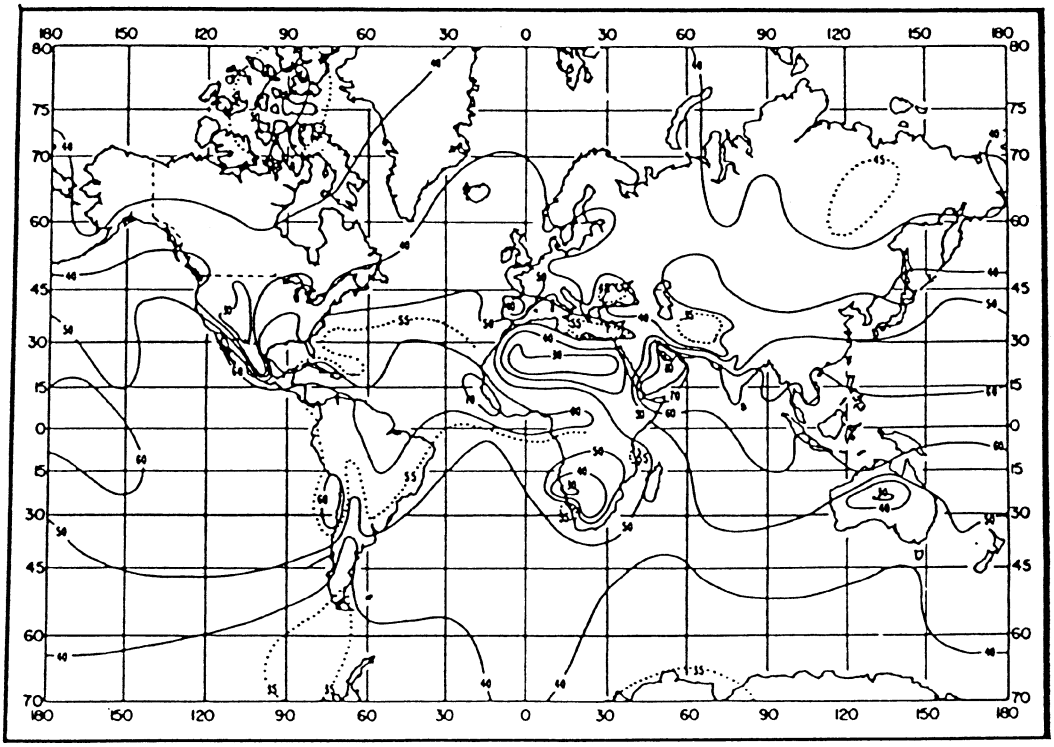

Figure 5.2

Global Distribution of Annual Mean Refractivity Gradient to 1 Km.

(Bean et al. 1966)

mobile receiver and perhaps at a mid-station shore point. More often, refractivity effects are determined directly as a by-product of baseline range calibration procedures performed at fixed locations in the vicinity of the survey area. A discussion of these procedures is given by Cooper (1979), Riemersma (1979), and Van Kujik (1984). This latter technique has a three-fold advantage in that:

1.) A direct indication of the integrated refractivity and effective propagation velocity along the transmission path can be obtained,

2.) The level of measurement instability arising from scattering can be more precisely determined and related to prevailing meteorological conditions, and

3.) The potential for real-time differential corrections based upon continuous baseline monitoring exists.

The disadvantages are that calibration measurements are more time consuming and costly than meteorological observations. In addition, they frequently involve measurements over coastal baselines where conditions may not be representative of those found further offshore, and the direct effects of refractivity may be masked or misinterpreted by the influence of instrumental, antenna, or terrain related effects. As a result tropospheric refractivity is generally poorly modelled in radio positioning and represents a fundamental accuracy limitation.

In the remaining sections of this chapter we present an assessment of refractivity variation for a typical coastal region in Atlantic Canada (Figure 3) and examine the significance of these variations given the commonly employed standard atmosphere refraction models described in Chapter 2.

5.1) Analysis of Radio Meteorological Data.

In this section we present an analysis of the principal sources of refractivity variation in Atlantic Canadian waters. For convenience, these results are presented in order of decreasing scale of influence, and surface and gradient effects are considered separately.

For this purpose surface and upper air meteorological data were obtained from the Canadian Atmospheric Environment Service (CAES) for three weather stations located along the southern coast of Nova Scotia from Halifax to Yarmouth as depicted in Figure 3. These were selected to provide coverage for UHF range measurements collected on three trans-horizon baselines monitored in cooperation with the Canadian Hydrographic Service (CHS) over a one month period in the winter of 1982/1983. Details of the CHS monitoring program have been described previously in Janes et al. (1985A, 1985B) and will be reviewed in section 2.

TABLE 5.1

Summary of Meteorological Observing Stations

Station	N.Lat.	W.Long.	Altitude	Designation
Halifax Airport	44° 53'	63° 31'	145 m	surface
Sable Island	43° 56'	60° 02'	5 m	surface + upper air
Shelburne	43° 46'	65° 14'	28 m	surface + upper air

The location, altitude, and type of observation made at each station are summarized in Table 1. Hourly observations of surface wet and dry bulb temperature and atmospheric pressure were obtained for all three sites for the period January1, 1982 to February 1, 1983. Upper air observations of pressure, temperature and relative humidity from radiosonde ascents taken twice daily at the Shelburne and Sable Island sites over the same period were also obtained. These were then examined to determine the range of seasonal, monthly, and daily variation in surface refractivity and the refractivity gradient, the extent of layering in the lower atmosphere, and the influence of weather systems and topography on the homogeneity of the refractivity field over the test area.

Hourly surface refractivity data are summarized in Appendix II. Tables II.1 to II.9 present a monthly statistical summary of the hourly variations in surface refractivity and its components observed at the Shelburne, Halifax Airport, and Sable Island sites. In addition, Figures II.1 to

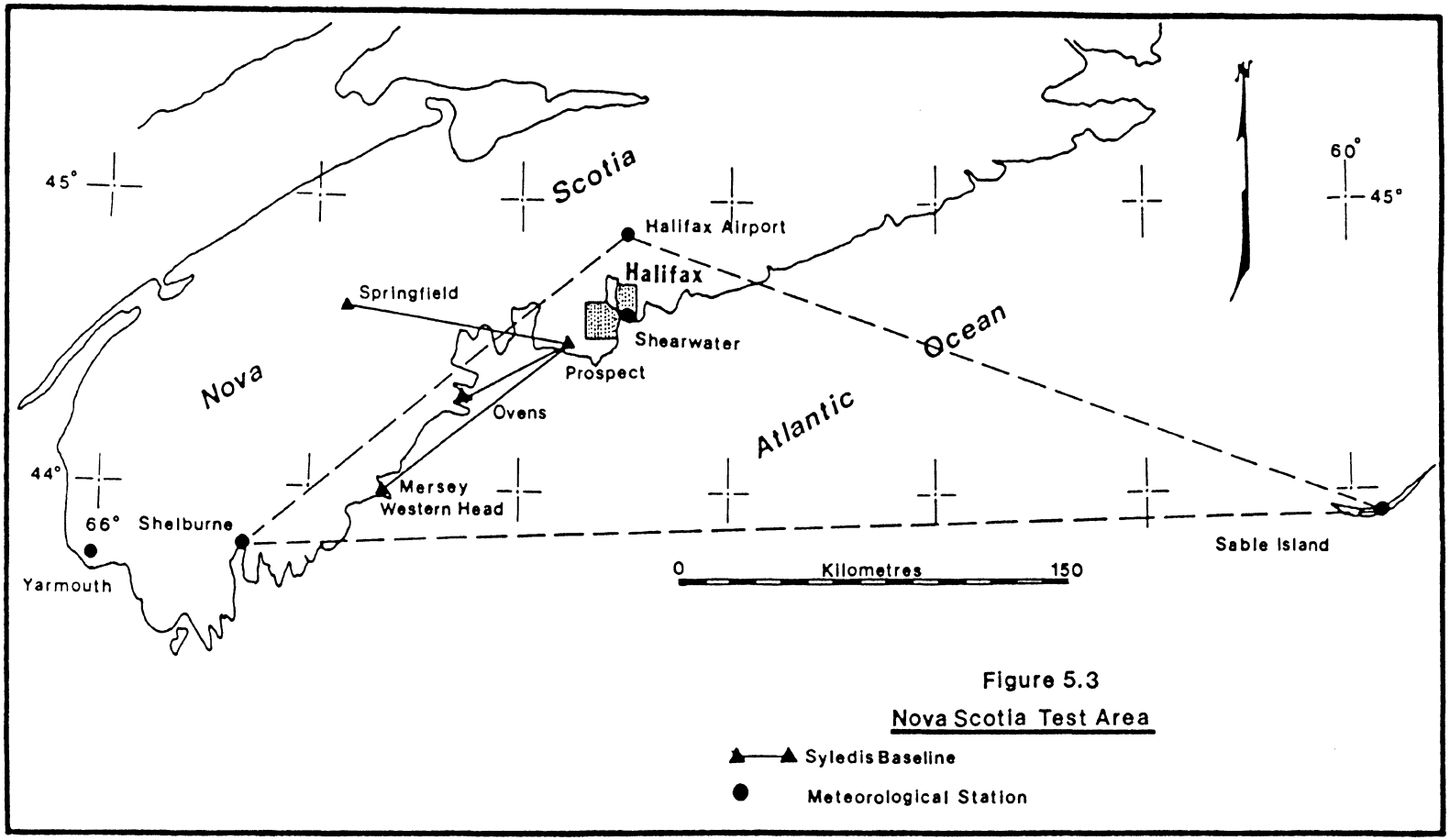

Figure 5.3

Nova Scotia Test Area

II.24 depict the hourly variation in surface meteorology and refractivity at each station for the four seasonally representative months of January, April, July, and October, 1982. Surface refractivity values were computed on the basis of the Goff-Gratch water vapour and Smith-Weintraub refractivity formulae given in Chapter 2. Temperature values have a quoted accuracy of 0.1 °C, atmospheric pressure of 0.1 mb, and water vapour pressure of 1 mb, yielding an estimated accuracy for the corresponding refractivity values of the order of 2-3 N units.

A seasonal variation in monthly mean surface refractivity of the order of 30-40 N units peak to peak is clearly evident in the tabulated data. The RMS spread associated with these monthly mean values varies from a low of the order of 5 N units in winter, to a high of 10-15 N units in summer. Moreover, the maximum range of monthly variation increases from a low of 40-50 N units to as high as 70-80 N units winter to summer. Maximum daily variations in the dry component of refractivity are found in the winter months when temperature and pressure variability is greatest, and reach as high as 40-50 N units. Conversely, the largest daily variations in the wet component of refractivity occur in summer due to the predominant influence of water vapour variability. These reach as high as 70-80 N units.

The principal sources of day-to-day variation in surface refractivity arise due to the combined effects of earth rotation and weather disturbances. The effect of earth rotation is most apparent in the summer months, when a diurnal cycle in surface refractivity is clearly evident at all three stations and arises as a result of strong daily variations in surface temperature and water vapour content. The range of diurnal variation is roughly of the order of 15-20 N units during the summer months, 5-10 N units in the spring and autumn, and barely perceptible in winter. Weather system influences are most clearly apparent in the winter months when the effects of surface heating are smallest. They are characterized by apparently random and abrupt changes in surface temperature, pressure, and water vapour values over relatively short periods of time. Variations of the order of 20-40 N units or more over a period of one to two days appear to be fairly commonplace at all times of the year, with the largest variations occurring in summer months.

The degree to which regional observations of surface meteorology provide a valid indication of these changes over an extended survey area ultimately depends upon the horizontal homogeneity of the refractivity field. Tables II.10 to II.12 summarize by month the hourly correlation in surface refractivity and its components at the Shelburne, Halifax Airport, and Sable Island sites. Given approximately 700 hourly values per month, a statistically significant degree of correlation exists at the 95% confidence level for values of the correlation coefficient exceeding 0.08 (Crow and Davis, 1978). Correlation coefficients for the surface refractivity of the order of 0.7-0.8 appear typical, with occasional excursions as high as 0.95 and as low as 0.45.

As might be expected, correlations are generally lowest in the summer months due principally to increased wet component variability. The Shelburne and Halifax sites, separated by 190 Km, show the highest degree of correlation, followed by Shelburne and Sable Island (435 Km), and Halifax and Sable Island (305 Km). This latter level of agreement may be understood when one considers that Halifax Airport is some 20 Km inland, while Sable Island is approximately 280 Km offshore. As a result, considerable differences in local surface conditions can be expected.

Despite the high degree of correlation existing between the stations, fairly large differences in simultaneously recorded hourly values were found. These are also listed according to month in Tables II.10 to II.12. The maximum regional discrepancies again occur during the summer months, and reach as high as 40 N units for the Shelburne-Halifax pairing, and 60 N units when either of these stations is compared to the Sable Island site.

Daily upper air refractivity data for the Shelburne and Sable Island sites are presented in Appendix III. Tables III.1 and III.2 present a statistical summary of daily variations in the mean refractivity lapse determined by linear least squares fit to twice daily radiosonde ascents. Ascents were rejected whenever fewer than four soundings were taken over the first tropospheric kilometre, or whenever a gap greater than 500 metres existed between consecutive soundings. Typically 40-60 acceptable ascents were available each month. The monthly mean value of the refractivity lapse at both stations ranges from 35 N/Km in February to 50-55 N/Km in August.

The standard deviations associated with these monthly mean values similarly increases from the 5-10 N/km level in winter to the 10-15 N/Km level in summer.

Figures III.1 to III.8 depict the daily variation in the mean refractivity lapse and its correlation with surface refractivity for the four seasonally representative months at both stations. The maximum daily variation in refractivity lapse increases from 30 N/Km during winter months to 70-80 N/Km in summer. Moreover, daily variations in lapse rate are generally poorly correlated with surface refractivity values. Given 40-60 ascents each month a statistically significant correlation exists at the 95% confidence level for values of the correlation coefficient exceeding 0.31 (Crow and Davis, 1978). In both cases, the monthly value of the correlation coefficient typically ranged from 0.10 to 0.35, with only occasional excursions above this level. In addition, the degree of correlation between the two stations was typically of the order of 0.1-0.3 .

Tables III.3 to III.6 summarize the extent of layering encountered in the refractivity profile at the Shelburne and Sable Island sites. The quoted accuracy of the radiosonde observations is of the order of 0.1 °C for temperature, 1 mb for pressure, and 3% for relative humidity, yielding an estimated accuracy for the refractivity at each reported level of the order of 5 N units. However, potential sources of error in reported data arise from improper initialization of the sonde at the surface, and from lag in the humidity sensors. These effects are discussed more fully by Helvey (1983). Initialization errors give the appearance of strong surface based gradients, whereas sensor lag tends to smooth the profile and mask extreme gradients at greater elevations. Consequently, some caution must be used in interpreting the data. However, a general indication of the linearity of the profile can be obtained. Some measure of reliability is indicated by the fact that the figures quoted agree within a few percentage points with those of a similar three year study of gradients at the Sable Island site reported in Segal and Barrington (1977).

Fully 5-10% of the twice daily radiosonde ascents registered in the winter months contain layers whose lapse rates exceed the critical value of 150 N/Km. This value increases to 20-30% in summer. The majority of these are elevated layers with base heights ranging from 500-700

metres and thicknesses ranging over several tens of metres. Often, these would undergo considerable variation in base height and thickness over a period of a few days. The most active periods of layering appear to be related to weather disturbances, as characterized by rapid changes in surface temperature, pressure, or humidity levels over a one or two day period. As a rule, layer thickness increases in the summer months for both elevated and surface layers, while the average base height of elevated layers decreases. However, significant differences in the time of occurrence, elevation, thickness, and duration of layers were found in comparing coincident data for the Shelburne and Sable Island sites.

Figures III.9 to III.16 depict the most graphic examples of atmospheric layering recorded at the Shelburne and Sable Island stations in each of the four seasonally representative months of January, April, July, and October. In every case, layering is associated with a small temperature inversion accompanied by an abrupt decrease in water vapour pressure. Consequently, the layering influence enters primarily through the wet component profile, while the dry component profile remains predictably linear. The thickness and severity of the layerings increase markedly in the summer. The most severe layer gradient was encountered on July 14 at the Shelburne station and is depicted in figure III.11. In this case, a strong humidity lapse of the order of 20 Mb and a temperature inversion of approximately 5 °C are encountered at an altitude of 400 metres and produce a total refractivity deficit of the order of 90 N units over a height interval of 100 metres. While this may be considered an extreme case, fully 10-15% of the ascents taken during the summer months contain layers with gradients exceeding -200 N/Km.

5.2) Analysis of Range Measurement Data.

Surface and upper air meteorological data of the type examined in the previous section provide little indication of the magnitude or scale of the refractive index irregularities generated in the lower atmosphere by the action of turbulent mixing. Scattering from these irregularities has a twofold effect, in that it provides a principal source of field energy beyond the standard radio horizon at UHF wavelengths, but introduces significant short term phase instabilities into the

range measurement. These latter instabilities are a function of the degree of turbulence and extent of layering existing in the lower atmosphere, and vary according to prevailing meteorological conditions, and the influence of weather systems and topography.

To examine these effects, range measurement data were collected on three baselines located in the vicinity of Mahone Bay, Nova Scotia over a six week period during December and January 1982/1983. These observations were conducted as part of a comprehensive field evaluation of the Sercel Syledis UHF radio positioning system undertaken by the Canadian Hydrographic Service, Atlantic Region. Details of this evaluation are presented in Janes et al. (1984) and Janes et al. (1985). A further technical description of the Syledis system may be found in Nard and Laurent (1975).

The results of this phase of our investigation are summarized in Appendix IV. Table IV.1 summarizes the station locations and baseline distances defining the test network depicted in Figure 3. Reference stations were established at each of the Western Head/Mersey, Ovens, and Springfield sites and monitored at the Prospect location using a Syledis MR3 receiver. Range monitoring was performed simultaneously on all three baselines by recording observation sets of fifty range measurements taken over a two minute period once each half hour. These were then reduced to a mean value and associated standard deviation for each half hourly epoch. First order corrections for the effects of propagation speed and ray curvature were applied to the mean values as per equation 2.59, assuming an average surface refractivity value of 320 N and a standard refractivity lapse rate of 40 N/Km. Reduced values were then compared with ground truth distances computed by geodetic inverse between station coordinates, using Vincenty's inverse algorithm (Delorme, 1978), to define a mean ranging error for each half hourly epoch. Station locations were established by the CHS from existing control using conventional survey techniques and the resulting ground truth distances are estimated to be accurate to within 1-2 m.

Figures IV.1 to IV.3 depict the time history of mean ranging error and standard deviation observed on each of the four baselines over the month of January, 1983. Although these are marred by frequent gaps in coverage, a considerable difference in ranging performance is found

when the baselines are contrasted. Whereas ranging stability on the Western Head/Mersey baselines, shown here together in Figure IV.3, varies erratically between the 5m and 30 m levels, that of the Springfield and Ovens baselines remains consistantly below the 5 m level. Moreover, no significant degree of correlation was found to exist in comparing the variation in mean ranging error between baselines. In large part these differences appear related to the radio horizon distances separating the stations, and hence, to differences in the predominant mode of propagation. In effect, the elevation of the stations is such that the Ovens and Springfield baselines fall just within the standard radio horizon from Prospect, and thus within the direct and surface diffraction propagation zones, while the Western Head and Mersey baselines extend to approximately twice the standard radio horizon distance, and consequently fall within the range of troposcatter propagation.

In general, no significant correlation was found to exist in comparing the variation in mean ranging error with hourly surface refractivity values determined for the surrounding meteorological stations. However, this is not suprising when one considers that computed surface refractivity values generally varied by less than 20 ppm over the month, and hence fall within the 1-2 metre instrumental noise of the range measurements themselves, and that the nearest meteorological site was some 50 Km away. The hourly variation in surface refractivity and its components for the Shelburne station is depicted in Figure IV.4. Unfortunately, baseline endpoint measurements of surface meteorology were not observed as part of the monitoring procedure, leaving some uncertainty as to the influence of large scale refractivity variations.

However, the periods of maximum troposcatter instability do appear to closely coincide with local weather disturbances. These are indicated in Figure VI.5 which depicts the hourly variation in surface meteorology at the nearby Shelburne site. Low pressure weather fronts, characterized by a rapid drop in atmospheric pressure and accompanied by sharp increases in temperature and water vapour content, appear to produce the greatest instabilities. Enhanced layering in the lower atmosphere also appears to occur during these periods, as indicated by the layer gradient values of Figure IV.6.

5.3) Discussion of Results.

Table 2 summarizes the results of the foregoing analysis. It seems clear that the assumptions of a quasi-static, horizontally homogeneous, and vertically linear refractivity structure have little validity when considering small scale variations in the refractivity field. Earth rotation and weather influences combine to produce day-to-day variations in surface refractive index of the order of several parts in 10^5 , and contribute to a strongly layered structure in the lower atmosphere. As a result, the average refractivity lapse over the first kilometre of the troposphere is in general poorly correlated with surface refractivity. Differences in local surface conditions at coastal and offshore locations introduce spatial variations of the same order of magnitude over distances of a few hundred kilometres.

Table 5.2

Effects of the Troposphere in UHF radio Positioning

Influence	Time Scale	Space Scale	Magnitude
Seasonal	one year	-	40 ppm
Diurnal	24 hours	-	10-30 ppm
Topographic	-	200-500 Km.	50^+ ppm
Weather systems	hours to days	200-500 Km.	50+ ppm
Turbulence/Layering	seconds	50^+ Km.	50-500 ppm (RMS)
			RSS 100-500 ppm

Consequently, a high temporal and spatial sampling rate involving both surface and upper air measurements is likely to be required before these effects can be significantly reduced. Possible alternatives include the regular observation of surface and upper air meteorology at representative locations within the survey area, or the use of differential corrections based upon the continuous monitoring of range measurements over fixed baselines. In either case, further study is required to establish appropriate procedures, and to determine the extent to which these

may reduce the level of range measurement bias error introduced by small scale variability in the refractivity field.

The stability of the troposcatter propagation mechanism used in extended range UHF radio positioning is strongly influenced by the degree of turbulent activity and the extent of non-standard layering found in the lower atmosphere. RMS stability over a two minute period was found to vary from the 5-10 m level during more standard atmospheric conditions, to 30-40 m or more during periods of maximum turbulence and layering. The greatest instabilities were observed during changes in the prevailing weather conditions and appear related to enhanced scattering from anomalous refractivity layers in the lower atmosphere. While temporal averaging over periods of a few minutes does appear to improve ranging precision, significant bias errors of the order of 5-10m are still evident. These may be related to undetected variations in the average structure of the local refractivity field. Further investigation is required to determine the magnitude, statistical distribution, and temporal period of scattering under varying weather conditions, and to establish the extent to which these may be reduced through space diversity or recursive filtering techniques.

6. CONCLUSIONS AND RECOMMENDATIONS.

Herein, the effects of a non-homogeneous and time varying troposphere on the accuracy of UHF range measurement have been considered. A description of the structure of tropospheric refractivity has been presented that is at once consistent with the physical theories of micro-meteorology and atmospheric turbulence and the study of electromagnetic wave propagation in layered and random media. A detailed assessment of the nature of refractive index variability in Atlantic Canada and its influence on the accuracy of UHF radio positioning has been presented. Finally, the limitations inherent in present approaches to the modelling of tropospheric refractivity in ranging applications have been examined.

6.1) Summary of Results and Their Significance.

A variety of natural influences impose upon the refractivity structure variations of differing characteristic amplitude, period, and spatial scale. Based upon the analysis presented in Chapter 5 these can be summarized for Atlantic Canadian waters as follows:

1.) Climatic influences produce a latitude dependent variation in annual mean surface refractivity of the order of 80 N, and a corresponding variation in the annual mean refractivity

lapse of the order of 20 N/Km. These variations occur gradually and uniformally over spatial scales of several hundred kilometres and may be described in terms of long term median tropical, temperate, and polar meteorological conditions.

2.) Seasonal influences contribute variations of the order of 40 N in the monthly mean surface refractivity winter to summer. Gradient variations are less severe, being of the order of 25 N/Km. These occur gradually over a period of months and uniformally over distances of several hundred kilometres.

3.) Earth rotation produces a daily cycle of variation in surface temperature and water vapour concentration which results in significant changes in surface refractivity over periods of a few hours. The amplitude of diurnal variation is greatest in the summer months due to the increased effect of water vapour and decreases to negligible levels in winter. A maximum daily cycle of variation of the order of 20 N units peak-to-peak may be expected.

4.) Weather system influences are characterized by abrupt and apparently random changes in surface meteorology over relatively short periods of time. Variations in surface refractivity of the order of 20-40 N units or more over a period of a few days appear to be fairly commonplace at all times of the year, with the largest variations occuring in summer months.

5.) Both earth rotation and weather system influences contribute to layering in the lower atmosphere. Anomalous refractivity layers were encountered up to 30% of the time during summer months and were frequently associated with weather system disturbances. The majority of the layers encountered were of the elevated variety with base heights ranging from 500-700 metres and thicknesses ranging over several tens of metres. Layering entered predominantly through variations in the wet term profile. By contrast, the dry component of refractivity remained closely linear under all but the most severe conditions.

6.) Regional variations in surface refractivity of the order of 50 N units were found in comparing hourly values between sites separated by a few hundred kilometres, and differences in the time of occurrence, altitude, and thickness of refractivity layers were frequently encountered in comparing the same sites. As might be expected, the largest discrepencies were found when

comparing coastal and offshore locations, and arose principally due to water vapour content variations.

7.) The combined effect of turbulence and layering in the lower atmosphere is most evident in the troposcatter propagation zone. Short term ranging stability over trans-horizon distances of the order of 80 Km was found to vary from the 5-10 metre level during more standard atmospheric conditions, to 20-30 metre level during periods of maximum turbulence and layering. These periods were frequently associated with changes in prevailing weather conditions. Conversely, surface diffraction measurements performed simultaneously over similar distances were virtually unaffected and were consistantly accurate to within the 5 metre level.

6.2) Implications for Field Operations.

It seems clear on the basis of the above discussion that the traditional approach to modelling tropospheric refractivity variations based upon the assumptions of a quasi-static, horizontally homogeneous, and vertically linear refractivity lapse have limited validity when applied to trans-horizon UHF range measurement. Earth rotation and weather influences combine to produce daily variations in surface refractivity of the order of several parts in 10^5, and contribute to a strongly non-standard layer structure in the lower atmosphere which is poorly correlated with surface conditions. Differences in local surface meteorology introduce spatial variations of the same order of magnitude over distances of a few hundred kilometres or less. As a result, a high temporal and spatial sampling rate is likely to be required before these effects can be significantly reduced.

Possible alternatives include the regular observation of surface and upper air meteorology at representative locations within the survey area, or the use of differential corrections based upon the continuous monitoring of fixed baselines. The latter technique offers a potential threefold advantage in that it provides a direct indication of integrated refractivity along the transmission path, assists in determining more precisely the level of measurement instability resulting from scattering effects and in relating these to local meteorology, and offers the potential for real-time

differential corrections. In either case, further study is required to establish appropriate procedures, and to quantify the degree of improvement possible.

The stability of troposcatter ranging is strongly influenced by the degree of turbulence and non-standard layering present in the lower atmosphere. While these effects can in general be linked to models of atmospheric stability, they cannot be reliably predicted on the basis of standard surface meteorological observations alone. Consequently, further range measurement studies offer the greatest potential for determining the degree of ranging stability to be expected under various atmospheric conditions, and to quantify climatic and regional differences in performance.

In the absence of corrective measures tropospheric influences would appear to limit the accuracy of UHF ranging to approximately 100-200 ppm depending upon prevailing conditions. Given careful consideration of refractivity effects through detailed meteorological or differential baseline observations coupled with space diversity or recursive filtering techniques, this limit could perhaps be reduced to 50-100 ppm. However, this latter estimate is largely speculative at the present time given the lack of a comprehensive data base.

6.3) Recommendations for Further Research.

The analysis of tropospheric effects in UHF radio positioning presented herein can be extended and improved upon in several ways:

1.) A more comprehensive study of surface and upper air meteorological records at various coastal locations throughout Canada should be undertaken to better determine the nature and magnitude of refractivity variation in Canadian coastal waters and the influence of regional variations in climate and topography. Such a study would be of direct benefit to all users of radio positioning, result in improved accuracy levels in all frequency bands, and be a natural extension to the existing Refractivity Atlas of Canada as compiled by Segal and Barrington (1977).

2.) Further study is required to establish more appropriate procedures for the correction of tropospheric effects in UHF radio positioning through the use of meteorological observations or

differential range measurement techniques. Minimum criteria for the spatial and temporal resolution of meteorological observation should be investigated.

3.) A more detailed investigation of the characteristics of UHF trans-horizon ranging should be undertaken. Baseline observations at various representative times of the year and over distances of varying length and transmission path characteristics are required to better determine the magnitude of short term phase instabilities and the degree to which ranging accuracy can be improved through the application of space diversity or recursive filtering techniques.

4.) The use of spectral analysis as a diagnostic tool in the study of tropospheric refractive index variability should be investigated. Such an approach would be particularly well suited to the study of variations in the amplitude, scale, and spectrum of troposcatter ranging instability, and would assist in separating the inter-related influences of weather and earth rotation in hourly surface refractivity data.

LIST OF REFERENCES

Abramowitz, M. and I. Stegun (1965). *Handbook of Mathematical Functions.* Dover Publications, Inc., New York.

Almond, T., and J. Clark (1983). "Considerations of the usefulness of microwave propagation prediction methods on air-to-ground paths." *Proceedings of the Institute of Electrical Engineers*, F130(7), pp. 649-656.

Baumgartner, G. B., H. V. Hitney, and R. A. Pappert (1983). "Duct propagation modelling for the integrated-refractive-effects prediction system (IREPS)." *Proceedings of the Institute of Electrical Engineers*, F130(7), pp. 630-642.

Barrow, B. B. (1968). "Troposcatter measurements using a rake receiver." Proceedings of the IEE Conference on Tropospheric Wave Propagation, IEE Conference Publication 48, pp. 125-137.

Bean, B. R. and F. M. Meaney (1955). "Some applications of the monthly median refractivity gradient in tropospheric propagation." *Proceedings of the Institute of Radio Engineers*, 43(10), pp. 1419-1431.

Bean, B. R. and B. A. Cahoon (1957). "The use of surface weather observations to predict total atmospheric bending of radio waves at small elevation angles." *Proceedings of the Institute of Radio Engineers*, 45(11), pp. 1545-1546.

Bean, B. R. and G. D. Thayer (1959). "Models of the atmospheric radio refractive index." *Proceedings of the Institute of Radio Engineers*, 47(5), pp. 740-755.

Bean, B. R. and E. J. Dutton (1966). " Radio Meteorology." National Bureau of Standards Monograph 92, U.S. Government Printing Office, Washington, U.S.A.

Bean, B. R. , C. A. Samson, and G. D. Thayer (1966). "A world atlas of atmospheric radio refractivity." Environmental Sciences Services Administration Monograph 1, U.S. Government Printing Office, Washington, U.S.A.

Bean, B. R., C. B. Emmanual, and R. W. Krinks (1967). "Some spectral characteristics of the radio refractivity in the surface layer of the atmosphere." *Radio Science*, 2(5), pp. 503-510.

Beckmann, P., and A. Spizzichino (1963). *The Scattering of Electromagnetic Waves from Rough Surfaces.* The MacMillan Company, New York.

Bell, C. P. (1968). "A survey of UHF tropospheric propagation measurements carried out by the BBC." Proceedings of the IEE Conference on Tropospheric Wave Propagation, IEE Conference Publication 48, pp. 101-109.

Birnbaum, G., and H. E. Bussey (1955). "Amplitude, scale, and spectrum of refractive index inhomogeneities in the first 125 metres of the atmosphere." *Proceedings of the Institute of Radio Engineers*, 43(10), pp. 1412-1418.

Black, H. D. and A. Eisner (1983). "Correcting Doppler data for tropospheric effects." Applied Physics Laboratory Report SDO6777, John Hopkins University, Maryland, U.S.A.

Boithias, L. and J. Battesti (1983). "Propagation due to tropospheric inhomogeneities." *Proceedings of the Institute of Electrical Engineers*, F130(7), pp. 657-664.

Booker, H. G. and W. Walkinshaw (1946). "The mode theory of tropospheric refraction and its relation to wave-guides and diffraction." *Meteorological Factors in Radio-Wave Propagation*, The Physical Society of London, London.

Booker, H. G. and W. E. Gordon (1950). "A theory of radio scattering in the troposphere." *Proceedings of the Institute of Radio Engineers*, 38(4), pp. 401-412.

Born, M. and E. Wolf (1965). *Principles of Optics*. Pergamon Press, New York.

Bowditch, N. (1981). *American Practical Navigator*. Defence Mapping Agency Hydrographic Center Publication 9 Vol. II, U.S. Government Printing Office, Washington, U.S.A.

Brekhovskikh, L. M. (1980). *Waves in Layered Media (2 ed.)*. Academic Press, New York.

Bremmer, H. (1949). *Terrestrial Radio Waves; Theory of Propagation*. Elsevier Co., New York.

Brunner, F. K. (Ed.) (1984). *Geodetic Refraction: Effects of Electromagnetic Wave Propagation Through The Atmosphere*, Springer-Verlag, New York

Budden, K.G. (1961). *The Wave-Guide Mode Theory of Wave Propagation*. Prentice-Hall Inc., Englewood Cliffs, New Jersey.

Bugnolo, D. S. (1960). "On the question of multiple scattering in the troposphere." *Journal of Geophysical Research*, 65(3), pp. 879-884.

Bull, G. (1966). "Power spectra of atmospheric refractive index from microwave refractometer measurements." *Journal of Atmospheric and Terrestrial Physics*, 28(5), pp. 513-519.

Bullington, K. (1957). "Radio propagation fundamentals." *Bell System Technical Journal*, 36(3), pp. 593-626.

Bullington, K., W. J. Inkster, and A. L. Durkee (1955). "Results of propagation tests at 505 MHz and 4090 MHz on beyond horizon paths." *Proceedings of the Institute of Radio Engineers*, 43(10), pp. 1306-1316.

Cartwright, N. E., and R. L. Tattersall (1977). "Simultaneous measurements of radio refractivity and multipath fading on July 2nd 1975 at 11, 19, and 36 GHz on a 7.5 Km path." *Electronics Letters*, 13(7), pp. 208-210.

Chang, H. T. (1971). "The effect of tropospheric layer structures on long range VHF radio propagation." *IEEE Transactions on Antennas and Propagation*, 19(6), pp. 751-756.

Chernov, L. A. (1960). *Wave Propagation in a Random Medium*. McGraw-Hill Book Company, Inc., New York.

Chisholm, J. H., W. E. Morrow, B. E. Nichols, J. F. Roche, and A. E. Teachman (1962). "Properties of 400 CPS long distance troposcatter circuits." *Proceedings of the Institute of Radio Engineers*, 50(12), pp. 2464-2482.

Cho, S. H., and J. R. Wait (1978). "Analysis of microwave ducting in an inhomogeneous troposphere." *Pure and Applied Geophysics*, 166, pp. 1118-1142.

Clark, D. , R. Lowen, E. Munden, G. Peterkin, and B. Segal (1978). "Use of the Canadian refractivity atlas for terrestrial radio link design." Unpublished Report of the Canadian Radio Technical Planning Board, Department of Communications, Ottawa, Canada.

Cooper, A. H. (1979). "Standard test procedures for precise positioning systems." *Proceedings of Commission 4 of the 15th International Congress of Surveyors*, Montreaux, Switzerland, pp. 403.1-403.12.

Corson, D. and P. Lorrain (1970). *Electromagnetic Fields and Waves*. W. H. Freeman and Sons, San Francisco.

Crain, C. M., A. P. Deam, and J. R. Gerhardt (1953). "Measurement of the tropospheric index of refraction fluctuations and profiles." *Proceedings of the Institute of Radio Engineers*, 41(2), pp. 284-290.

Crawford, A. B., D. C. Hogg, and W. H. Kummer (1959). "Studies in tropospheric propagation beyond the horizon." *Bell System Technical Journal*, 38, pp. 1067-1178.

Crow, E. L. and F. A. Davis (1978). *Statistics*. Coles Publishing Ltd., Toronto.

David, P. and J. Voge (1969). *Propagation of Waves*, Pergamon Press Ltd., Oxford.

Delorme, P. (1978). "Evaluation direct and inverse geodetic algorithms." Bedford Institute of Oceanography Computer Note C-78-2, Dartmouth, Nova Scotia.

Dennis, A. S. (1962). "Correlation between hourly median scattered signals and simple refractivity parameters." *Journal of Research of the National Bureau of Standards*, 66D(3), pp. 285-289.

Dougherty, H. T. and B. A. Hart (1979). "Recent Progress in Duct Propagation Prediction." *IEEE Transactions on Antennas and Propagation*, 27(4), pp. 542-548.

Dubin, M. , N. Sissenwine, and H. Wexler (1962). "U.S. Standard Atmosphere 1962." National Aeronautics and Space Administration Technical Report, U.S. Government Printing Office, Washington, U.S.A.

Du Castel, F., P. Misme, A. Spizzichino, and J. Voge (1962). "On the role of the process of reflection in radio wave propagation." *Journal of Research of the National Bureau of Standards*, 66D(3), pp. 273-284.

Dutton, J. A. and H. A. Panofsky (1970). "Clear Air Turbulence: a mystery may be unfolding." *Science*, 167(3920), pp. 937-944.

Elmore, W. C. and M. A. Heald (1969). *Physics of Waves*. McGraw-Hill Book Company, Inc., New York.

Essen, L. (1953). "Refractive indices of water vapour, air, oxygen, nitrogen, hydrogen, deuterium, and helium." *Proceedings of the Physical Society of London*, B66, pp. 189-193.

Essen, L. and K. D. Froome (1951). The refractive indices and dielectric constants of air and its principle constituents at 24,000 Mc/s." *Proceedings of the Physical Society of London.* B64, pp. 862-875.

Fehlhaber, L. (1968). "Results of the theory of tropospheric scattering derived from propagation measurements." Proceedings of the IEE Conference on Tropospheric Wave Propagation, IEE Conference Publication 48, pp. 37-42.

Fleagle, R. G. and J. A. Businger (1980). *An Introduction to Atmospheric Physics.* Academic Press, New York.

Friis, H. T., A. B. Crawford, and D. C. Hogg (1957). "A reflection theory for propagation beyond the horizon." *Bell System Technical Journal*, 36(3), pp. 627-644.

Gjessing, D. T. and J. A. Borreson (1968). "The influence of an irregular refractive index structure on the spatial field strength correlation of a scattered radio wave." Proceedings of the IEE Conference on Tropospheric Wave Propagation, IEE Conference Publication 48, pp. 43-50.

Gordon, W. E. (1955). "Radio scattering in the troposphere." *Proceedings of the Institute of Radio Engineers*, 43(1), pp. 23-28.

Gossard, E. E. (1960A). "Power spectra of temperature, humidity, and refractive index from aircraft and tethered balloon measurements." *IRE Transactions on Antennas and Propagation*, 8(2), pp. 186-201.

Gossard, E. E. (1960B). "Spectra of atmospheric scalars." *Journal of Geophysical Research*, 65(10), pp. 3339-3351.

Hall, M. P. (1968A). "VHF radio propagation by double hop reflection from a tropospheric layer." *Proceedings of the Institute of Electrical Engineers*, 115(4), pp. 503-506.

Hall, M. P. (1968B). "Further evidence of VHF propagation by successive reflections from an elevated layer in the troposphere." *Proceedings of the Institute of Electrical Engineers*, 115(11), pp. 1595-1596.

Hall, M. P. (1979). *Effects of the Troposphere on Radio Communication.* Peter Peregrinus Ltd., London.

Hall, M. P., and C. M. Comer (1969). "Statistics of tropospheric radio refractive index soundings taken over a 3-year period in the UK." *Proceedings of the Institute of Electrical Engineers*, 116(5), pp. 685-690.

Hall, M. P., and C. M. Comer (1970). "Changes in the radio field strength at VHF and UHF due to disintegration of reflecting layers in the troposphere." *Proceedings of the Institute of Electrical Engineers*, 117(12), pp. 1925-1932.

Helvey, R. A. (1983). "Radiosonde errors and spurious surface based effects." *Proceedings of the Institute of Electrical Engineers*, F130(7), pp. 643-648.

Herbstreit, J. W. and M. C. Thompson (1955). "Measurement of the phase of radio waves received over transmission paths with electrical lengths varying as a result of atmospheric turbulence." *Proceedings of the Institute of Radio Engineers*, 43(10), pp. 1391-1401.

Hopfield, H. S. (1969). "Two quartic tropospheric refractivity profile for correcting satellite data." *Journal of Geophysical Research*, 74(18), pp. 4487-4499.

Hopfield, H. S. (1971). "Tropospheric effect on electromagnetically measured range: Prediction from surface weather data." *Radio Science*, 6(3), pp. 357-367.

Hopfield, H. S. (1972). Tropospheric range error parameters: Further studies." Applied Physics Laboratory Report CP015, Johns Hopkins University, Maryland, U.S.A.

Hopfield, H.S. (1976). "Tropospheric effects on signals at very low elevation angles." Applied Physics Laboratory Technical Memorandum TG1291, Johns Hopkins University, Maryland, U.S.A.

Hudson, R. P. (Ed.) (1984) "Documents concerning the new definition of the metre." *Metrologia*, 19(4), pp. 163-177.

Janes, H. W., R. M. Eaton, and J. Wilson (1985). "UHF Syledis for coastal survey positioning." *International Hydrographic Review*, LXII(2), pp. 59-73

Janes, H. W., D. E. Wells, and J. Tranquilla (1985). "Accuracy considerations in UHF radiopositioning." Proceedings of the Canadian Hydrographic Service 1st Bienniel Conference, Halifax, Nova Scotia, (in press).

Jeske, H. and K. Brocks (1966). "Comparison of experiments on duct propagation above the sea with the mode theory of Booker and Walkinshaw." *Radio Science*, 1(8), pp. 891-895.

Jones, L. M. (1979). *An Introduction to Mathematical Methods in Physics.* The Benjamin/Cummings Publishing Company, Inc., Menlo-Park, Calif.

Jordan, E. D., and K. G. Balmain (1968). *Electromagnetic Waves and Radiating Systems (2nd ed.)* Prentice-Hall Inc., Englewood Cliffs, New Jersey.

Joseph, R. I. and G. D. Smith (1972). "Propagation in an evaporation duct: Results in some simple analytical models." *Radio Science*, 7(4), pp. 433-441.

Kerr, E. D. (Ed.) (1951). *Propagation of Short Radio Waves.* McGraw-Hill Book Company Inc., New York.

Lane, J. A. (1965). "Some investigations of the structure of elevated layers in the troposphere." *Journal of Atmospheric and Terrestrial Physics*, 27(9), pp. 969-978.

Lane, J. A. (1968). "Small-scale variations of radio refractive index in the troposphere: Part 1, Relation to meteorological conditions." *Proceedings of the Institute of Electrical Engineers*, 115(9), pp. 1227-1234.

Lane, J. A. and P. W. Sollum (1965). "VHF transmission over distances of 140 and 300 Km." *Proceedings of the Institute of Electrical Engineers*, 112(2), pp. 254-258.

Lane, J. A. and G. W. Paltridge (1968). "Small-scale variations of radio refractive index in the troposphere: Part 2, Spectral characteristics." *Proceedings of the Institute of Electrical Engineers*, 115(9), pp. 1235-1239.

Larsen, R. (1968). "A comparison of some troposcatter prediction methods." Proceedings of the IEE Conference on Tropospheric Wave Propagation, IEE Conference Publication 48, pp. 110-117.

Laurila, S. H. (1969). Statistical analysis of refractive index through the troposphere and stratosphere." *Bulletin Geodesique*, 92, pp. 139-154.

Laurila, S. H. (1976). *Electronic Surveying and Navigation*. John Wiley and Sons, New York.

List, R. J. (1971). *Smithsonian Meteorological Tables*. Smithsonian Institution Press, Washington.

Livingston, D. C. (1970). *The Physics of Microwave Propagation*. Prentice-Hall Inc, Englewood Cliffs, New Jersey.

Lumley, J. L. and H. A. Panofsky (1964). *The Structure of Atmospheric Turbulence*. John Wiley and Sons, Inc., New York.

Matthews, P. A. (1965). *Radio Wave Propagation, VHF and Above*. Chapman and Hall Ltd., London.

Matthews, P. A. and S. Dufu (1968). "The effect of reflecting layers in the troposphere on trans-horizon propagation." Proceedings of the IEE Conference on Tropospheric Wave Propagation, IEE Conference Publication 48, pp. 22-29.

Meeks, M. L. (1982). *Radar Propagation at Low Altitudes*. Artech House Inc., Washington.

Megaw, E. C. S. (1950). "Scattering of electromagnetic waves by atmospheric turbulence.", *Nature*, 166(4235), pp. 1100-1104.

Megaw, E. C. S. (1957). "Fundamental radio scatter propagation theory.", Proceedings of the Institute of Electrical Engineers, 104C, pp. 441-455.

Menzel, D. H. (Ed.) (1960). *Fundamental Formula of Physics*. Dover Reprint, New York.

Minzner, R. A. and others (1976). "U.S. standard atmosphere 1976." National Aeronautics and Space Administration Technical Report R-549, U.S. Government Printing Office, Washington, U.S.A.

Monin, A. S. and A. M. Yaglom (1971). *Statistical Fluid Mechanics: Mechanics of Turbulence* (2 vol.), The MIT Press, Cambridge, Mass.

Muchmore, R. B. and A. D. Wheelon (1955). "Line of sight propagation phenomena.", *Proceedings of the Institute of Radio Engineers*, 43(10), pp. 1437-1458.

Murdoch, G. E. (1978). "A formula for computing refraction effects on range measurements." *Radio Science*, 13(3), pp. 509-510.

Norton, K. A. (1959). "Recent experimental evidence favoring the $\rho K_1(\rho)$ correlation function for describing turbulence of refractivity in the troposphere and stratosphere.", Journal of Atmospheric and Terrestrial Physics, 15(3), pp. 206-227.

Norton, K. A., P. L. Rice, and L. E. Vogler (1955A). The use of angular distance in estimating transmission loss and fading range for propagation through a turbulent atmosphere over irregular terrain.", *Proceedings of the Institute of Radio Engineers*, 43(10), pp. 1488-1526.

Norton, K. A., P. L. Rice, H. B. Janes, and A. P. Barsis (1955B). "The rate of fading in propagation through a turbulent atmosphere." *Proceedings of the Institute of Radio Engineers*, 43(10), pp. 1341-1353.

Panofsky, H. A. and J. A. Dutton (1984). *Atmospheric Turbulence: Models and Methods for Engineering Applications*. John Wiley and Sons, New York.

Pappert, R. A. and C. L. Goodhart (1977). "Case studies of beyond the horizon propagation in tropospheric ducting environments.", *Radio Science*, 12(1), pp. 75-87.

Picquenard, A. (1974). *Radio Wave Propagation*. John Wiley and Sons, New York.

Planck, V. G. (1959). "Convection and refractive index inhomogeneities.", *Journal of Atmospheric and Terrestrial Physics*, 15(3), pp. 228-247.

Rao, N. M. (1977). *Elements of Engineering Electromagnetics*. Prentice-Hall Inc., Englewood Cliffs, New Jersey.

Reed, H. R. and M. S. Russell (1953). *Ultra-High Frequency Propagation*. John Wiley and Sons, New York.

Rice, S. O. (1953). "Statistical fluctuations of radio field strength far beyond the horizon.", *Proceedings of the Institute of Radio Engineers*, 41(2), pp. 274-281.

Richter, J. H. and H. V. Hitney (1980). "The effects of atmospheric refractivity on microwave propagation." *Atmospheric Water Vapor*, A. Deepak, T. D. Wilkerson, and L.H. Ruhnke (Ed.), Academic Press, New York.

Riemersma, J. G. (1979). "Quality control of offshore positioning surveys." *Proceedings of the 1st International Hydrographic Technical Conference*, Ottawa, pp. 79-92.

Rueger, J. M. (1980). "Introduction to electronic distance measurement." School of Surveying Monograph 7, University of New South Wales, Kensington, Australia.

Saastamoinen, J. (1973). " Contributions to the theory of atmospheric refraction." *Bulletin Geodesique*, 107, pp. 13-34.

Saxton, J. A. (1951). "The propagation of metre radio waves beyond the normal horizon: Part 1, Some theoretical consideration with particular reference to propagation over land." *Proceedings of the Institute of Electrical Engineers*, 98(3), pp. 360-369.

Saxton, J. A., G. W. Luscombe, and G. H. Bazzard (1951). "The propagation of metre radio waves beyond the normal horizon: Part 2, Experimental investigations at frequencies of 90 and 45 MHz.", *Proceedings of the Institute of Electrical Engineers*, 98(3), pp. 370-378.

Saxton, J. A., J. A. Lane, R. W. Meadows, and P. A. Matthews (1964). "Layer structure of the Troposphere; Simultaneous radar and microwave refractometer investigations." *Proceedings of the Institute of Electrical Engineers*, 111(2), pp. 275-283.

Schelling, J. C. , C. R. Burrows, and E. B. Ferrell (1933). "Ultra-short-wave propagation." *Proceedings of the Institute of Radio Engineers*, 21(3), pp. 427-463.

Schulkin, M. (1952). "Average radio ray refraction in the lower atmosphere." *Proceedings of the Institute of Radio Engineers*, 40(5), pp 554-562.

Segal, B. and R. E. Barrington (1977). "The radio climatology of Canada, a tropospheric refractivity atlas for Canada." Communications Research Centre Report 1315-E, Department of Communications, Ottawa, Canada.

Silverman, R. A. (1955). "Some remarks on scattering from eddies.", *Proceedings of the Institute of Radio Engineers*, 43(10), pp. 1253-1254.

Silverman, R. A. (1956). "Turbulent mixing theory applied to radio scattering.", *Journal of Applied Physics*, 27, pp. 699-705.

Silverman, R. A. (1957). "Fading of radio waves scattered by dielectric turbulence.", *Journal of Applied Physics*, 28, pp. 506-511.

Smith, E. K. and S. Weintraub (1953). "The constants in the equation for atmospheric refractive index at radio frequencies." *Proceedings of the Institute of Radio Engineers*, 41(8), pp. 1035-1037.

Staras, H. (1955). "Forward scattering of radio waves by anisotropic turbulence.", *Proceedings of the Institute of Radio Engineers*, 43(10), pp. 1374-1380.

Staras, H. (1956). "Diversity reception with correlated signals.", *Journal of Applied Physics*, 27(1), pp. 93-94.

Straiton, A. W., A. P. Deam, and G. B. Walker (1962). "Spectra of radio refractive index between ground and 500 feet above ground.", IRE Transactions on Antennas and Propagation, 10(6), pp. 732-737.

Stratton, J. A. (1941). *Electromagnetic Theory.* McGraw-Hill Book Company, New York.

Sutton, O. G. (1953). *Micrometeorology.* McGraw-Hill Book Company, Inc., New York.

Tatarskii, V. I. (1961). *Wave Propagation in a Turbulent Medium.* McGraw-Hill Book Company, Inc., New York.

Thayer, G. D. (1967). "A rapid and accurate ray tracing algorithm for a horizontally stratified atmosphere." *Radio Science*, 1(2), pp. 249-252.

Thayer, G. D. (1970). "Radio reflectivity of atmospheric layers." *Radio Science*, 5(11), pp. 1293-1299.

Thayer, G. D. (1974). "An improved equation for the radio refractive index of air." *Radio Science*, 9(10), pp. 803-807.

Thompson, M. C. (1975). "Effects of the troposphere on the propagation time of microwave signals." *Radio Science*, 10(7), pp. 727-733.

VanMarcke, E. (1983). *Random Fields: Analysis and Synthesis*. The MIT Press, Cambridge, Mass.

Van Kuijik, E. (1984). "The establishment, calibration, and monitoring of a permanent combined Syledis/Argo navigation system offshore N.W. Borneo." *Proceedings of the 2nd International Hydrographic Technical Conference*, Plymouth, pp. 21.1-21.14.

Van Wambeck, S. H. and A. H. Ross (1951). "Performance of diversity receiving systems.", *Proceedings of the Institute of Radio Engineers*, 39(2), pp. 256-264.

Vigants, A. (1971). "Number and duration of fades at 6 and 4 GHz.", *Bell System Technical Journal*, 50(3), pp. 815-841.

Villars, F., and V. F. Weisskopf (1954). "The scattering of electromagnetic waves by turbulent atmospheric fluctuations.", *Physical Review*, 94(2),pp. 232-240.

Wait , J. R. (1962). *Electromagnetic Waves in Stratified Media*. The MacMillan Company, New York.

Wait, J. R., and C. M. Jackson (1964). "Influence of the refractive index profile in VHF reflection from a tropospheric layer." *IEEE Transactions on Antennas and Propagation*, 12(4), pp. 512-513.

Wait, J. R., and K. P. Spies (1969). "Internal guiding of microwaves by an elevated tropospheric layer." *Radio Science*, 4(4), pp. 319-326.

Waterman, A. T. (1958). "A rapid beam swinging experiment in trans-horizon propagation.", *IRE Transactions on Antennas and Propagation*, 6(10), pp. 338-340.

Wells, D. E. (1974). "Doppler satellite control." Department of Surveying Engineering Technical Report 29, University of New Brunswick, Fredericton, N.B., Canada.

Wheelon, A. D. (1955). "Near-field corrections to line-of-sight propagation.", Proceedings of the Institute of Radio Engineers, 43(10), pp. 1459-1466.

Wheelon, A. D. (1957A). "Relation of radio measurements to the spectrum of tropospheric dielectric fluctuation.", *Journal of Applied Physics*, 28, pp. 683-693.

Wheelon, A. D. (1957B). "Spectrum of turbulent fluctuations produced by convective mixing of gradients.", *Physical Review*, 105(6), pp. 1706-1710.

Wheelon, A. D. (1959). "Radio scattering by tropospheric irregularities.", *Journal of Atmospheric and Terrestrial Physics*, 15(3), pp. 185-205.

APPENDIX I

US STANDARD ATMOSPHERE: CONSTANTS AND PARAMETERS

TABLE I.1

US/ICAO Standard Atmosphere.

Primary Constants*

Lower Atmosphere: Sea Level to Tropopause.

	Parameter**	Value
P_o	Atmospheric Pressure	101.325 Kpa.
ρ_o	Atmospheric Density	1.2250 Kg/m^3
T_o	Atmospheric Temperature	288.15 °K (15 °C)
g_o	Gravitational Acceleration	980.665 Gal (ϕ=45°)
R	Gas Constant	8.31432 J/°K-Mole
M	Molecular Mass	28.9644
H_t	Tropopause Height	11,100 m
T_t	Tropopause Temperature	216.7 °K (-56.2 °C)
α	Mean Temperature Lapse Rate	0.0065 °C/m
∇g	Mean Gravitational Gradient	-0.3085 mGal/m

*Source: Dubin et al. (1962), Minzner et al. (1977).

**Subscript o denotes sea-level value.

TABLE I.2

US/ICAO Standard Atmosphere: Standard Profile Data*.

Lower Atmosphere: Sea Level to Tropopause.

H(m)	T(°C)	P(Kpa)	ρ(Kg/m^3)	g(Gal)
0	15.0	101.325	1.2250	980.66
100	14.4	100.125	1.2133	980.63
200	13.7	98.945	1.2017	980.60
300	13.1	97.773	1.1901	980.57
400	12.4	96.611	1.1786	980.54
500	11.8	95.461	1.1673	980.51
600	11.1	94.322	1.1560	980.48
700	10.5	93.194	1.1448	980.45
800	9.8	92.078	1.1337	980.42
900	9.1	90.971	1.1226	980.39
1000	8.5	89.876	1.1117	980.36
2000	2.0	79.501	1.0066	980.05
3000	-4.5	70.121	0.9093	979.74
4000	-11.0	61.660	0.8194	979.43
5000	-17.5	54.048	0.7364	979.12
6000	-24.0	47.218	0.6601	978.82
7000	-30.5	41.105	0.5900	978.51
8000	-37.0	35.652	0.5258	978.20
9000	-43.4	30.801	0.4671	977.89
10,000	-50.0	26.500	0.4135	977.59
11,000	-56.2	22.700	0.3648	977.28

*Source: Dubin et al. (1962).

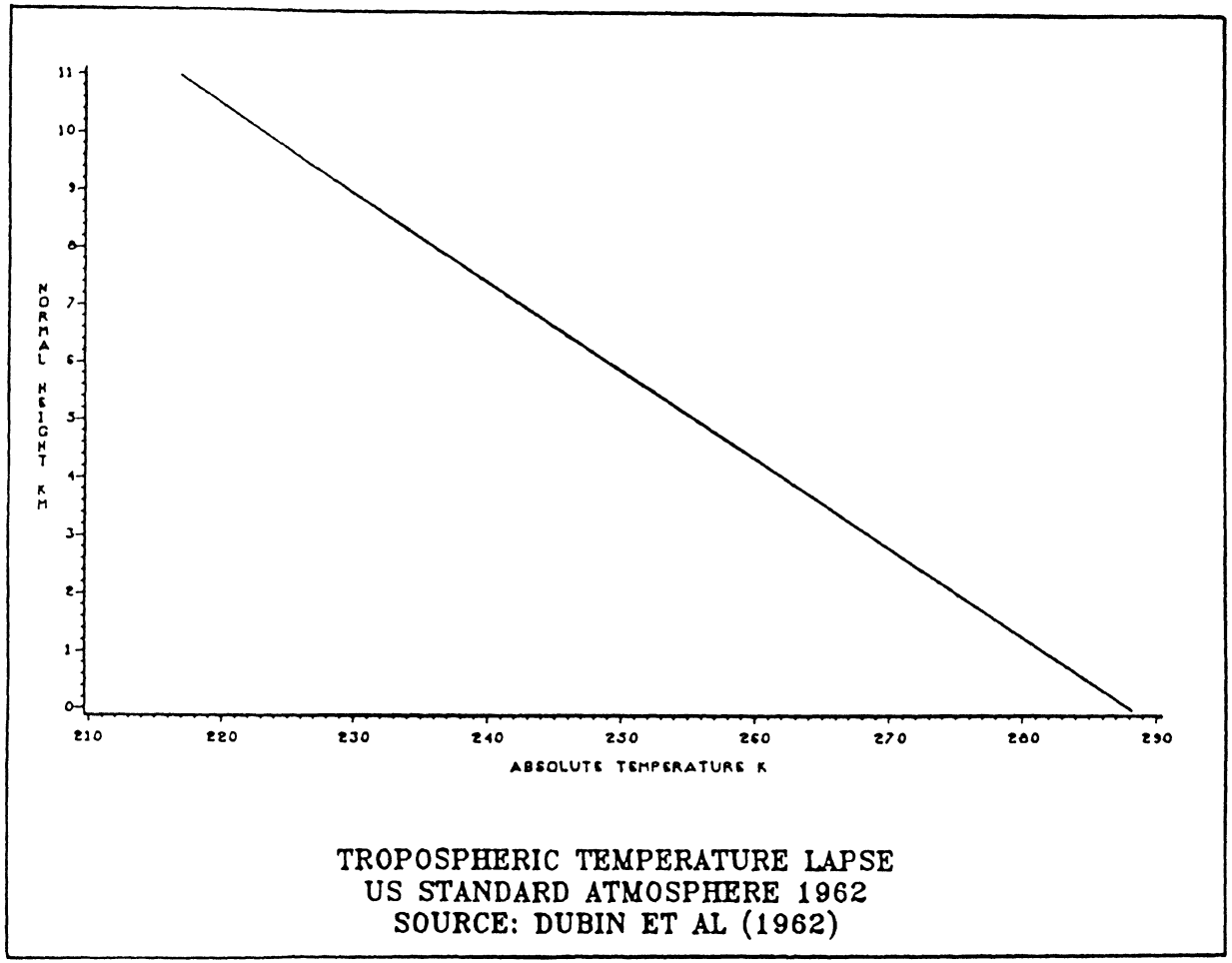

TROPOSPHERIC TEMPERATURE LAPSE
US STANDARD ATMOSPHERE 1962
SOURCE: DUBIN ET AL (1962)

Figure 1.1

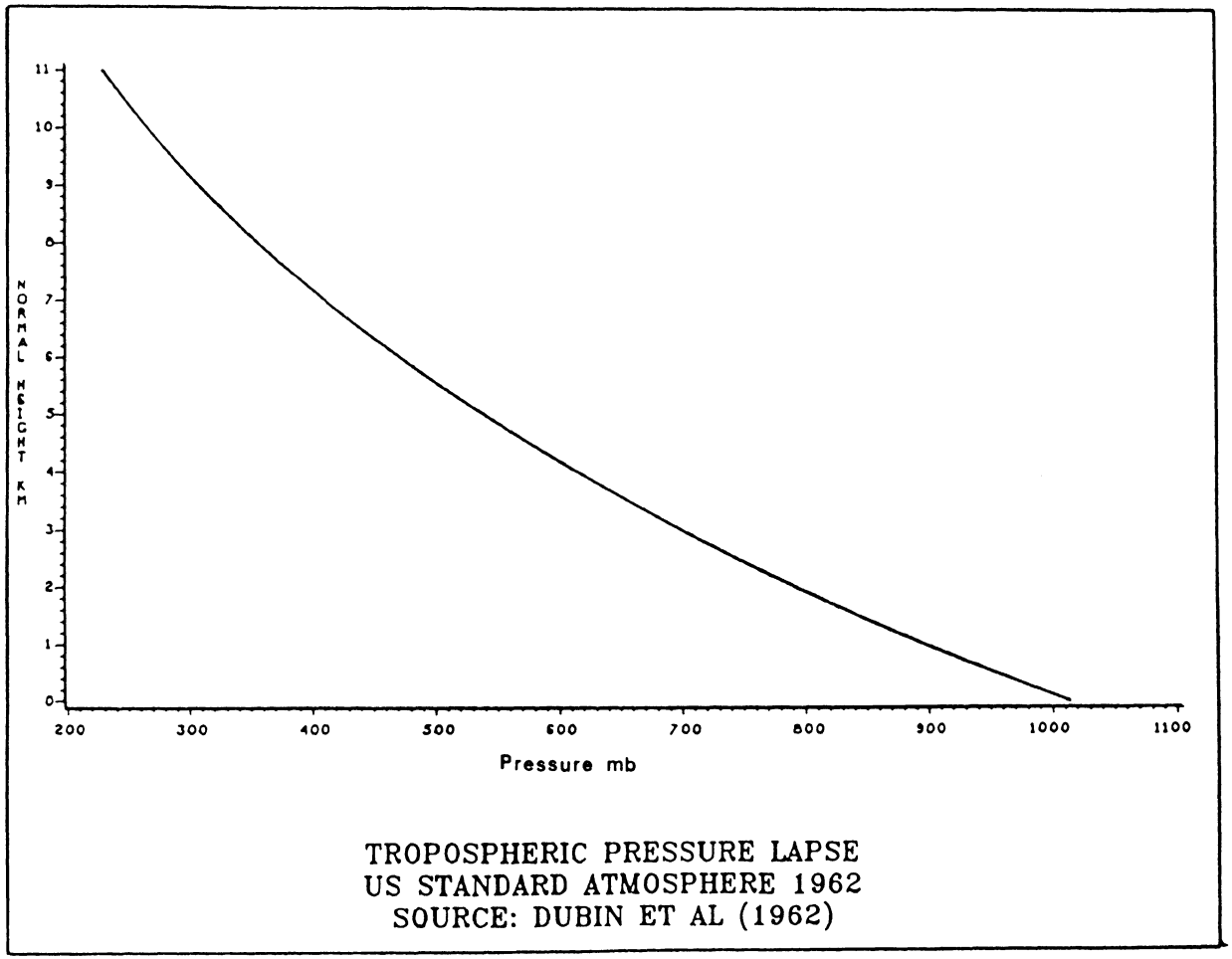

TROPOSPHERIC PRESSURE LAPSE
US STANDARD ATMOSPHERE 1962
SOURCE: DUBIN ET AL (1962)

Figure I.2

APPENDIX II

SUMMARY OF HOURLY VARIATIONS IN SURFACE REFRACTIVITY: SHELBURNE, HALIFAX AIRPORT, AND SABLE ISLAND, NOVA SCOTIA 1982

TABLE II.1

Statistical Summary of Hourly Surface Refractivity Variations

Shelburne, Nova Scotia

1982

Month	Mean	St.Dev	Minimum	Maximum	Range
Jan	---	---	---	---	---
Feb	---	---	---	---	---
Mar	313	8	288	331	43
Apr	313	10	288	336	48
May	321	9	294	346	52
Jun	329	10	297	350	53
Jul	339	13	302	368	66
Aug	340	12	298	363	65
Sep	338	10	308	362	54
Oct	323	9	298	351	53
Nov	323	12	301	356	55
Dec	318	8	300	343	43
Ann	---	---	---	---	---

TABLE II.2

Statistical Summary of Hourly Dry Refractivity Variations

Shelburne, Nova Scotia

1982

Month	Mean	St.Dev	Minimum	Maximum	Range
Jan	---	---	---	---	---
Feb	---	---	---	---	---
Mar	288	7	274	316	42
Apr	282	5	271	294	23
May	279	5	262	292	30
Jun	275	5	262	284	22
Jul	271	4	259	281	22
Aug	273	4	262	286	24
Sep	274	4	262	289	27
Oct	279	6	267	298	31
Nov	283	7	269	302	33
Dec	287	9	271	318	47
Ann	---	---	---	---	---

TABLE II.3

Statistical Summary of Hourly Wet Refractivity Variations

Shelburne, Nova Scotia

1982

Month	Mean	St.Dev	Minimum	Maximum	Range
Jan	---	---	---	---	---
Feb	---	---	---	---	---
Mar	25	10	6	56	50
Apr	31	11	13	57	44
May	42	10	18	76	58
Jun	54	12	26	86	60
Jul	69	14	35	101	66
Aug	67	13	27	98	71
Sep	64	12	33	93	60
Oct	44	12	15	84	69
Nov	41	18	10	86	76
Dec	31	15	6	70	64
Ann	---	---	---	---	---

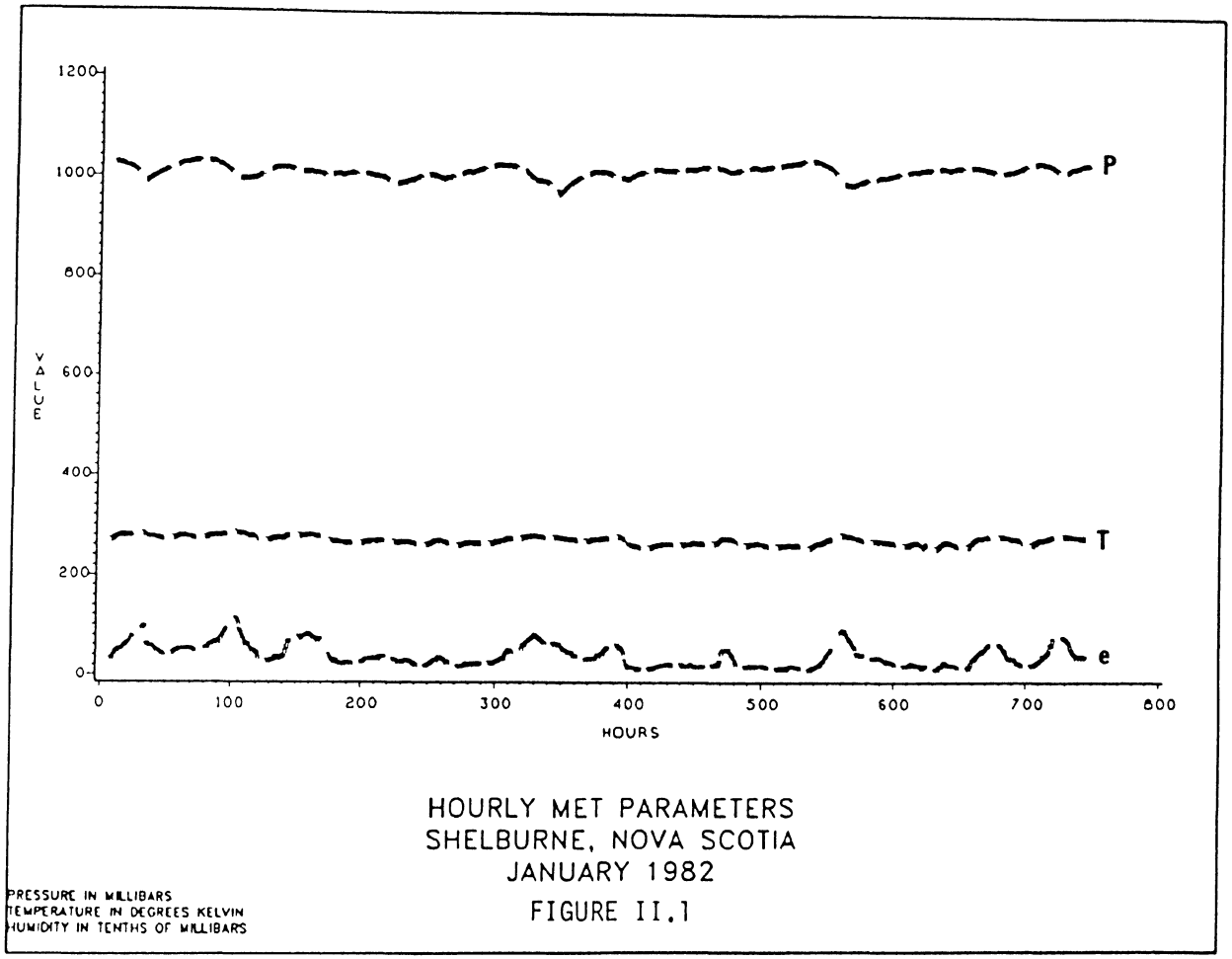

HOURLY MET PARAMETERS
SHELBURNE, NOVA SCOTIA
JANUARY 1982

FIGURE II.1

PRESSURE IN MILLIBARS
TEMPERATURE IN DEGREES KELVIN
HUMIDITY IN TENTHS OF MILLIBARS

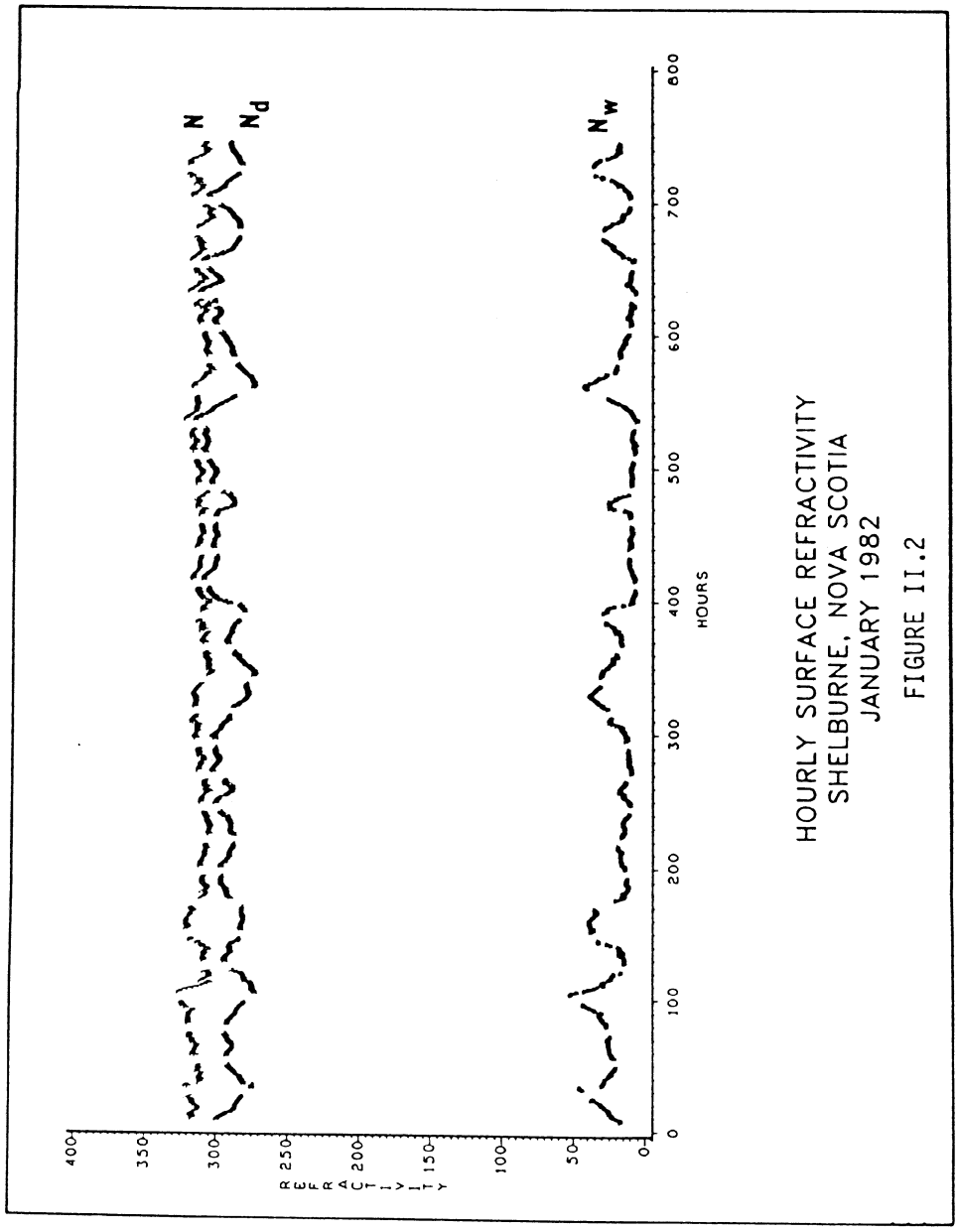

HOURLY SURFACE REFRACTIVITY
SHELBURNE, NOVA SCOTIA
JANUARY 1982

FIGURE II.2

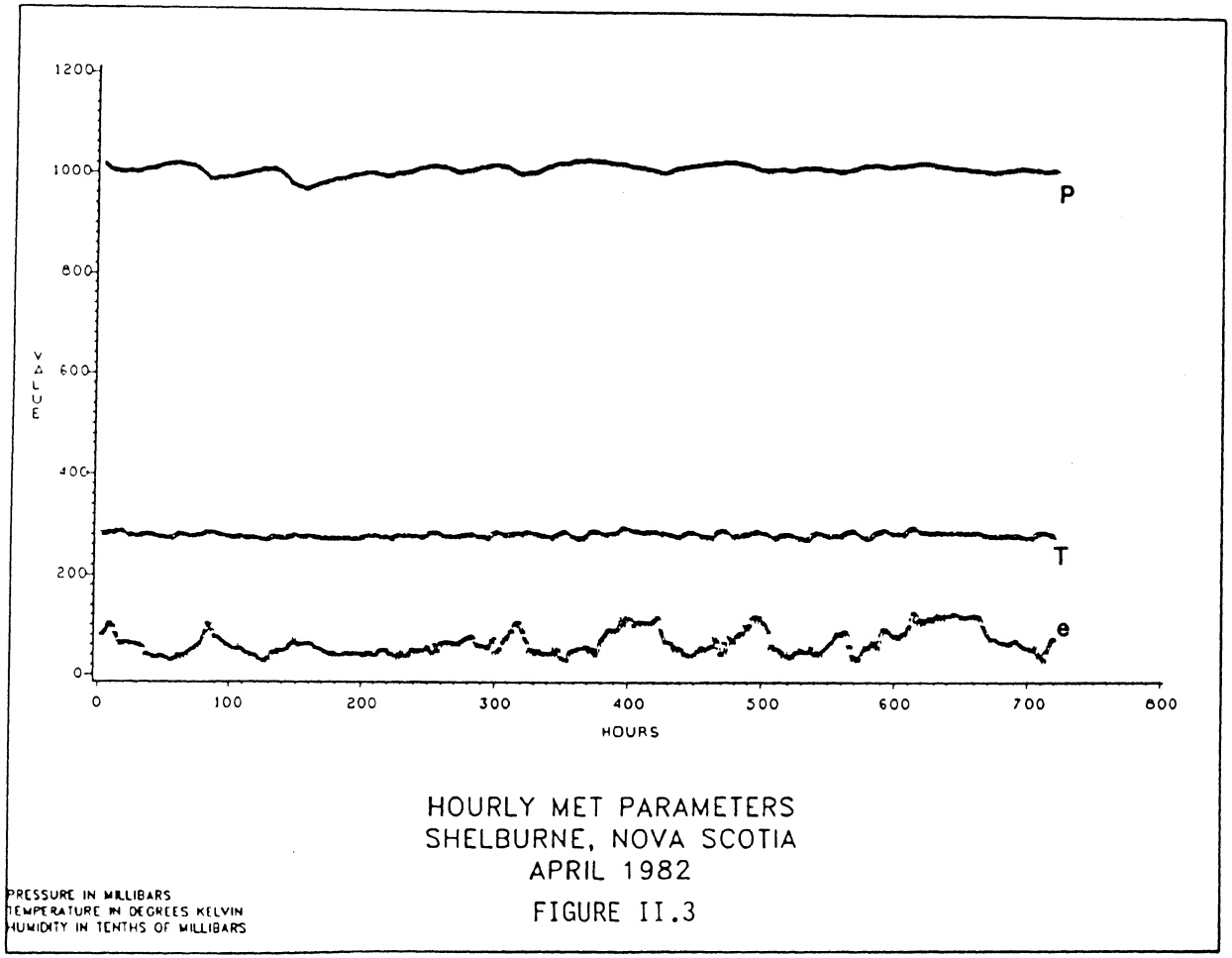

HOURLY MET PARAMETERS
SHELBURNE, NOVA SCOTIA
APRIL 1982

FIGURE II.3

PRESSURE IN MILLIBARS
TEMPERATURE IN DEGREES KELVIN
HUMIDITY IN TENTHS OF MILLIBARS

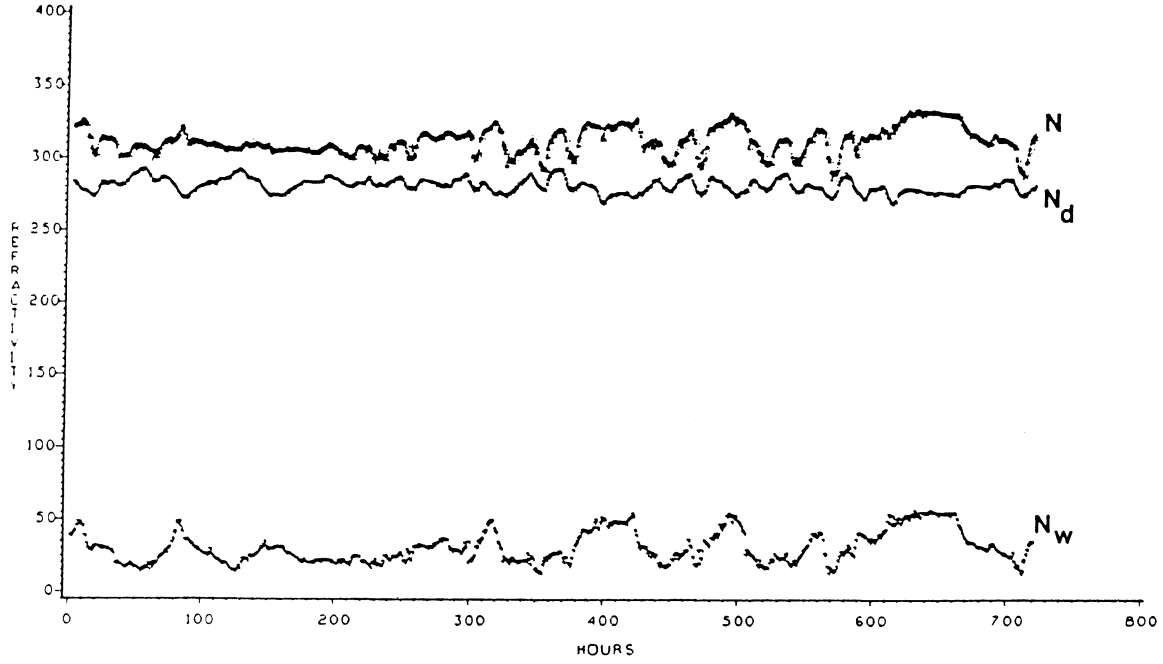

HOURLY SURFACE REFRACTIVITY
SHELBURNE, NOVA SCOTIA
APRIL 1982
FIGURE II.4

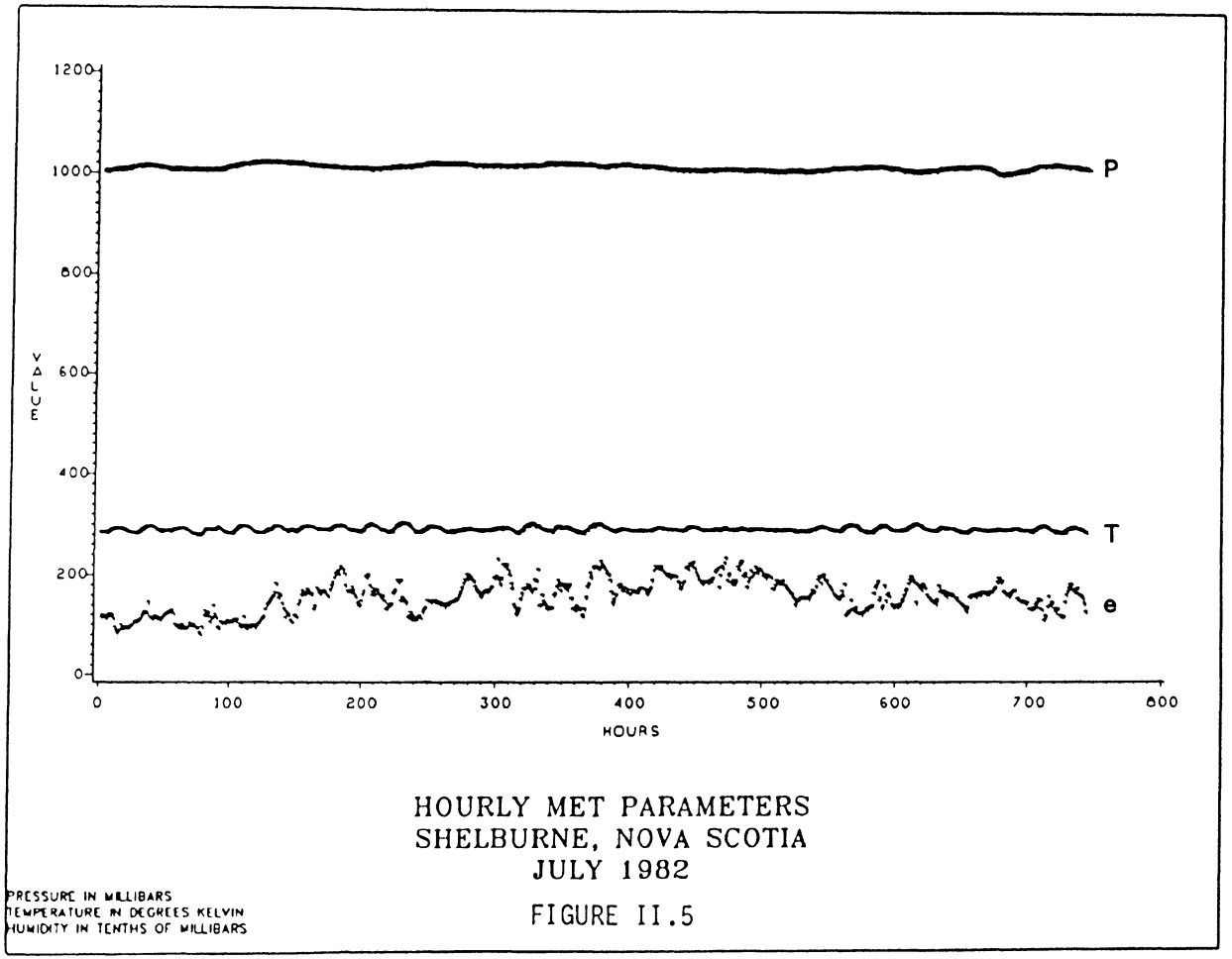

HOURLY MET PARAMETERS
SHELBURNE, NOVA SCOTIA
JULY 1982

FIGURE II.5

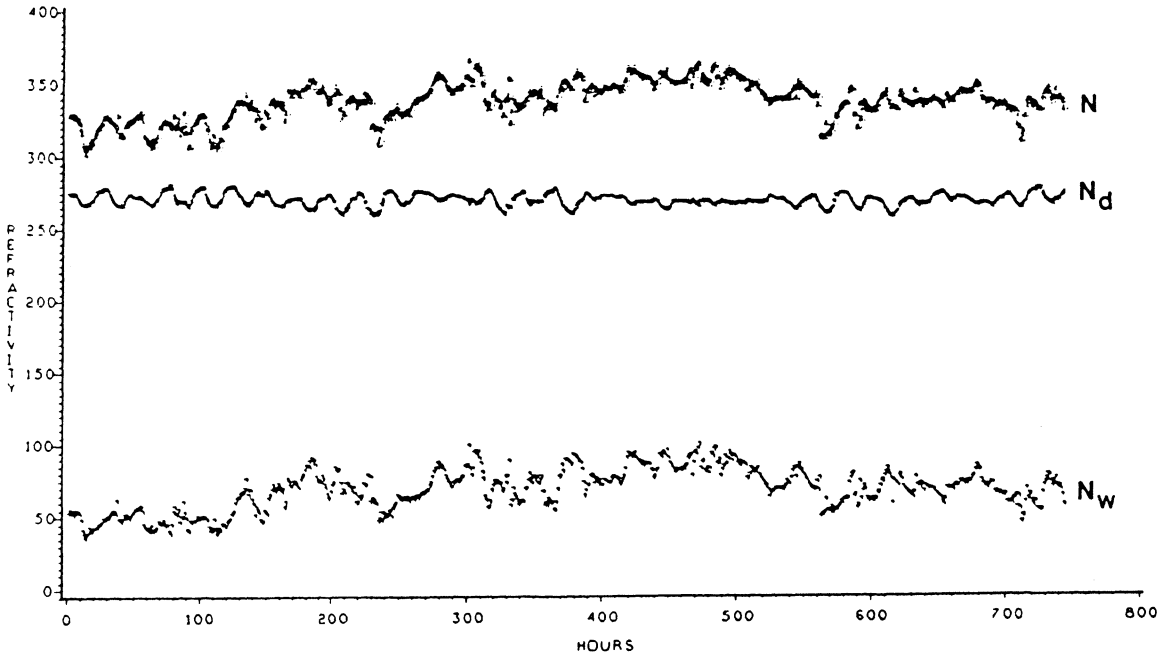

HOURLY SURFACE REFRACTIVITY
SHELBURNE, NOVA SCOTIA
JULY 1982

FIGURE II.6

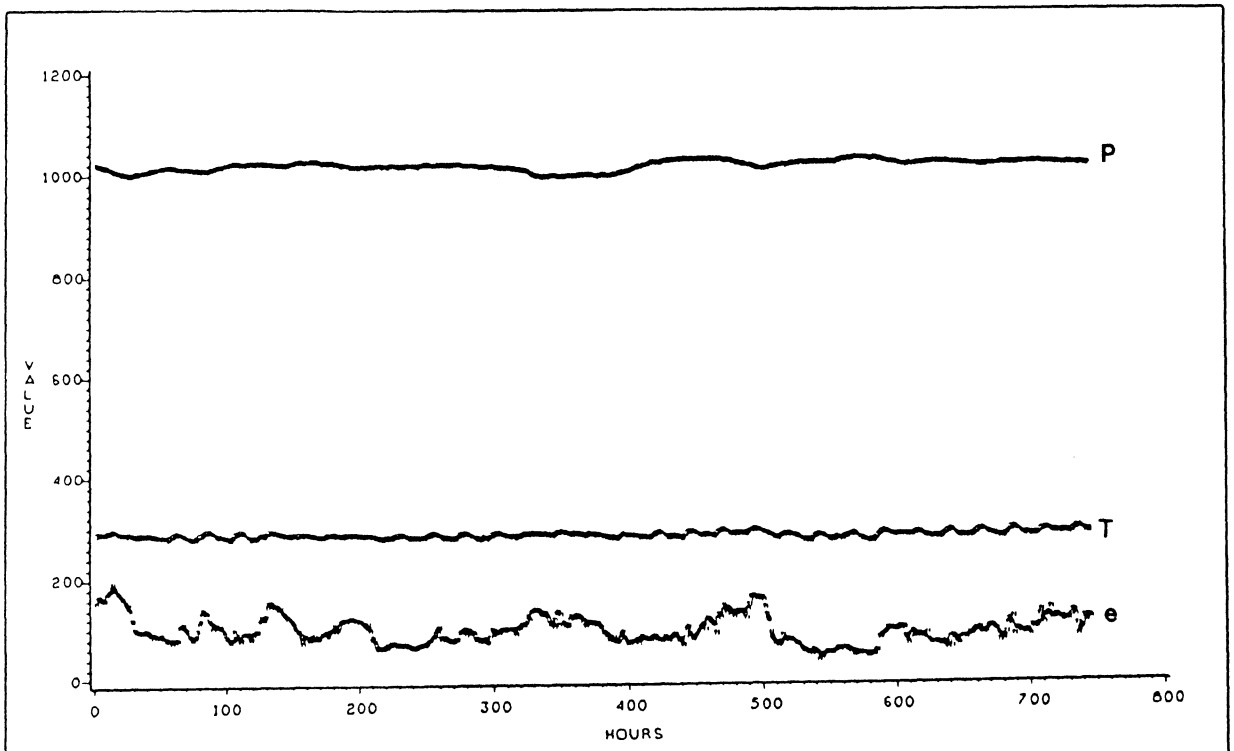

HOURLY MET PARAMETERS
SHELBURNE, NOVA SCOTIA
OCTOBER 1982
FIGURE II.7

PRESSURE IN MILLIBARS
TEMPERATURE IN DEGREES KELVIN
HUMIDITY IN TENTHS OF MILLIBARS

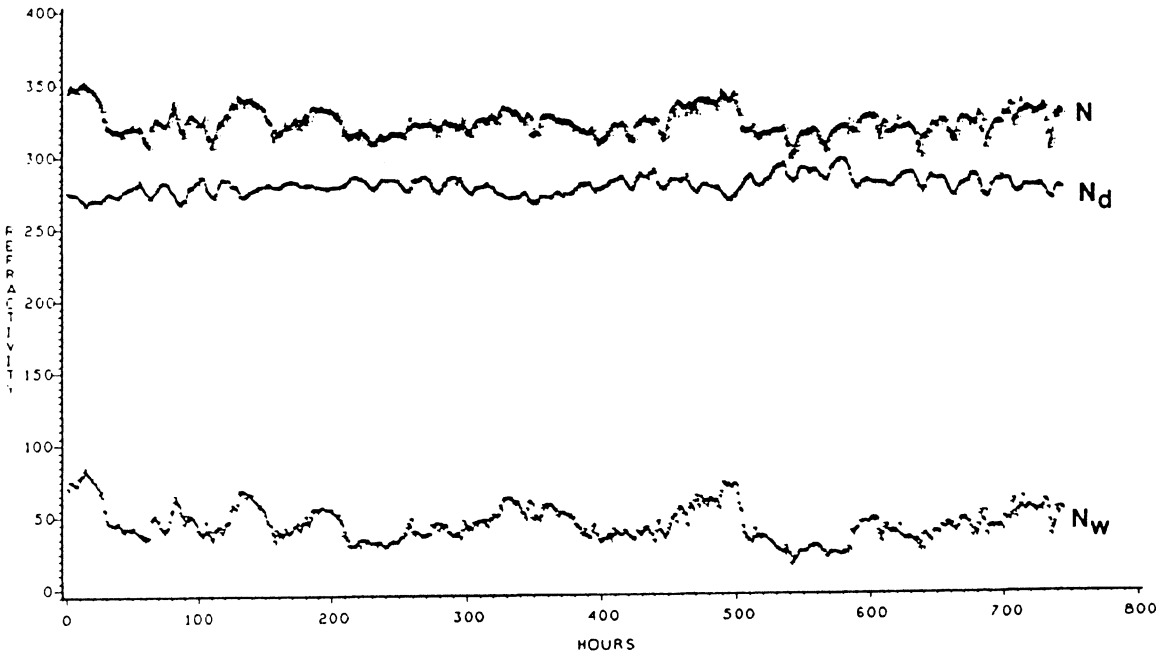

HOURLY SURFACE REFRACTIVITY
SHELBURNE, NOVA SCOTIA
OCTOBER 1982

FIGURE II.8

TABLE II.4

Statistical Summary of Hourly Surface Refractivity Variations

Halifax Airport, Nova Scotia

1982

Month	Mean	St.Dev	Minimum	Maximum	Range
Jan	307	5	294	321	27
Feb	307	5	293	325	32
Mar	307	8	287	327	40
Apr	307	10	287	337	50
May	315	11	287	341	54
Jun	323	13	287	350	63
Jul	334	16	290	371	81
Aug	333	12	294	362	68
Sep	332	11	304	355	51
Oct	317	8	295	343	48
Nov	317	13	297	358	61
Dec	313	8	298	338	40
Ann	318	11	287	371	84

TABLE II.5

Statistical Summary of Hourly Dry Refractivity Variations

Halifax Airport, Nova Scotia

1982

Month	Mean	St.Dev	Minimum	Maximum	Range
Jan	291	10	268	313	45
Feb	290	8	273	307	34
Mar	285	7	269	311	42
Apr	278	5	265	290	25
May	275	5	255	287	32
Jun	270	5	260	282	22
Jul	265	4	255	274	19
Aug	268	4	257	281	24
Sep	270	4	259	282	23
Oct	276	5	262	290	28
Nov	280	8	263	299	36
Dec	285	9	267	309	42
Ann	278	9	255	313	58

TABLE II.6

Statistical Summary of Hourly Wet Refractivity Variations

Halifax Airport, Nova Scotia

1982

Month	Mean	St.Dev	Minimum	Maximum	Range
Jan	17	10	3	52	49
Feb	18	10	6	50	44
Mar	22	11	5	58	53
Apr	28	12	8	65	57
May	40	12	15	75	60
Jun	53	15	17	85	68
Jul	69	17	28	109	81
Aug	66	14	26	99	73
Sep	62	13	35	90	55
Oct	41	12	15	79	64
Nov	38	19	12	92	80
Dec	28	15	6	68	62
Ann	40	19	3	109	106

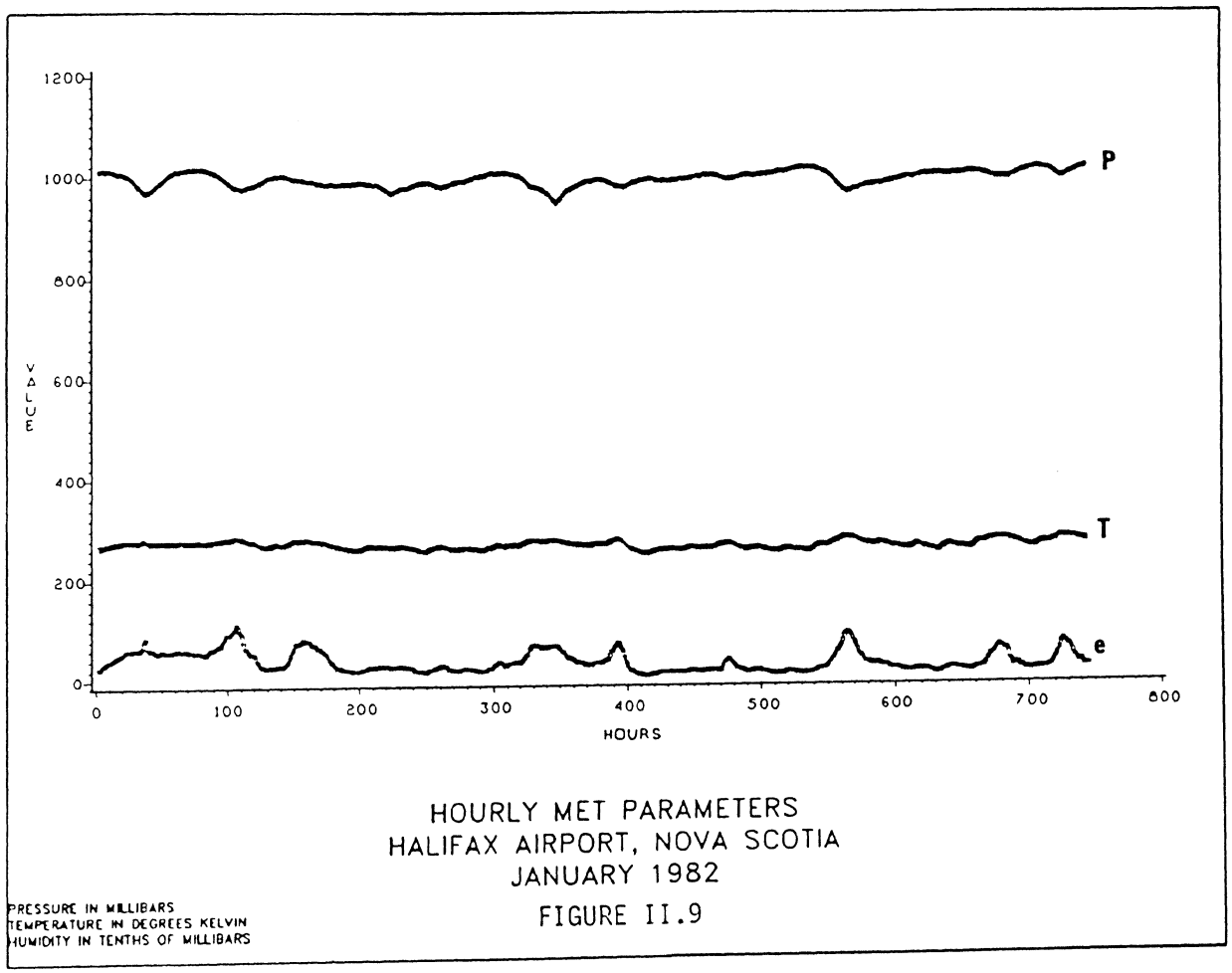

HOURLY MET PARAMETERS
HALIFAX AIRPORT, NOVA SCOTIA
JANUARY 1982

FIGURE II.9

PRESSURE IN MILLIBARS
TEMPERATURE IN DEGREES KELVIN
HUMIDITY IN TENTHS OF MILLIBARS

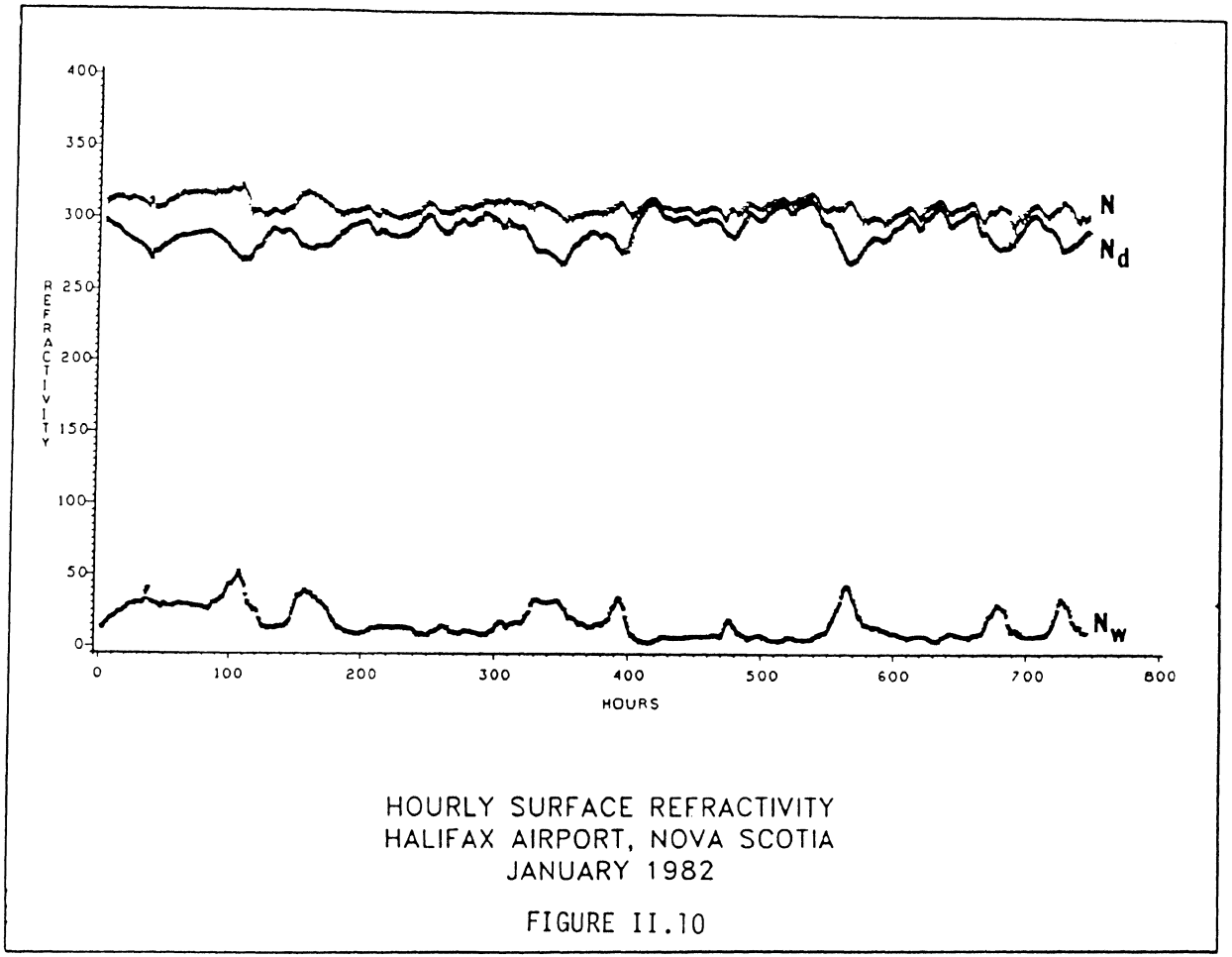

HOURLY SURFACE REFRACTIVITY
HALIFAX AIRPORT, NOVA SCOTIA
JANUARY 1982

FIGURE II.10

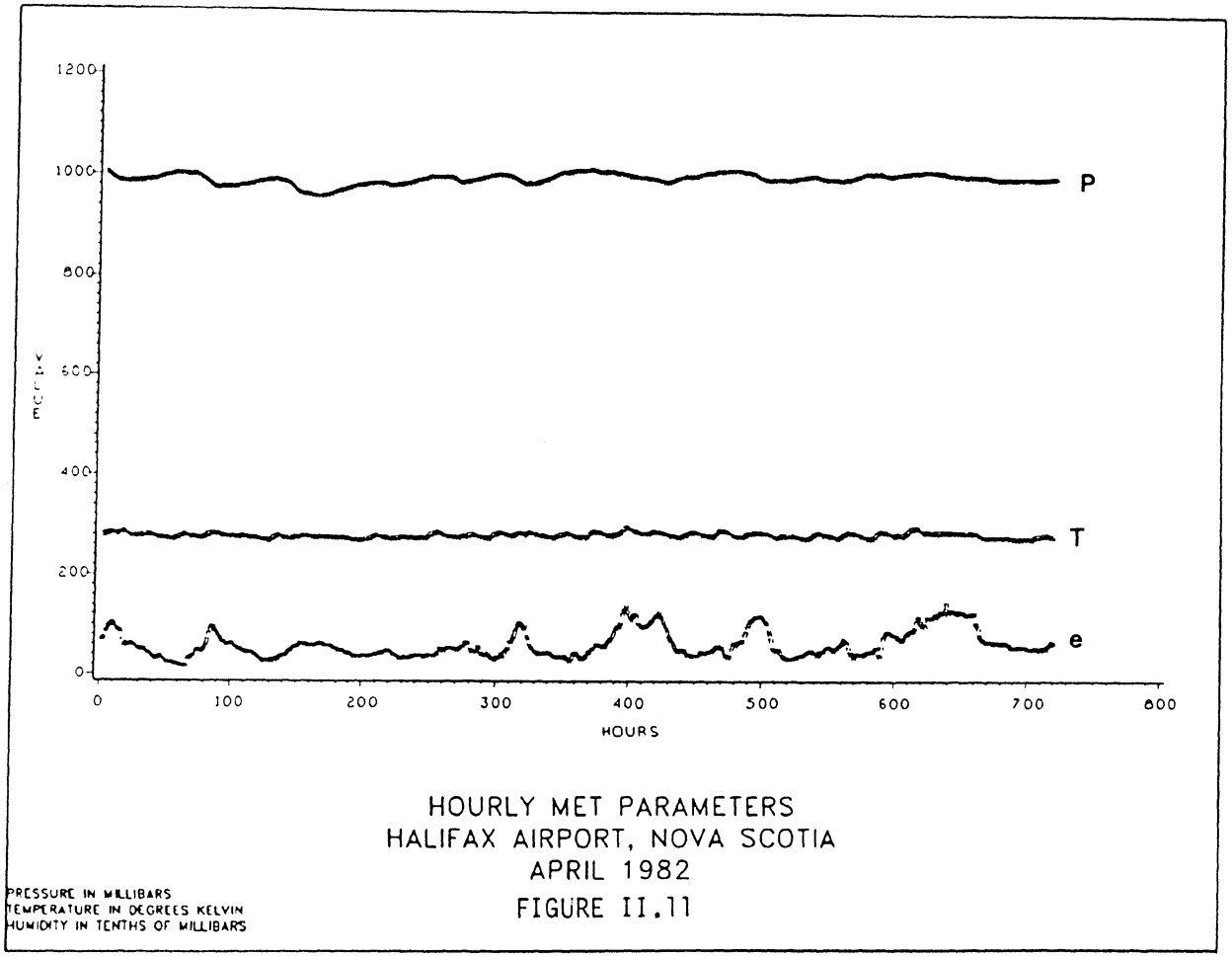

HOURLY MET PARAMETERS
HALIFAX AIRPORT, NOVA SCOTIA
APRIL 1982
FIGURE II.11

PRESSURE IN MILLIBARS
TEMPERATURE IN DEGREES KELVIN
HUMIDITY IN TENTHS OF MILLIBARS

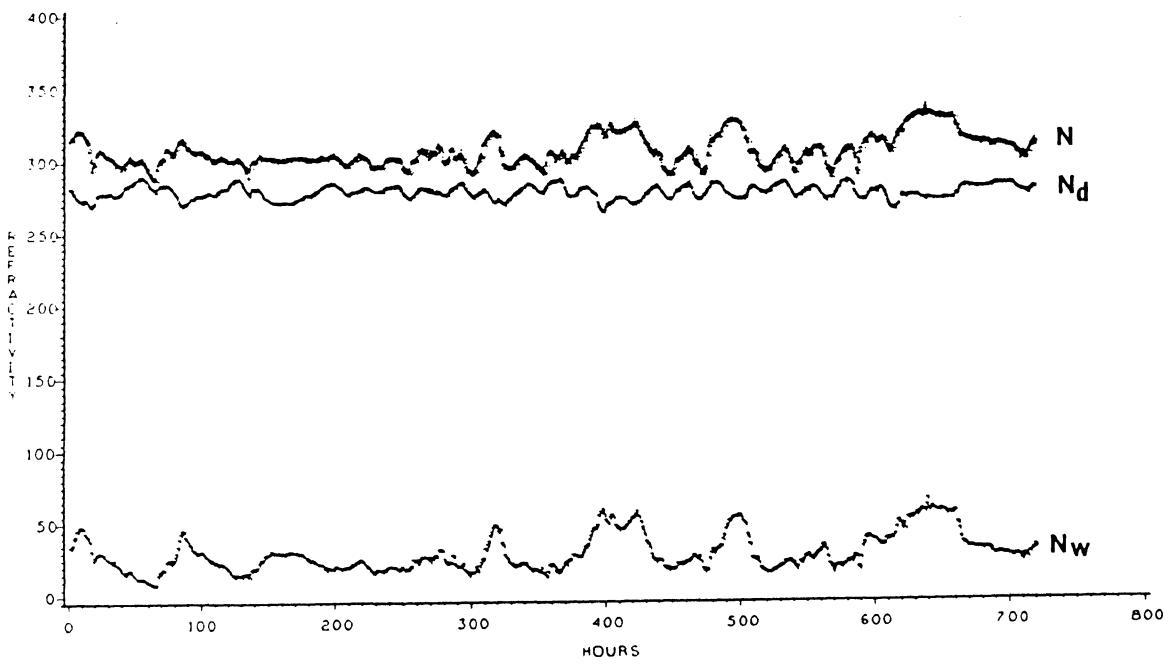

HOURLY SURFACE REFRACTIVITY
HALIFAX APORT, NOVA SCOTIA
APRIL 1982
FIGURE II.13

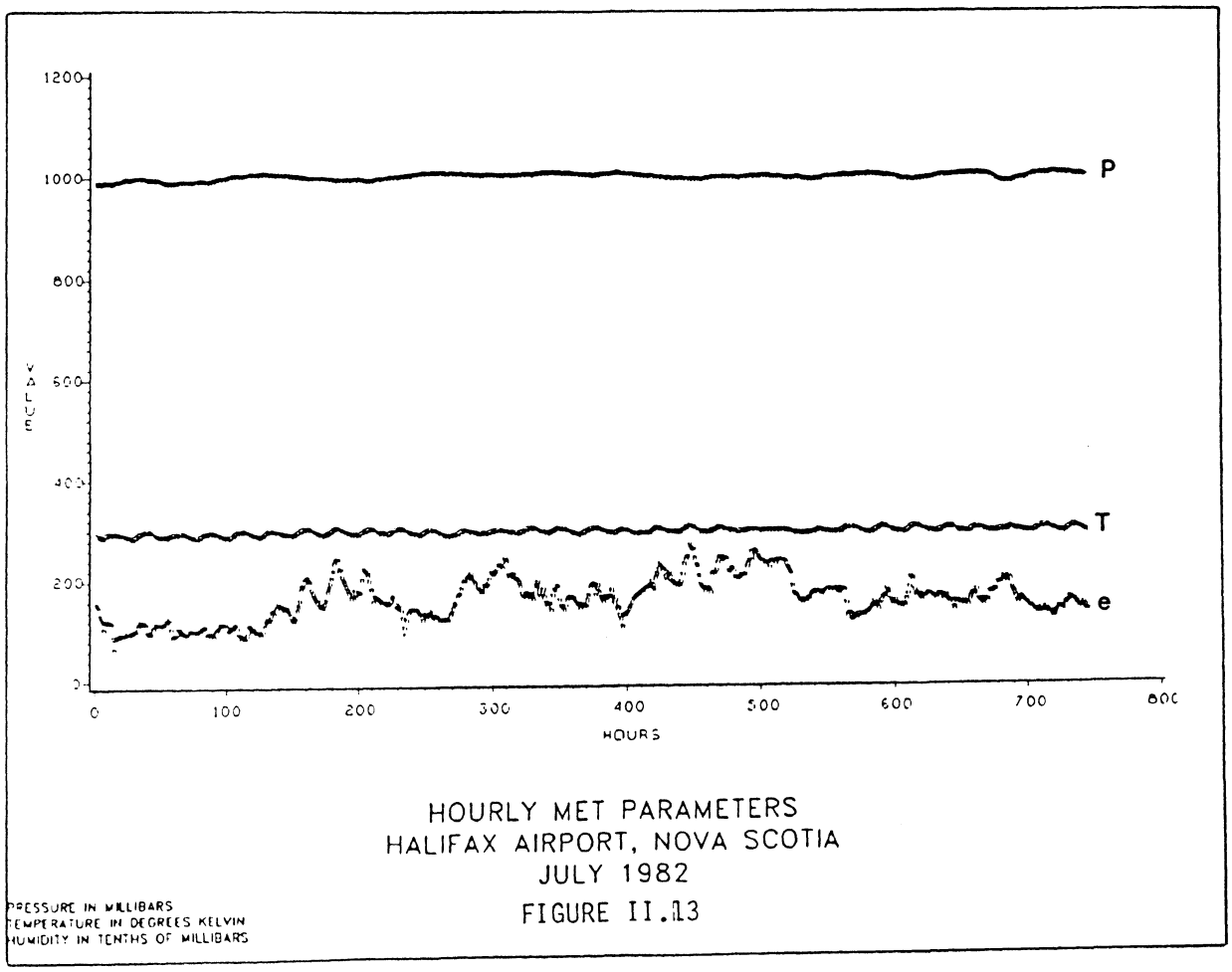

HOURLY MET PARAMETERS
HALIFAX AIRPORT, NOVA SCOTIA
JULY 1982
FIGURE II.13

PRESSURE IN MILLIBARS
TEMPERATURE IN DEGREES KELVIN
HUMIDITY IN TENTHS OF MILLIBARS

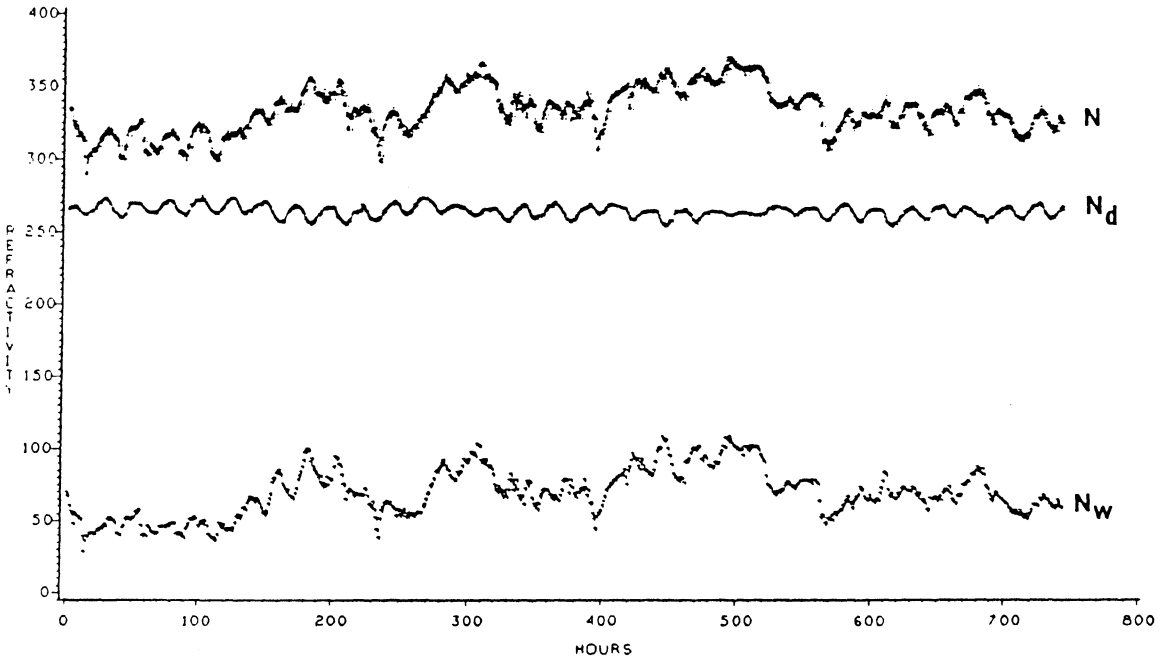

HOURLY SURFACE REFRACTIVITY
HALIFAX APORT, NOVA SCOTIA
JULY 1982

FIGURE II.14

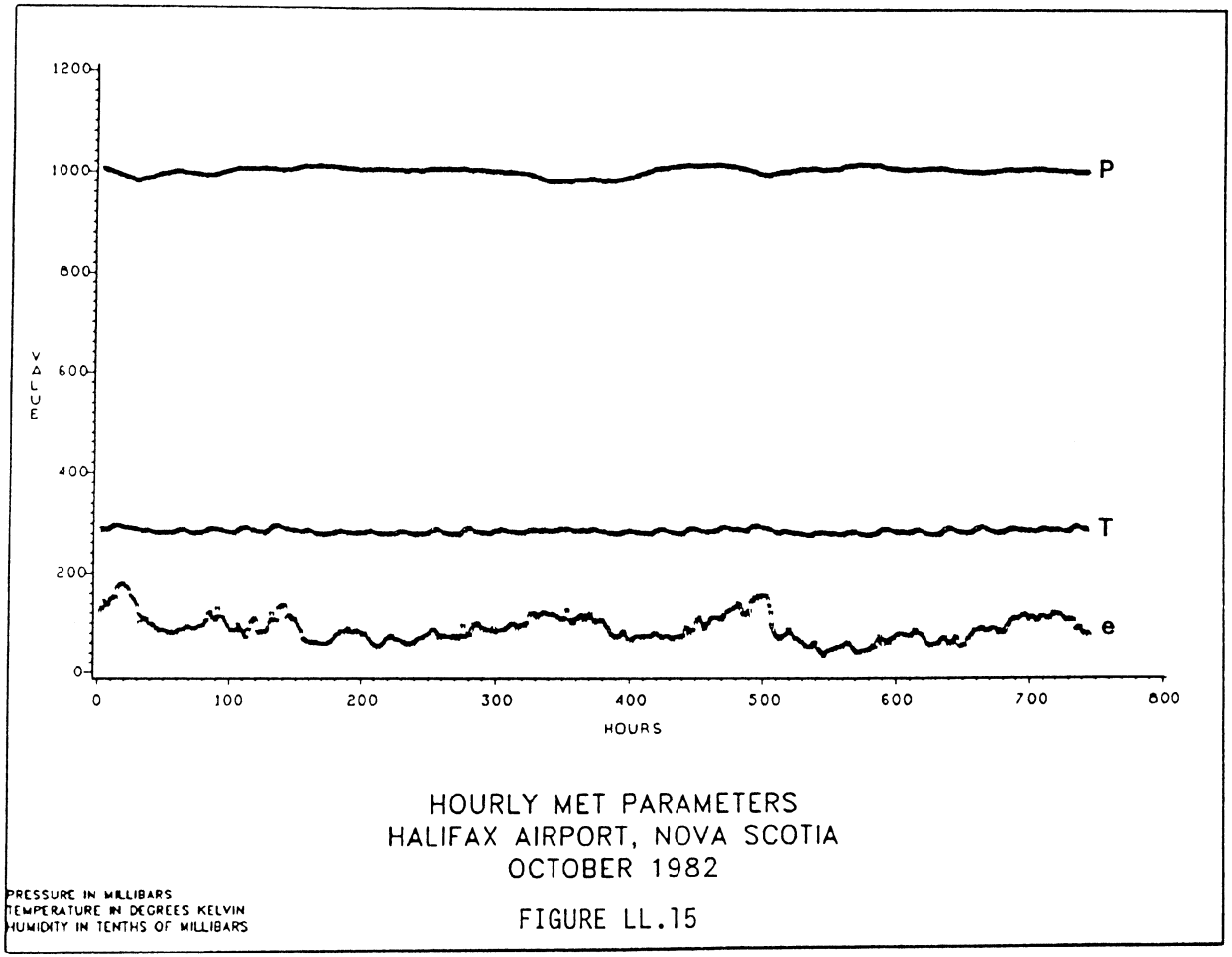

HOURLY MET PARAMETERS
HALIFAX AIRPORT, NOVA SCOTIA
OCTOBER 1982

PRESSURE IN MILLIBARS
TEMPERATURE IN DEGREES KELVIN
HUMIDITY IN TENTHS OF MILLIBARS

FIGURE LL.15

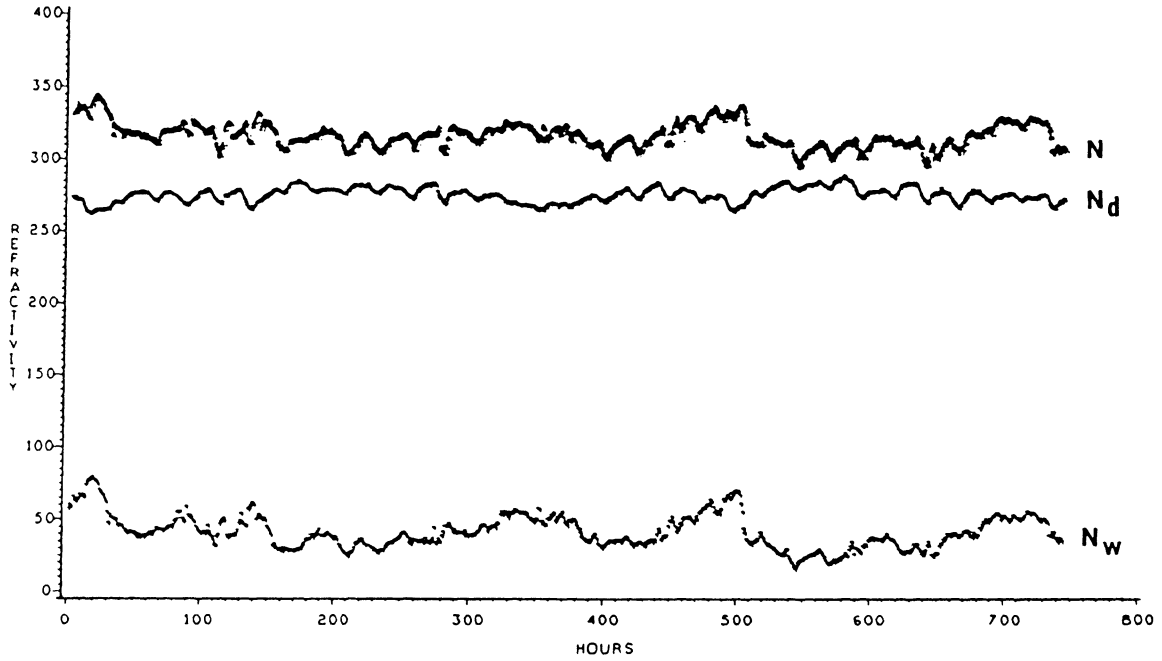

HOURLY SURFACE REFRACTIVITY
HALIFAX APORT, NOVA SCOTIA
OCTOBER 1982

FIGURE II.16

TABLE II.7

Statistical Summary of Hourly Surface Refractivity Variations

Sable Island, Nova Scotia

1982

Month	Mean	St.Dev	Minimum	Maximum	Range
Jan	313	5	296	326	36
Feb	315	5	302	331	29
Mar	316	5	302	334	32
Apr	317	7	301	334	33
May	323	5	308	336	28
Jun	330	5	317	343	26
Jul	343	9	323	363	40
Aug	348	10	312	370	58
Sep	349	12	314	369	55
Oct	329	10	309	362	53
Nov	326	11	306	351	45
Dec	320	8	306	343	37
Ann	327	13	301	370	69

TABLE II.8

Statistical Summary of Dry Refractivity Variations

Sable Island, Nova Scotia

1982

Month	Mean	St.Dev	Minimum	Maximum	Range
Jan	288	7	266	301	35
Feb	290	6	276	303	27
Mar	289	5	278	304	26
Apr	284	3	274	292	18
May	282	3	274	291	17
Jun	279	3	266	287	21
Jul	274	3	267	280	13
Aug	272	3	265	282	17
Sep	273	3	266	280	14
Oct	277	4	266	291	25
Nov	281	5	270	296	26
Dec	285	6	272	300	28
Ann	281	6	265	304	39

TABLE II.9

Statistical Summary of Hourly Wet Refractivity Variations

Sable Island, Nova Scotia

1982

Month	Mean	St.Dev	Minimum	Maximum	Range
Jan	26	10	8	53	45
Feb	25	9	7	49	42
Mar	27	9	8	54	46
Apr	33	8	16	54	38
May	41	7	23	61	38
Jun	51	7	36	72	36
Jul	70	10	48	94	46
Aug	76	12	40	101	61
Sep	76	14	38	101	63
Oct	52	13	29	94	65
Nov	44	15	14	76	62
Dec	34	13	10	67	57
Ann	46	19	7	101	94

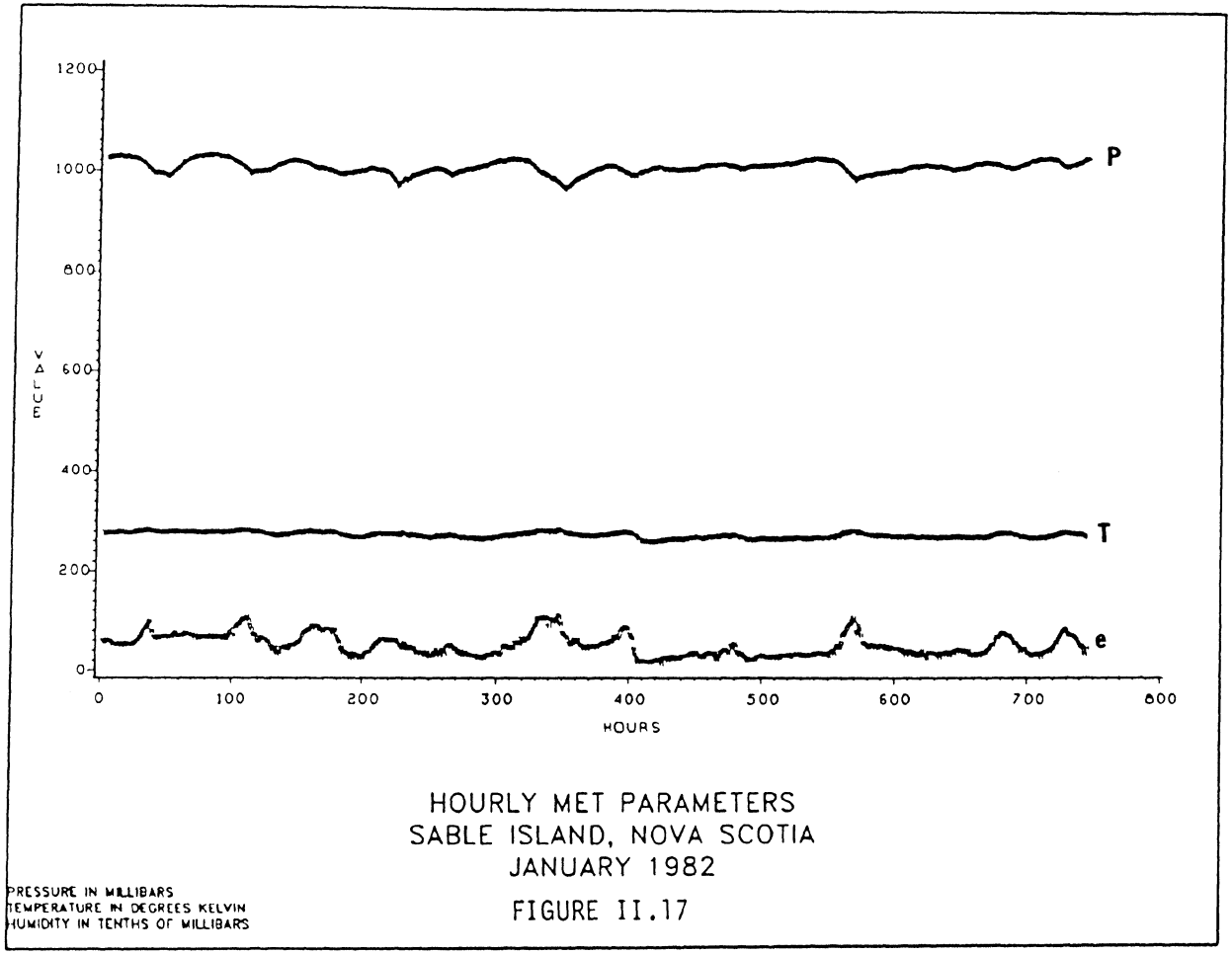

HOURLY MET PARAMETERS
SABLE ISLAND, NOVA SCOTIA
JANUARY 1982

FIGURE II.17

PRESSURE IN MILLIBARS
TEMPERATURE IN DEGREES KELVIN
HUMIDITY IN TENTHS OF MILLIBARS

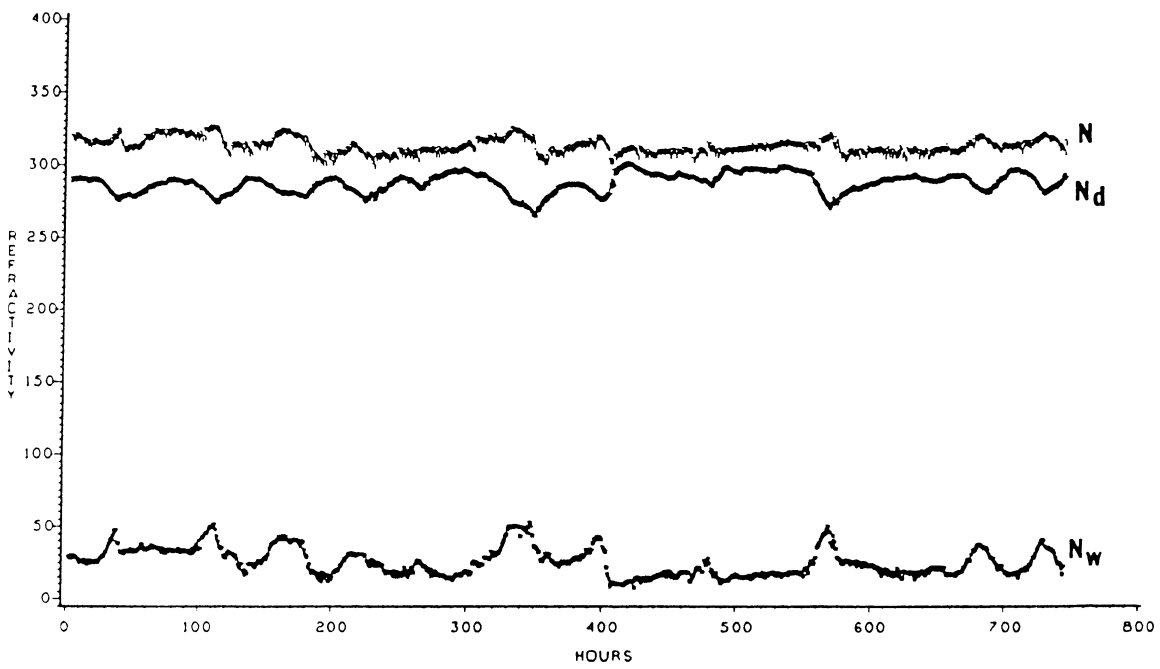

HOURLY SURFACE REFRACTIVITY
SABLE ISLAND, NOVA SCOTIA
JANUARY 1982

FIGURE II.18

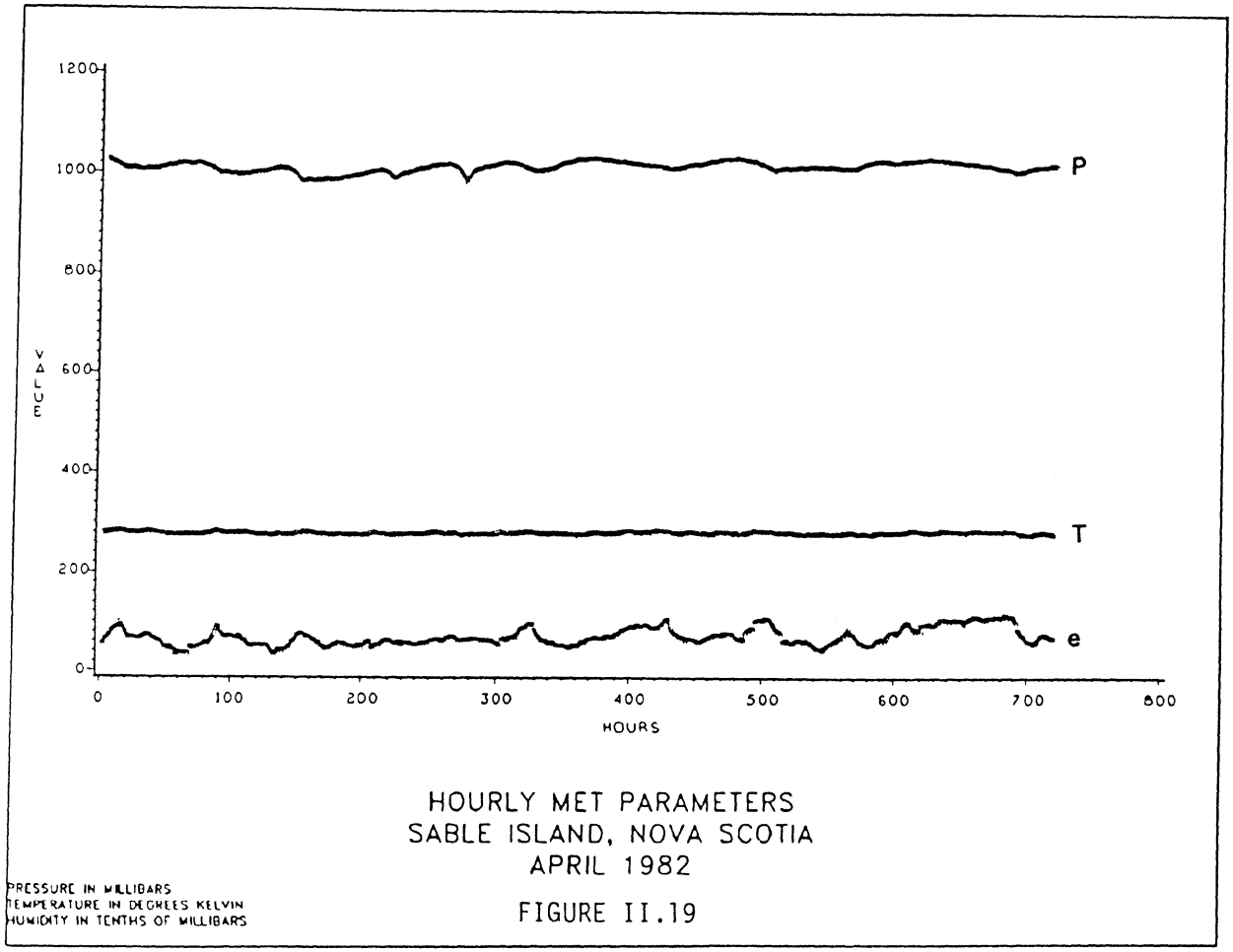

HOURLY MET PARAMETERS
SABLE ISLAND, NOVA SCOTIA
APRIL 1982

FIGURE II.19

PRESSURE IN MILLIBARS
TEMPERATURE IN DEGREES KELVIN
HUMIDITY IN TENTHS OF MILLIBARS

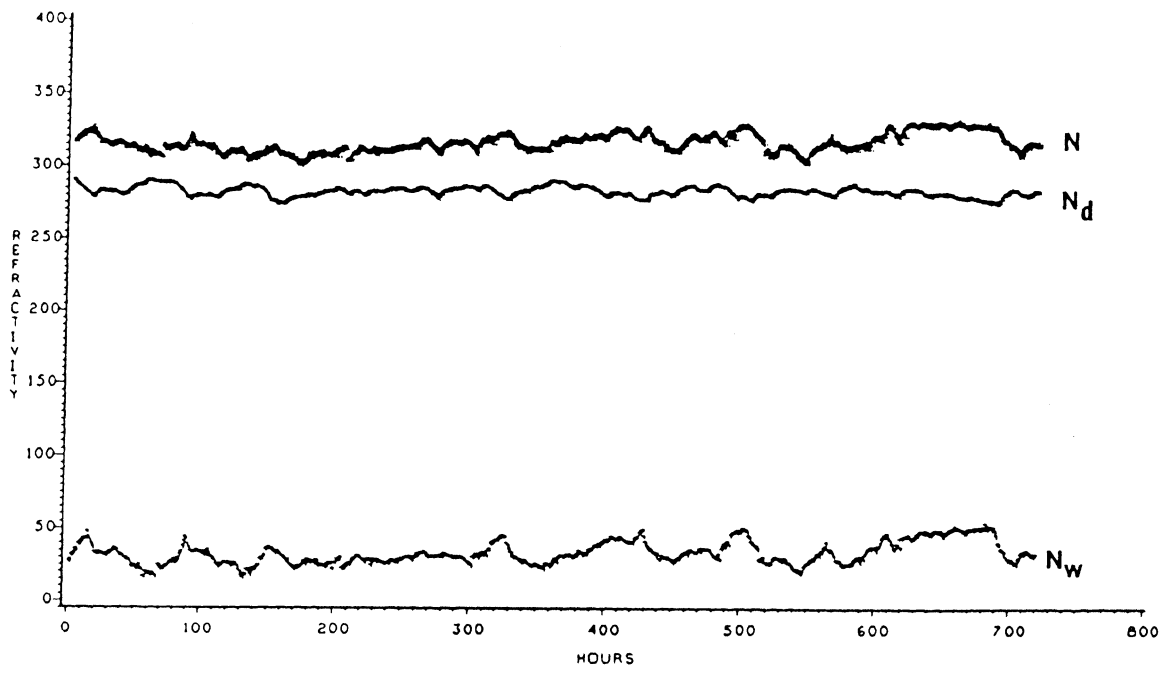

HOURLY SURFACE REFRACTIVITY
SABLE ISLAND, NOVA SCOTIA
APRIL 1982
FIGURE II.20

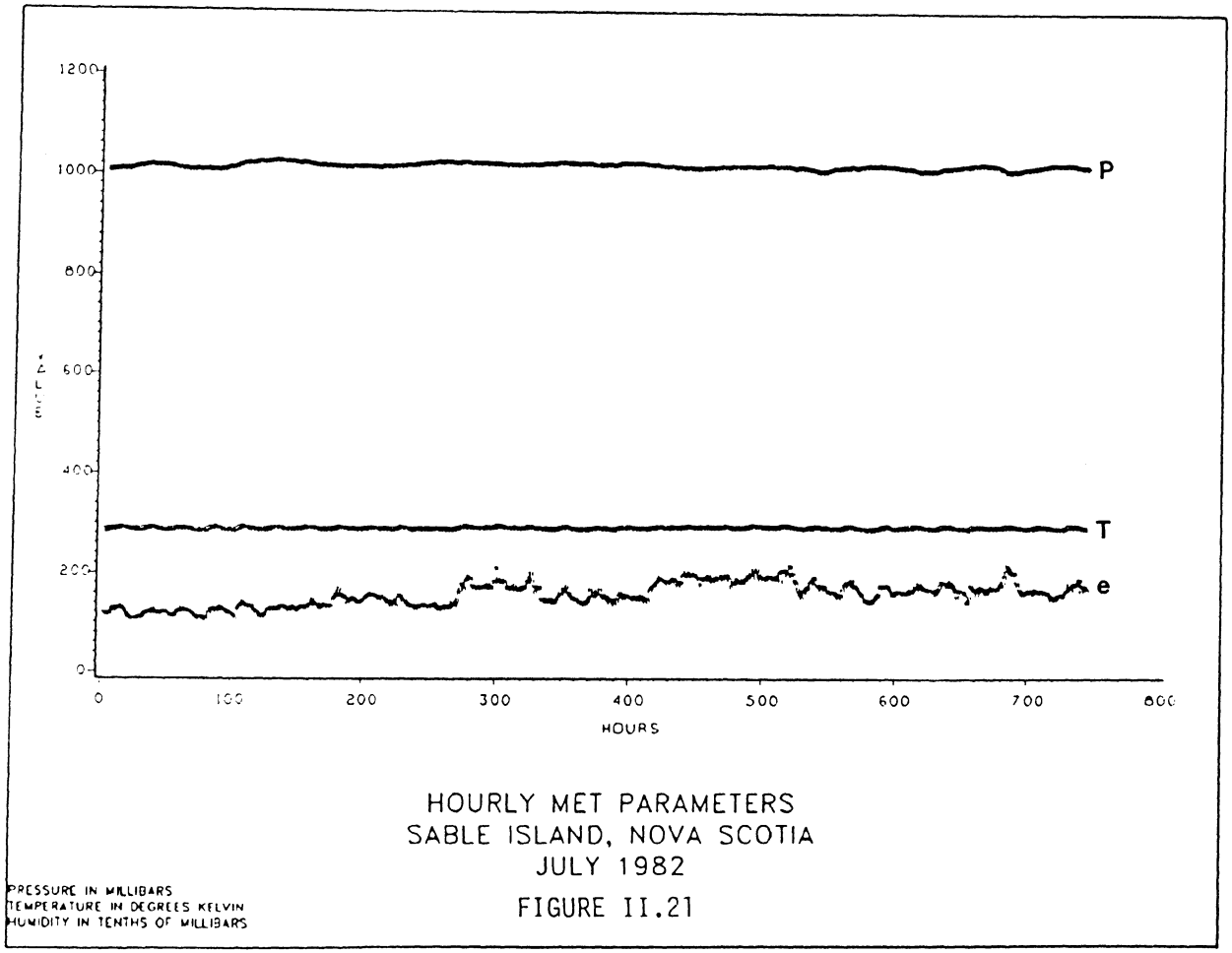

HOURLY MET PARAMETERS
SABLE ISLAND, NOVA SCOTIA
JULY 1982

FIGURE II.21

PRESSURE IN MILLIBARS
TEMPERATURE IN DEGREES KELVIN
HUMIDITY IN TENTHS OF MILLIBARS

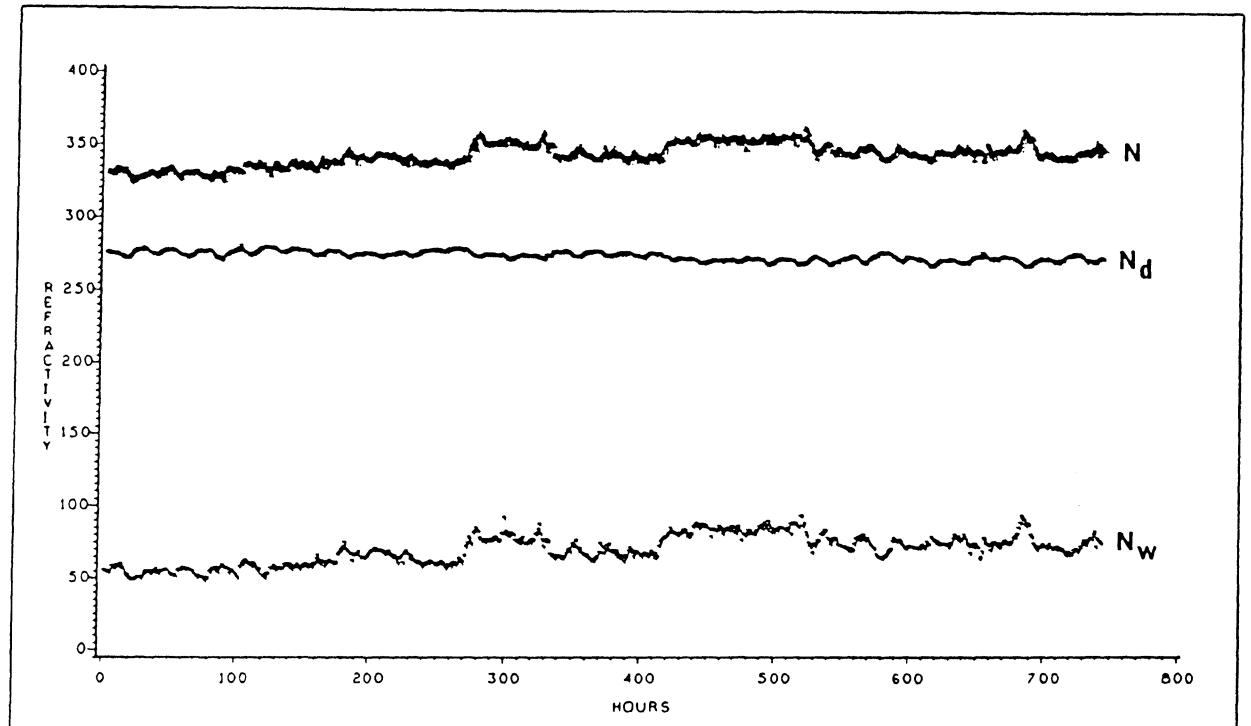

HOURLY SURFACE REFRACTIVITY
SABLE ISLAND, NOVA SCOTIA
JULY 1982

FIGURE II.22

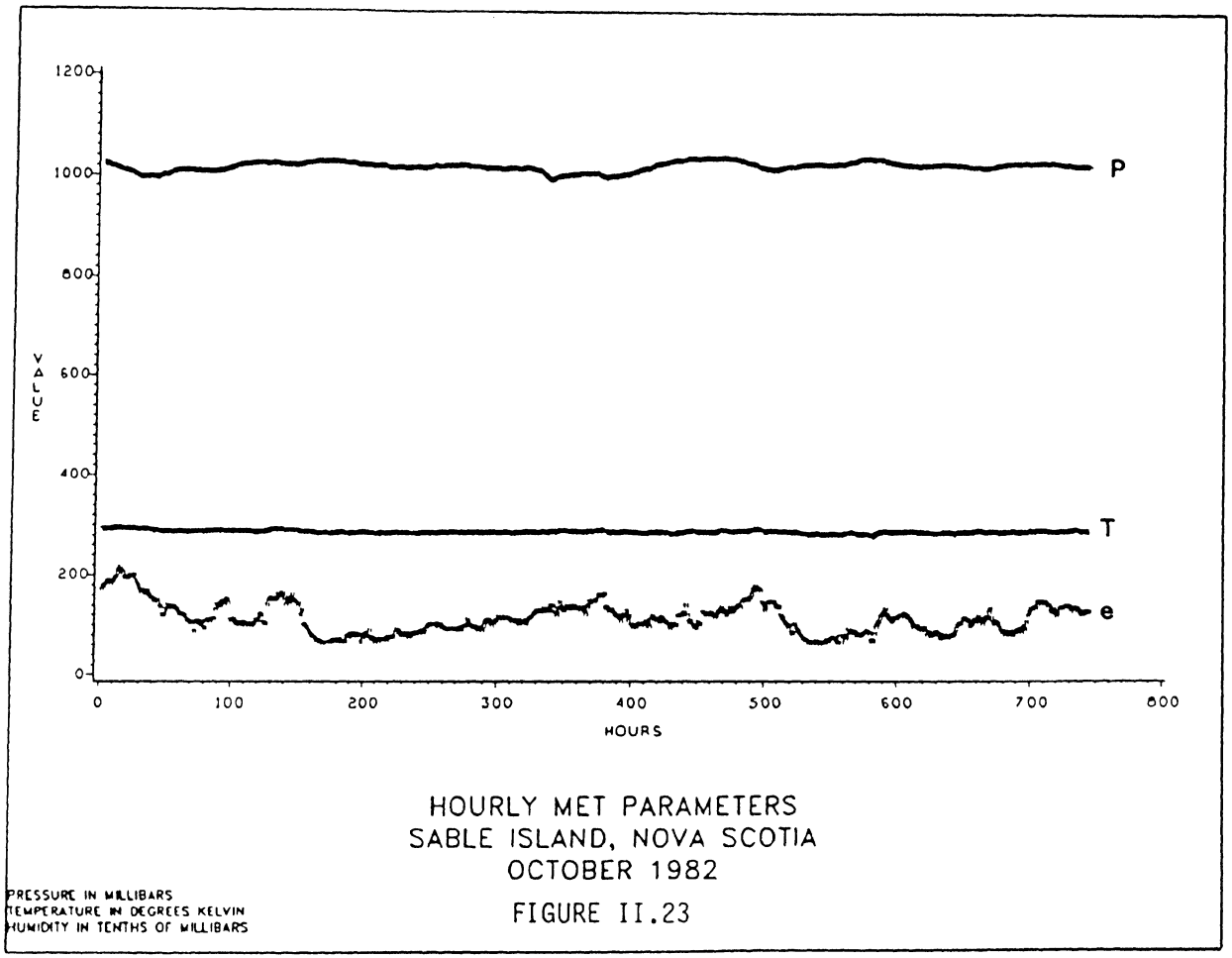

HOURLY MET PARAMETERS
SABLE ISLAND, NOVA SCOTIA
OCTOBER 1982

FIGURE II.23

PRESSURE IN MILLIBARS
TEMPERATURE IN DEGREES KELVIN
HUMIDITY IN TENTHS OF MILLIBARS

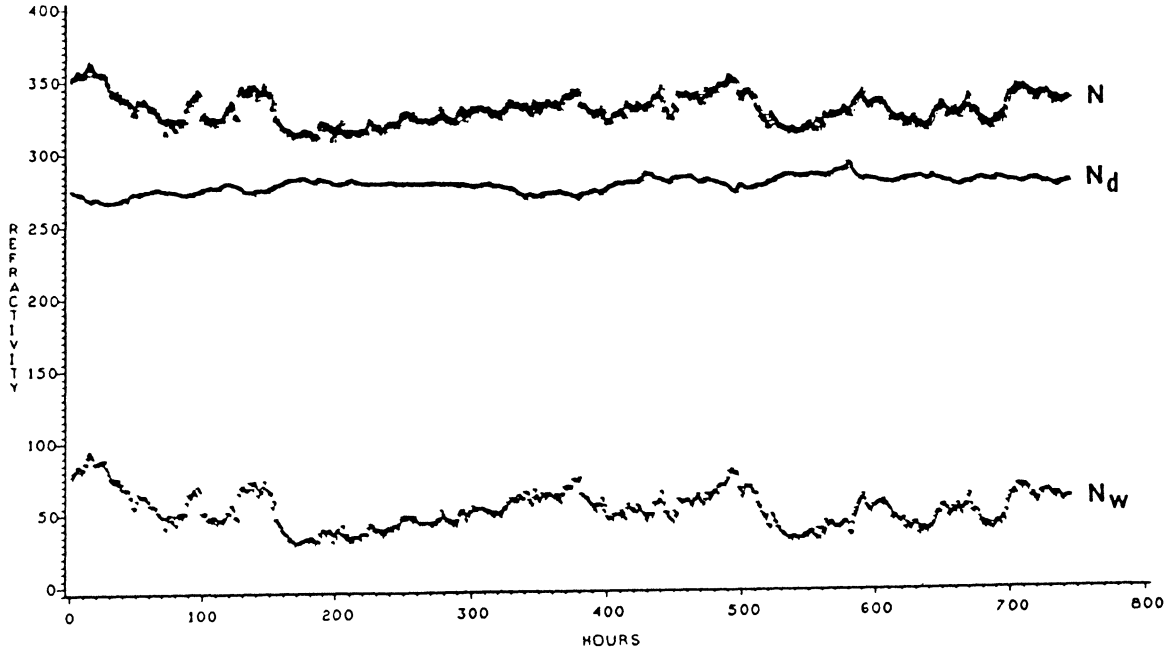

HOURLY SURFACE REFRACTIVITY
SABLE ISLAND, NOVA SCOTIA
OCTOBER 1982

FIGURE II.24

TABLE II.10

Regional Surface Refractivity Correlations and Maximum Hourly Differences

Shelburne, Halifax Airport, and Sable Island, Nova Scotia

1982

First column indicates the value of the correlation coefficient for the month.
Second column indicates the maximum monthly difference in hourly values.

Month	Shel-Hfax (190 Km)	Shel-Sable (435 Km)	Hfax-Sable (305 Km)
Jan	---	---	0.50 | 24
Feb	---	---	0.69 | 23
Mar	0.89 | 20	0.71 | 20	0.70 | 29
Apr	0.85 | 27	0.70 | 31	0.75 | 32
May	0.74 | 34	0.58 | 28	0.62 | 31
Jun	0.78 | 40	0.57 | 32	0.53 | 37
Jul	0.84 | 40	0.72 | 36	0.76 | 43
Aug	0.83 | 34	0.44 | 58	0.59 | 61
Sep	0.80 | 30	0.66 | 39	0.70 | 41
Oct	0.78 | 28	0.64 | 31	0.64 | 36
Nov	0.93 | 22	0.80 | 27	0.84 | 35
Dec	0.90 | 17	0.62 | 23	0.69 | 29

TABLE II.11

Regional Dry Refractivity Correlations and Maximum Hourly Differences

Shelburne, Halifax Airport, and Sable Island, Nova Scotia

1982

First column indicates the value of the correlation coefficient for the month.
Second column indicates the maximum monthly difference in hourly values.

Month	Shel-Hfax (190 Km)	Shel-Sable (435 Km)	Hfax-Sable (305 Km)
Jan	---	---	0.87 | 16
Feb	---	---	0.91 | 13
Mar	0.95 | 10	0.82 | 13	0.85 | 12
Apr	0.88 | 11	0.54 | 13	0.55 | 18
May	0.82 | 15	0.66 | 16	0.56 | 24
Jun	0.87 | 13	0.83 | 14	0.74 | 20
Jul	0.87 | 13	0.59 | 14	0.61 | 18
Aug	0.89 | 11	0.73 | 9	0.78 | 12
Sep	0.82 | 13	0.74 | 12	0.72 | 12
Oct	0.91 | 11	0.76 | 12	0.81 | 10
Nov	0.96 | 12	0.82 | 13	0.88 | 11
Dec	0.96 | 11	0.72 | 22	0.83 | 17

TABLE II.12

Regional Wet Refractivity Correlations and Maximum Hourly Differences

Shelburne, Halifax Airport, and Sable Island, Nova Scotia

1982

First column indicates the value of the correlation coefficient for the month.
Second column indicates the maximum monthly difference in hourly values.

Month	Shel-Hfax (190 Km)	Shel-Sable (435 Km)	Hfax-Sable (305 Km)
Jan	---	---	0.86 | 27
Feb	---	---	0.92 | 24
Mar	0.93 | 25	0.81 | 19	0.86 |20
Apr	0.90 | 20	0.71 | 25	0.77 | 26
May	0.84 | 22	0.67 | 27	0.70 | 25
Jun	0.84 | 32	0.73 | 30	0.68 | 32
Jul	0.84 | 32	0.74 | 30	0.77 | 32
Aug	0.85| 28	0.54 | 58	0.65 | 58
Sep	0.82 | 25	0.72 | 42	0.74 | 42
Oct	0.86 | 22	0.72 | 32	0.79 | 31
Nov	0.95 | 24	0.84 | 37	0.89 | 38
Dec	0.95 | 17	0.72 | 32	0.82 | 33

APPENDIX III

SUMMARY OF HOURLY VARIATIONS IN THE REFRACTIVITY GRADIENT:

SHELBURNE AND SABLE ISLAND, NOVA SCOTIA

1982

TABLE III.1

Statistical Summary of Variations in the Mean Refractivity Lapse to 1 Km.
Shelburne, Nova Scotia
1982

This table summarizes the range of daily variation in the mean gradient of refractivity determined by linear least squares fit to twice daily radiosonde soundings.

Month	Ascents	Mean	St.Dev.	Minimum	Maximum	Range
Jan	43	41.1	7.2	29.6	60.8	31.2
Feb	44	37.3	6.9	22.5	54.6	32.1
Mar	54	39.6	8.6	19.9	72.1	52.2
Apr	53	40.7	10.9	15.8	70.1	54.3
May	59	42.0	14.0	21.7	90.9	69.2
Jun	59	42.7	12.6	10.9	64.9	54.0
Jul	61	49.2	15.0	21.4	120.6	99.2
Aug	61	51.3	14.1	27.3	95.0	67.7
Sep	58	52.5	17.6	21.2	109.3	88.1
Oct	58	49.6	12.0	30.6	78.2	47.6
Nov	60	41.7	8.3	24.7	63.7	39.0
Dec	59	38.4	11.7	21.5	71.1	49.6
Annual		43.8	5.3	10.9	120.6	109.7

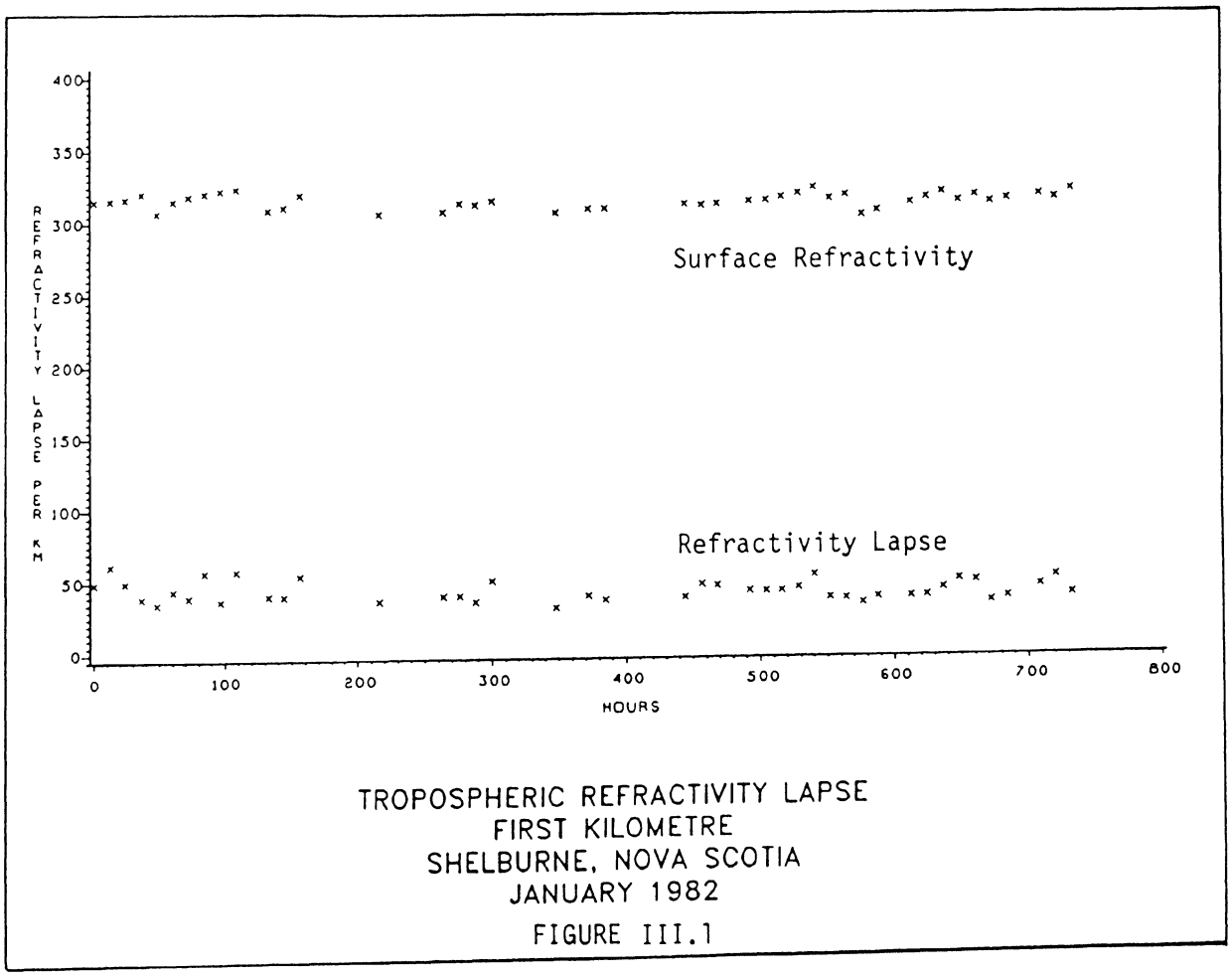

TROPOSPHERIC REFRACTIVITY LAPSE
FIRST KILOMETRE
SHELBURNE, NOVA SCOTIA
JANUARY 1982

FIGURE III.1

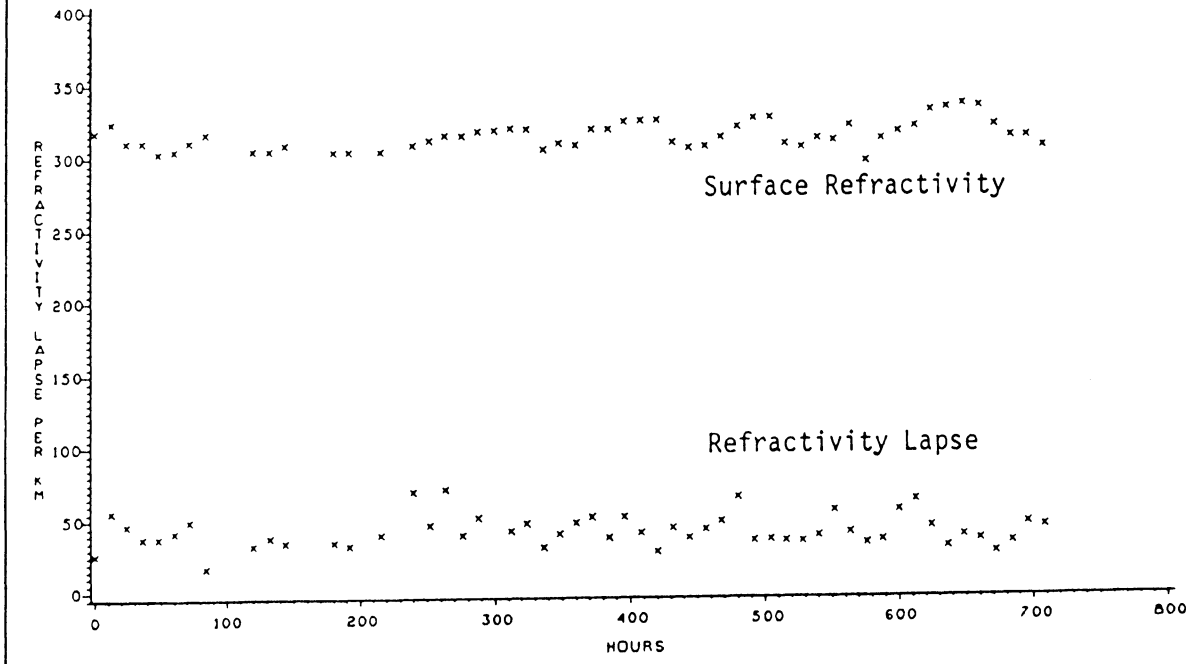

TROPOSPHERIC REFRACTIVITY LAPSE
FIRST KILOMETRE
SHELBURNE, NOVA SCOTIA
APRIL 1982

FIGURE III.2

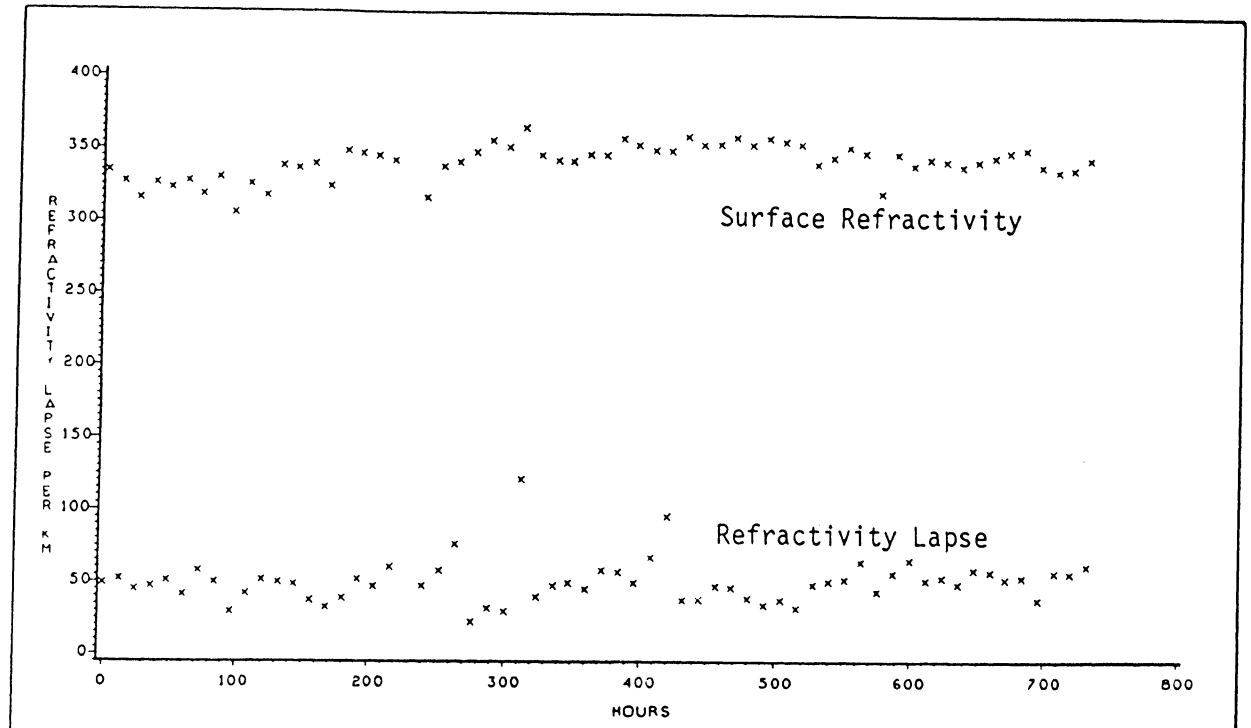

TROPOSPHERIC REFRACTIVITY LAPSE
FIRST KILOMETRE
SHELBURNE, NOVA SCOTIA
JULY 1982

FIGURE III.3

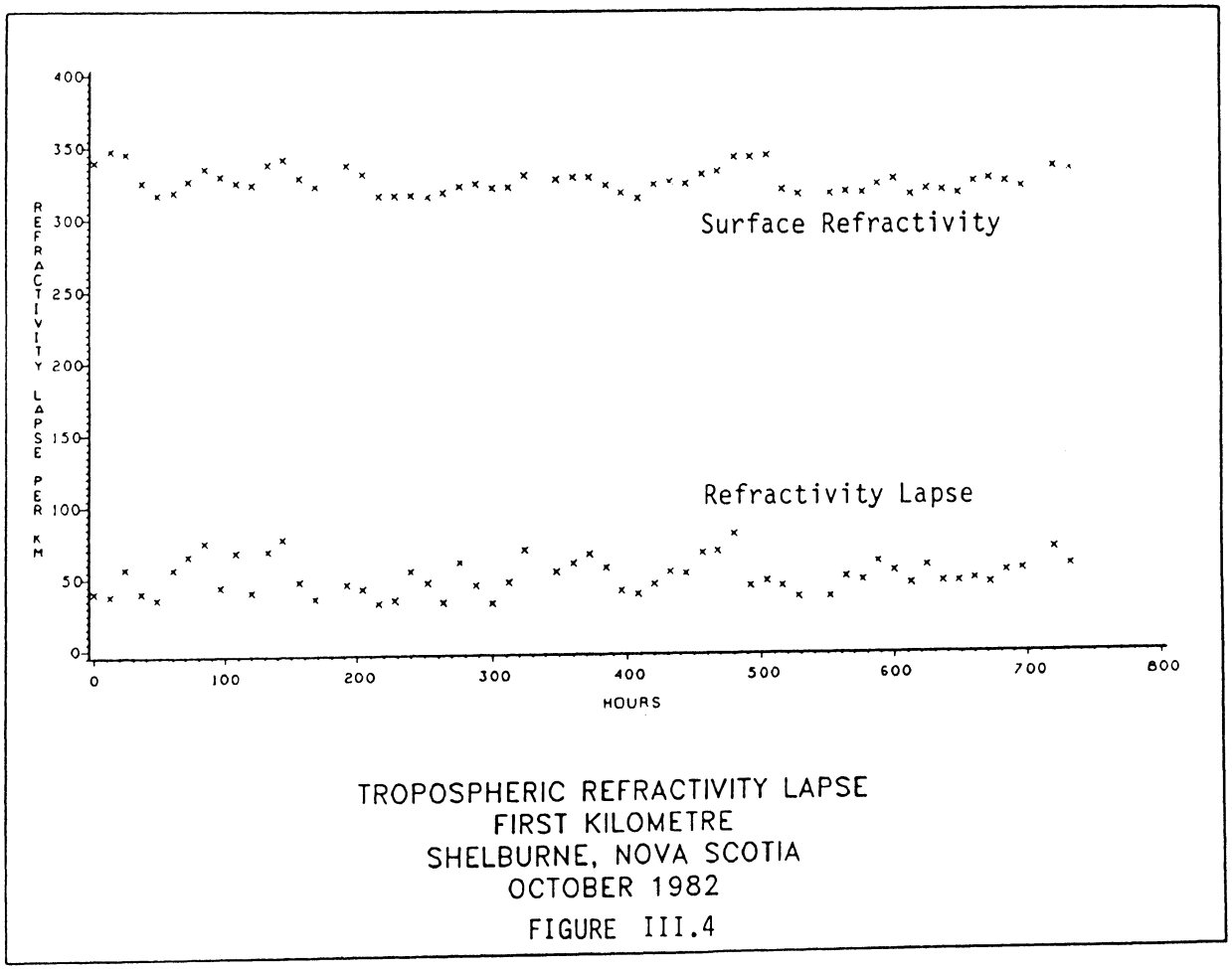

TROPOSPHERIC REFRACTIVITY LAPSE
FIRST KILOMETRE
SHELBURNE, NOVA SCOTIA
OCTOBER 1982

FIGURE III.4

TABLE III.2

Statistical summary of variations in the mean refractivity lapse to 1 Km.
Sable Island, Nova Scotia
1982

This table summarizes the range of daily variation in the mean gradient of refractivity determined by linear least squares fit to twice daily radiosonde soundings.

Month	Ascents	Mean	St.Dev.	Minimum	Maximum	Range
Jan	49	37.2	6.1	28.2	57.4	29.2
Feb	44	36.6	8.4	25.8	67.3	41.5
Mar	53	36.6	8.5	10.5	55.0	44.5
Apr	54	42.7	8.6	24.1	63.1	39.0
May	61	40.1	10.4	20.9	68.0	47.1
Jun	59	51.8	21.7	12.1	104.4	92.3
Jul	62	54.2	11.6	19.8	87.1	67.3
Aug	61	54.7	12.6	30.9	84.6	53.7
Sep	60	53.1	14.3	25.8	93.4	67.6
Oct	62	47.7	13.1	26.2	82.1	55.9
Nov	58	42.1	11.0	26.1	72.6	46.5
Dec	60	38.4	9.4	23.6	66.8	43.2
Annual		44.6	7.3	10.5	104.4	93.9

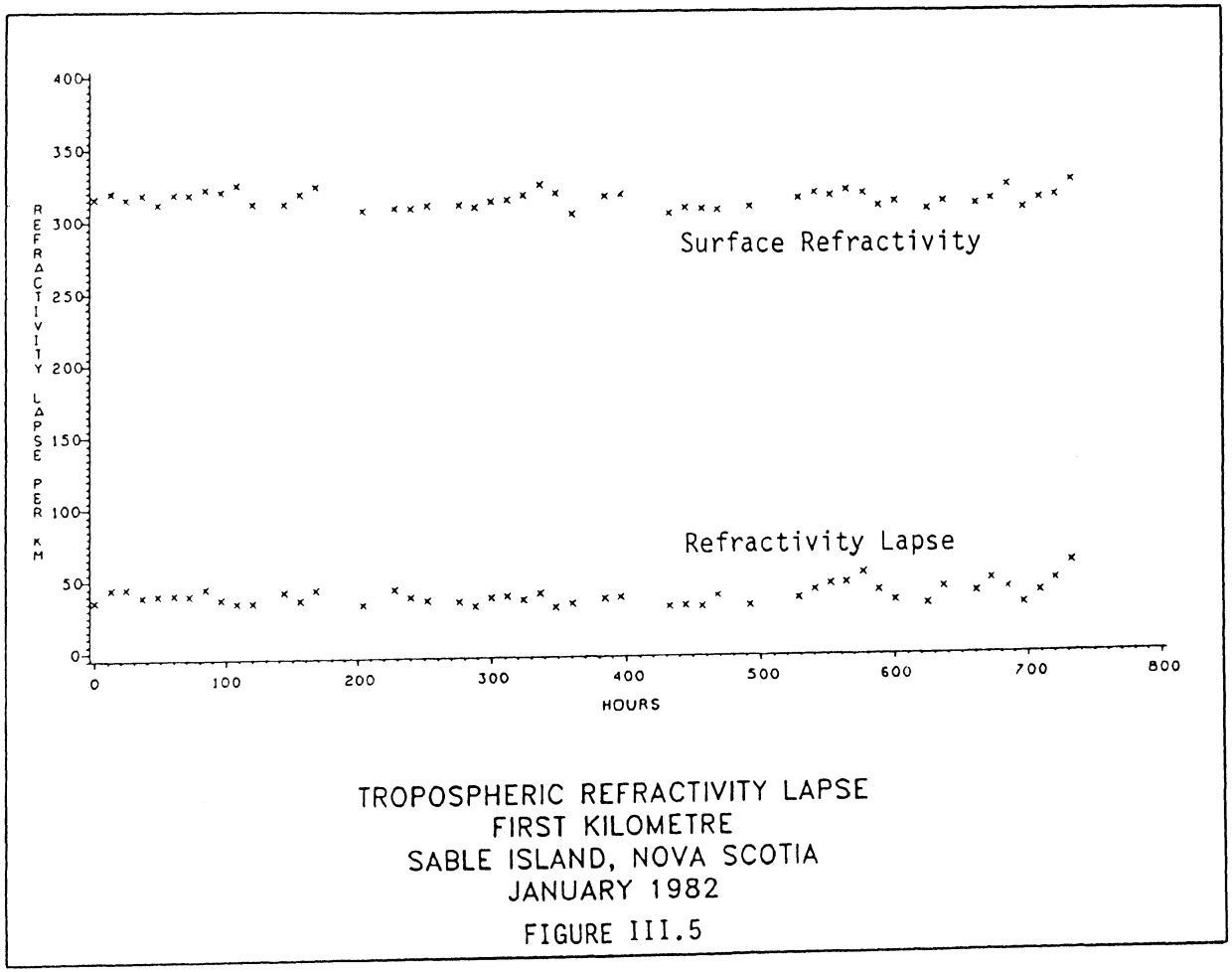

TROPOSPHERIC REFRACTIVITY LAPSE
FIRST KILOMETRE
SABLE ISLAND, NOVA SCOTIA
JANUARY 1982

FIGURE III.5

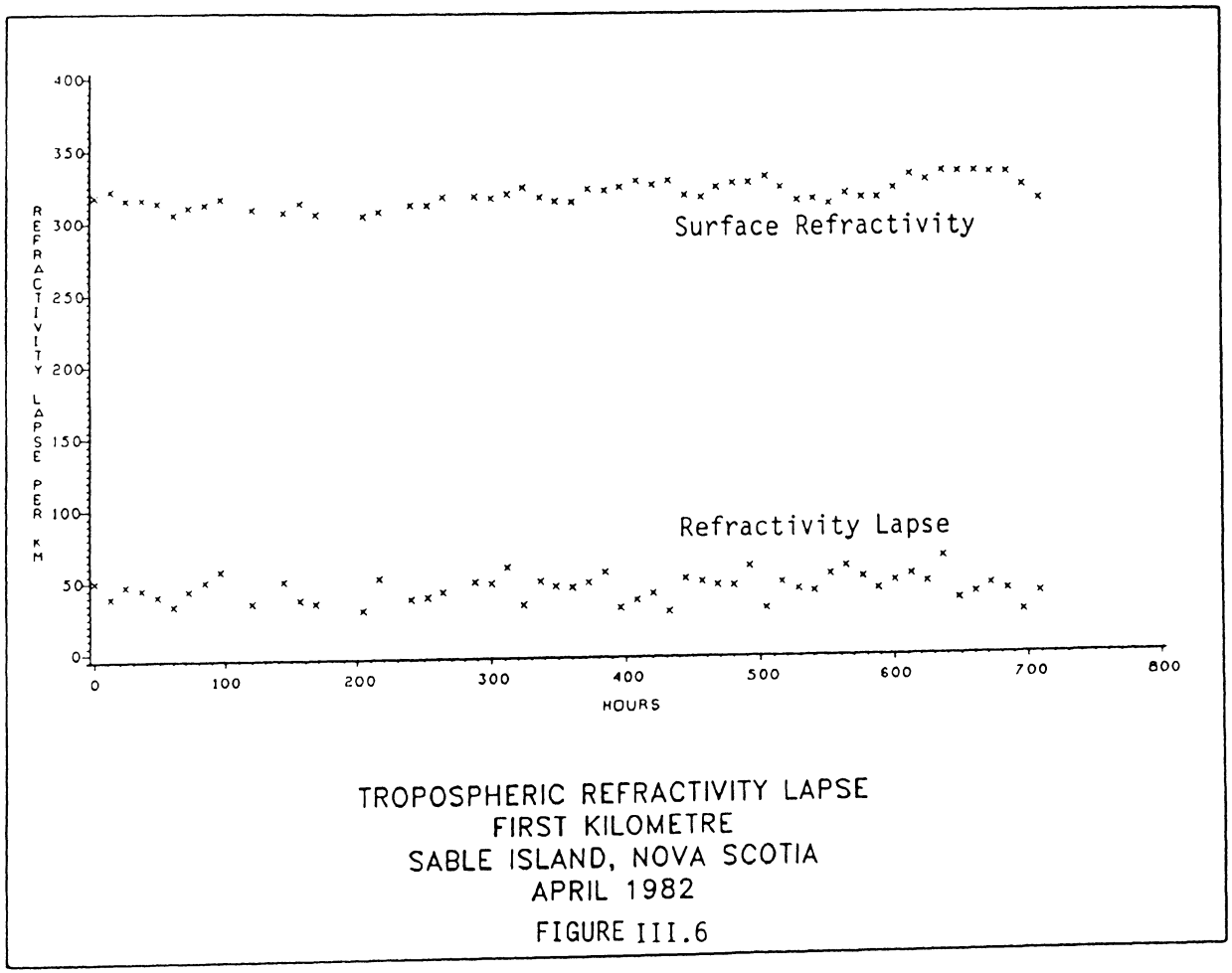

TROPOSPHERIC REFRACTIVITY LAPSE
FIRST KILOMETRE
SABLE ISLAND, NOVA SCOTIA
APRIL 1982

FIGURE III.6

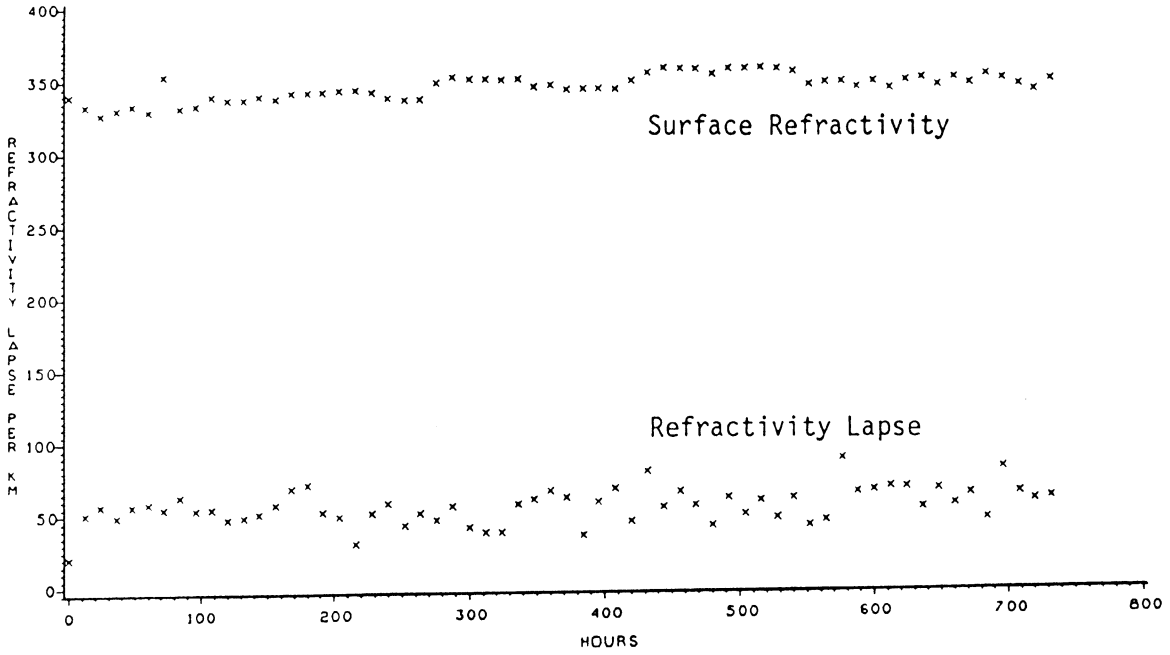

TROPOSPHERIC REFRACTIVITY LAPSE
FIRST KILOMETRE
SABLE ISLAND, NOVA SCOTIA
JULY 1982
FIGURE III.7

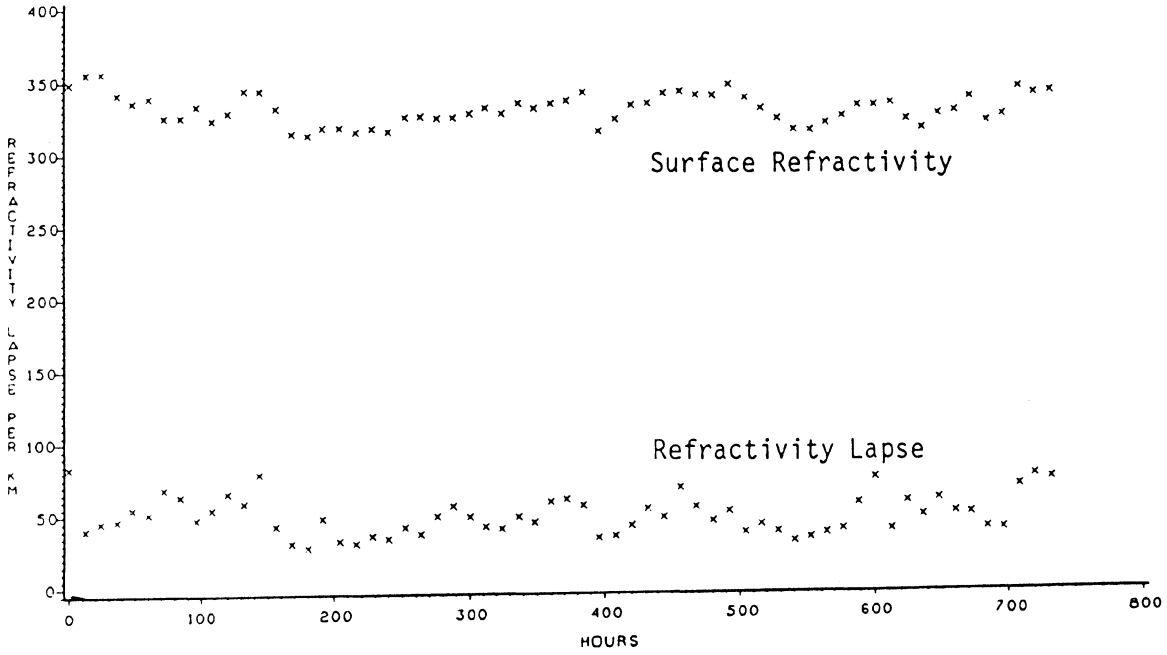

TROPOSPHERIC REFRACTIVITY LAPSE
FIRST KILOMETRE
SABLE ISLAND, NOVA SCOTIA
OCTOBER 1982

FIGURE III.8

TABLE III.3

Occurance of Extreme Refractivity Gradients
Shelburne, Nova Scotia
1982

This table lists the number of twice daily radiosonde ascents each month containing surface or elevated layers within the first kilometre of the troposphere whose gradients exceed the limits indicated.

Month	Ascents	-100 N/Km	-150 N/Km	-200 N/Km	Surface	Elevated
Jan	43	5	4	1	0	5
Feb	44	8	2	1	3	5
Mar	54	14	6	3	1	13
Apr	53	14	5	3	4	10
May	59	21	11	6	8	13
Jun	59	29	15	9	6	23
Jul	61	28	11	6	7	21
Aug	61	29	21	10	12	17
Sep	58	28	19	12	11	17
Oct	58	25	12	8	7	18
Nov	60	26	13	7	4	22
Dec	59	14	7	2	3	11
Annual	669	241	126	68	67	174

TABLE III.4

Occurance of Extreme Refractivity Gradients
Sable Island, Nova Scotia
1982

This table lists the number of twice daily radiosonde ascents each month containing surface or elevated layers within the first kilometre of the troposphere whose gradients exceed the limits indicated.

Month	Ascents	-100 N/Km	-150 N/Km	-200 N/Km	Surface	Elevated
Jan	49	14	7	1	3	11
Feb	44	12	4	1	0	12
Mar	53	9	3	1	0	9
Apr	54	13	4	1	5	8
May	61	21	8	5	2	19
Jun	59	31	20	16	3	28
Jul	62	40	23	11	18	22
Aug	61	32	12	7	12	20
Sep	60	29	17	8	13	16
Oct	62	22	14	6	3	19
Nov	58	24	14	6	5	19
Dec	60	13	7	0	1	12
Annual	683	260	133	63	61	199

TABLE III.5

Median Base Height and Thickness of Extreme Gradients
Shelburne, Nova Scotia
1982

First row indicates the mean base height and thickness of surface and elevated extreme gradient layers deduced from twice daily radiosonde soundings over the month. Second row is the standard deviation associated with these mean values.

Month	Surface Layers	Elevated Layers	
	Thickness (m)	Base Height (m)	Thickness (m)
Jan	---	712	75
		182	40
Feb	73	652	86
	29	290	35
Mar	---	647	105
		268	39
Apr	83	516	108
	15	302	24
May	141	540	145
	89	217	86
Jun	136	608	127
	87	284	48
Jul	96	424	152
	38	222	59
Aug	103	500	149
	39	295	90
Sep	136	607	167
	71	216	70
Oct	166	520	148
	156	202	53
Nov	97	722	122
	32	291	75
Dec	106	685	98
	33	219	26

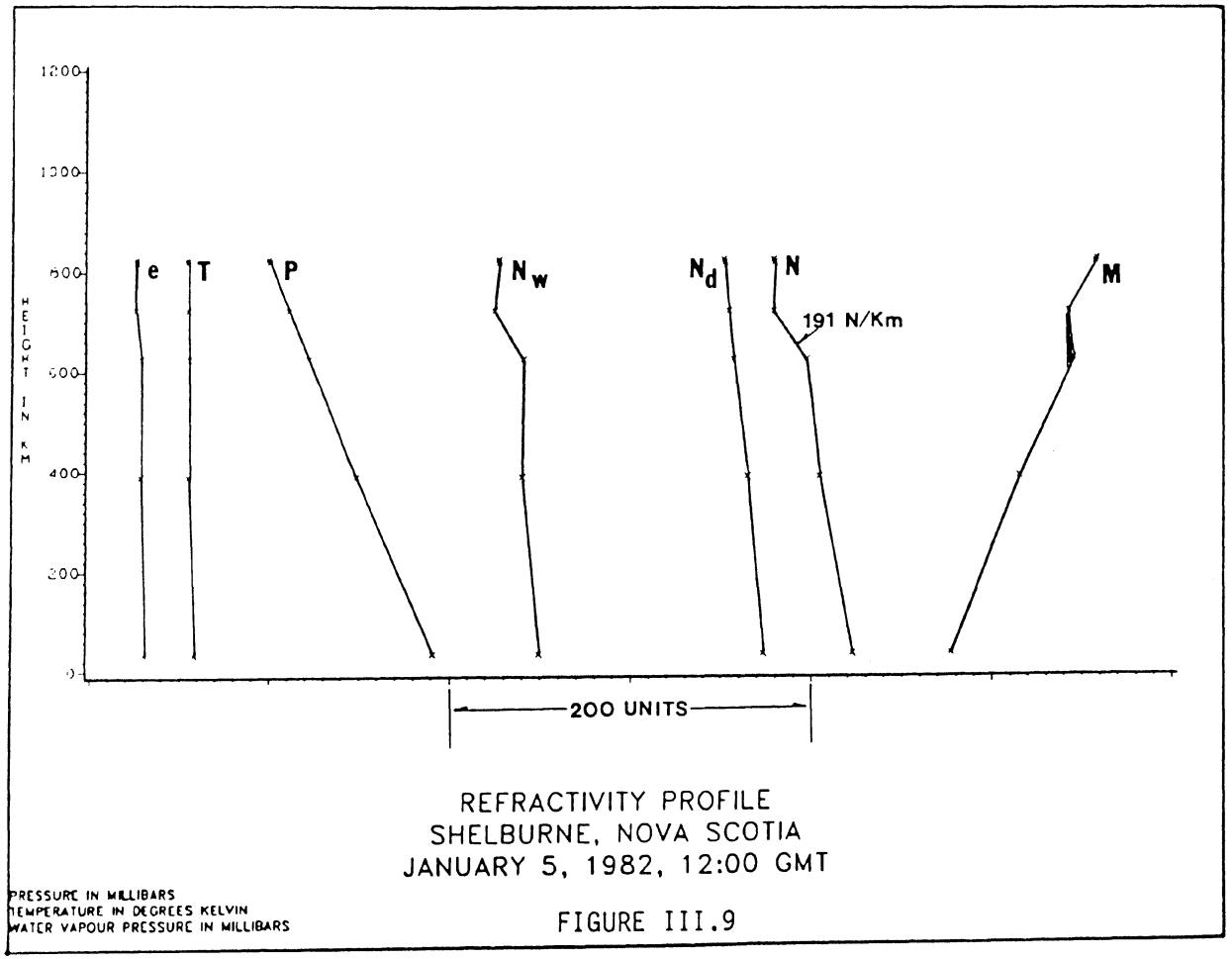

REFRACTIVITY PROFILE
SHELBURNE, NOVA SCOTIA
JANUARY 5, 1982, 12:00 GMT

PRESSURE IN MILLIBARS
TEMPERATURE IN DEGREES KELVIN
WATER VAPOUR PRESSURE IN MILLIBARS

FIGURE III.9

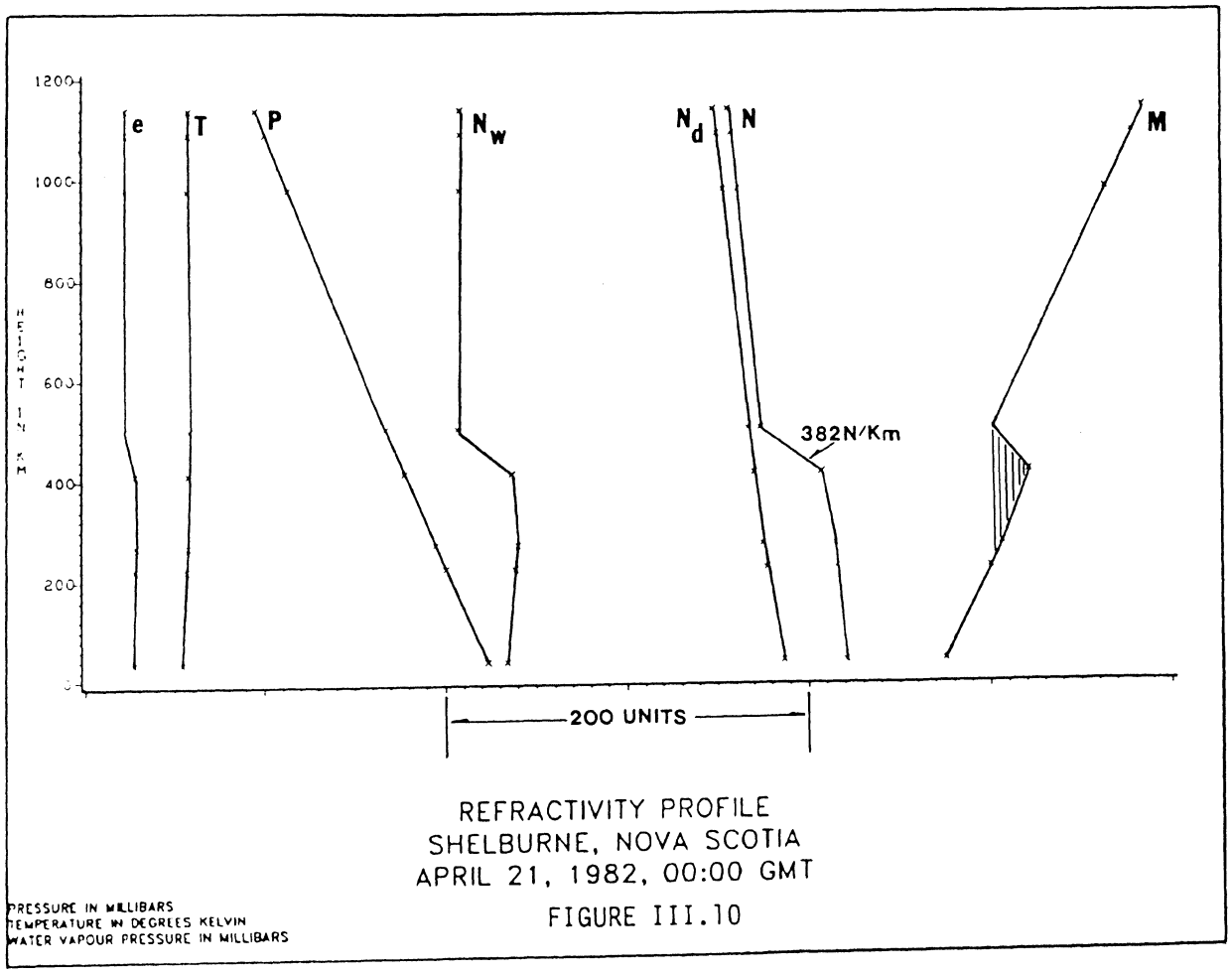

REFRACTIVITY PROFILE
SHELBURNE, NOVA SCOTIA
APRIL 21, 1982, 00:00 GMT

FIGURE III.10

PRESSURE IN MILLIBARS
TEMPERATURE IN DEGREES KELVIN
WATER VAPOUR PRESSURE IN MILLIBARS

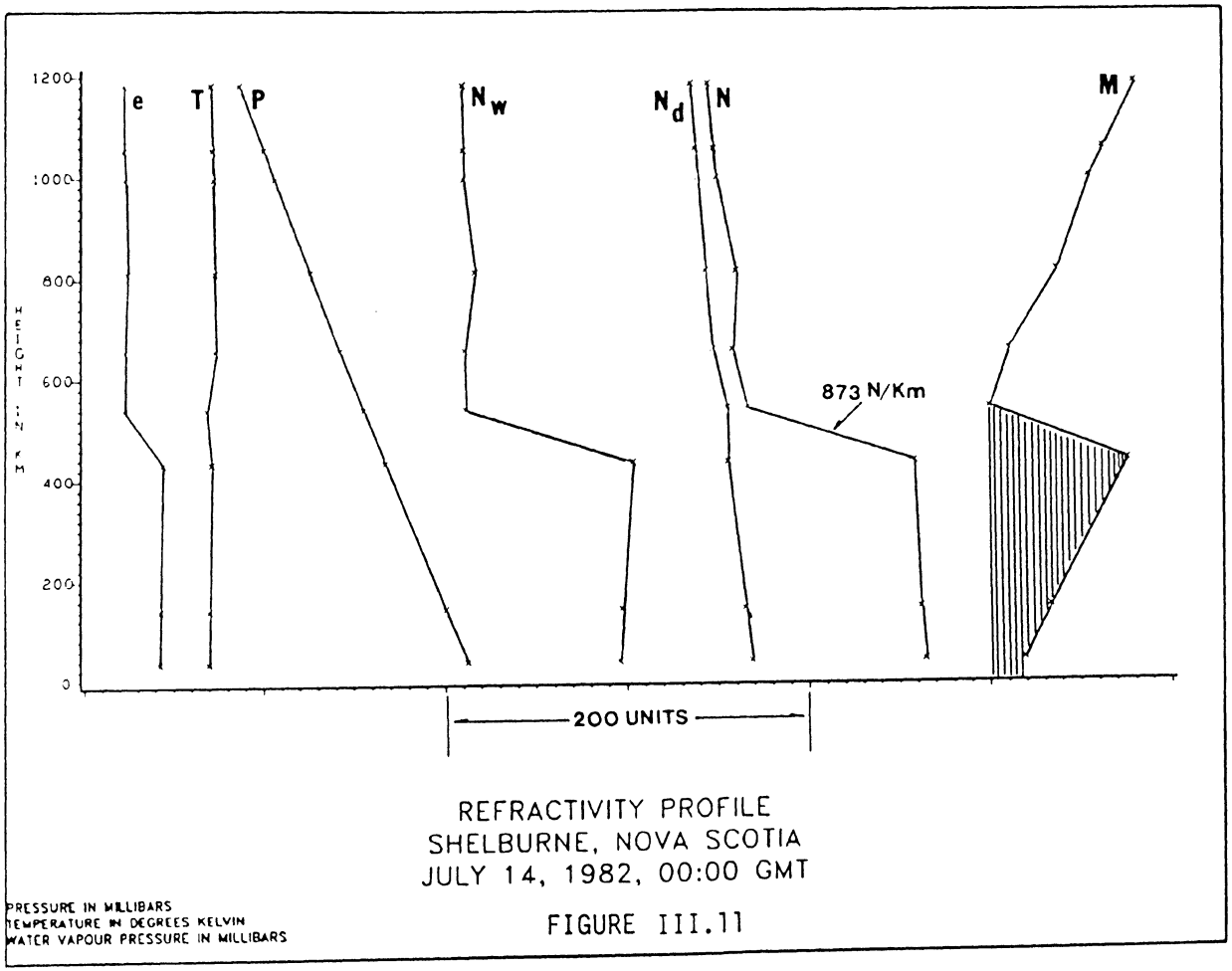

REFRACTIVITY PROFILE
SHELBURNE, NOVA SCOTIA
JULY 14, 1982, 00:00 GMT

FIGURE III.11

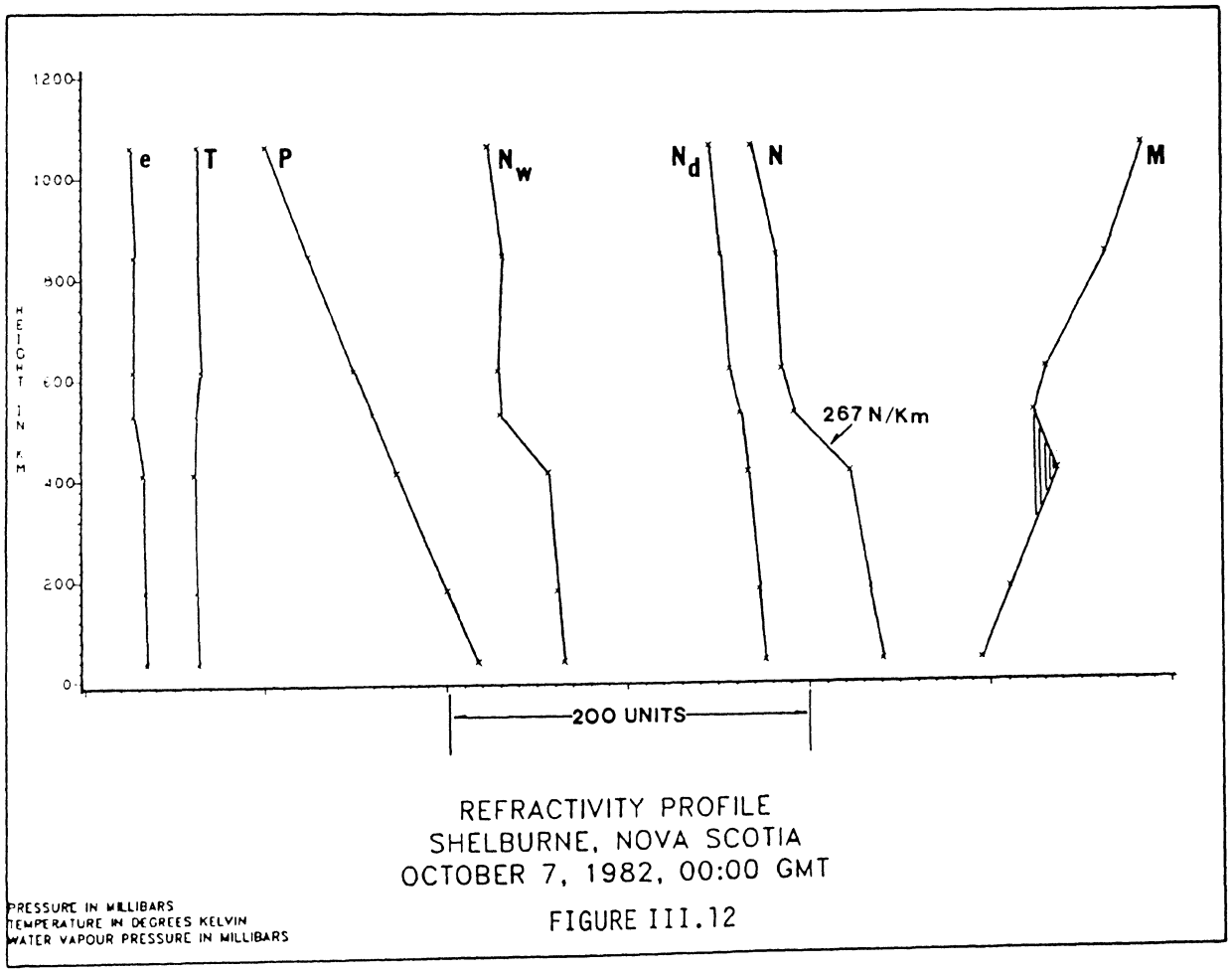

REFRACTIVITY PROFILE
SHELBURNE, NOVA SCOTIA
OCTOBER 7, 1982, 00:00 GMT

FIGURE III.12

PRESSURE IN MILLIBARS
TEMPERATURE IN DEGREES KELVIN
WATER VAPOUR PRESSURE IN MILLIBARS

TABLE III.6

Median Base Height and Thickness of Extreme Gradients
Sable Island, Nova Scotia
1982

First row indicates the mean base height and thickness of surface and elevated extreme gradient layers deduced from twice daily radiosonde soundings over the month. Second row is the standard deviation associated with these mean values.

Month	Surface Layers	Elevated Layers	
	Thickness (m)	Base Height (m)	Thickness (m)
Jan	54	701	103
	4	150	34
Feb	---	636	124
	---	265	59
Mar	---	622	110
	---	298	52
Apr	116	485	123
	82	252	60
May	123	678	113
	86	205	65
Jun	161	570	165
	68	194	93
Jul	149	593	235
	73	228	182
Aug	151	612	170
	71	284	82
Sep	190	580	172
	77	223	91
Oct	113	563	143
	67	259	77
Nov	164	686	109
	97	250	50
Dec	---	746	118
	---	341	51

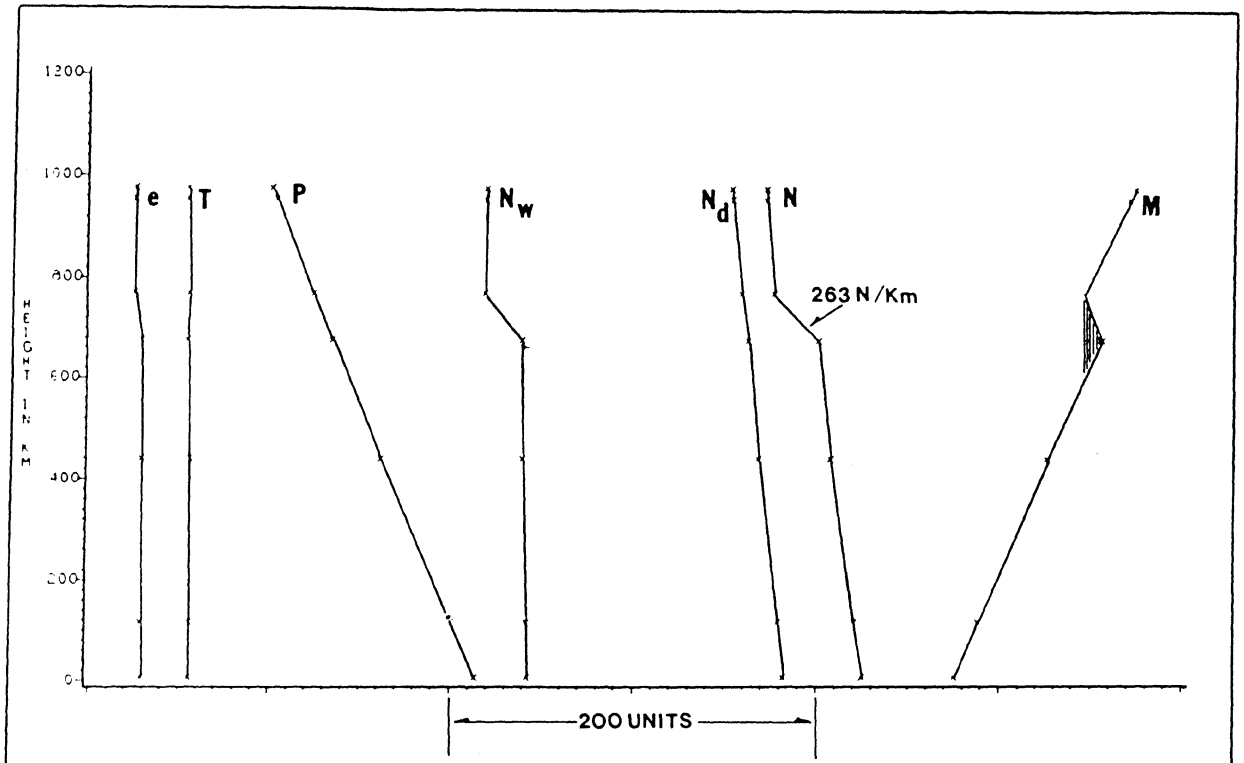

REFRACTIVITY PROFILE
SABLE ISLAND, NOVA SCOTIA
JANUARY 31, 1982, 12:00 GMT

FIGURE III.13

PRESSURE IN MILLIBARS
TEMPERATURE IN DEGREES KELVIN
WATER VAPOUR PRESSURE IN MILLIBARS

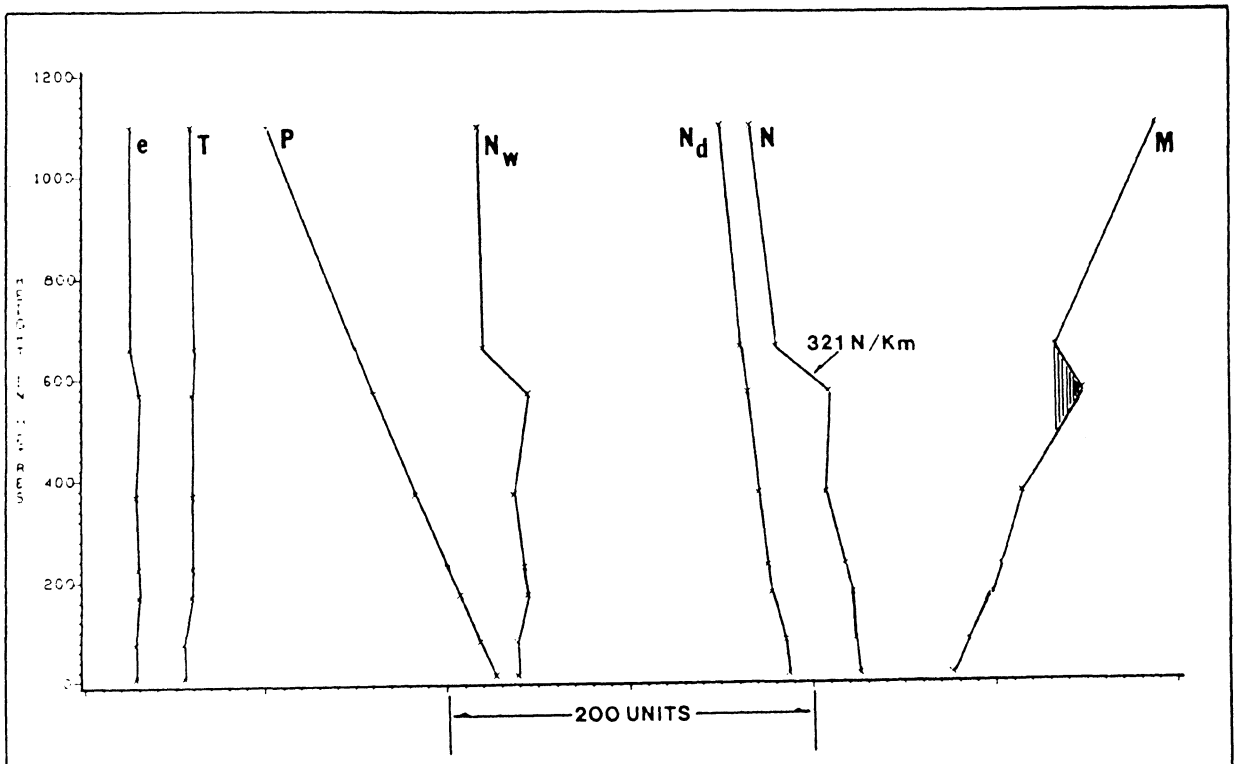

REFRACTIVITY PROFILE
SABLE ISLAND, NOVA SCOTIA
APRIL 21, 1982, 12:00 GMT

FIGURE III.14

PRESSURE IN MILLIBARS
TEMPERATURE IN DEGREES KELVIN
WATER VAPOUR PRESSURE IN MILLIBARS

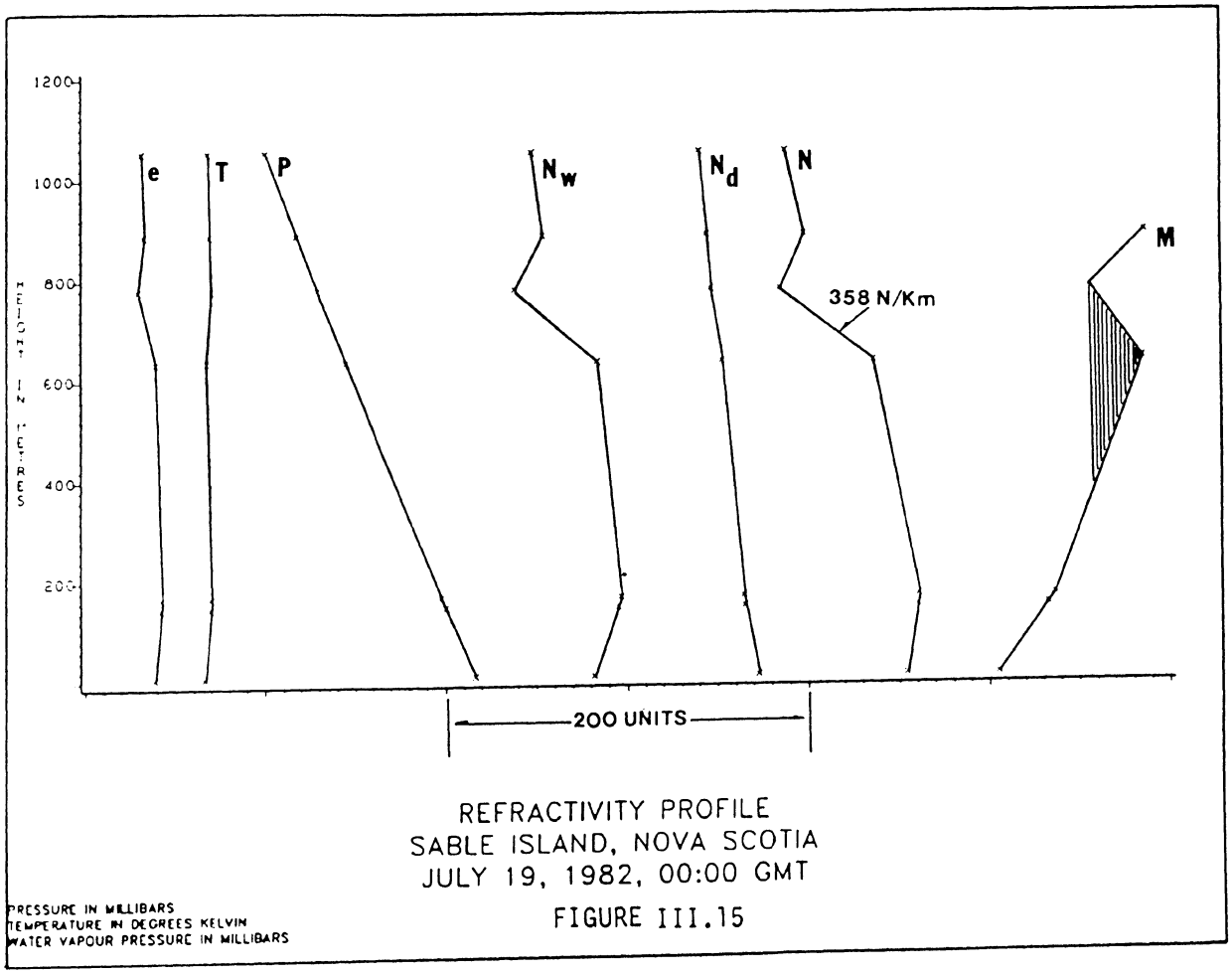

REFRACTIVITY PROFILE
SABLE ISLAND, NOVA SCOTIA
JULY 19, 1982, 00:00 GMT

FIGURE III.15

PRESSURE IN MILLIBARS
TEMPERATURE IN DEGREES KELVIN
WATER VAPOUR PRESSURE IN MILLIBARS

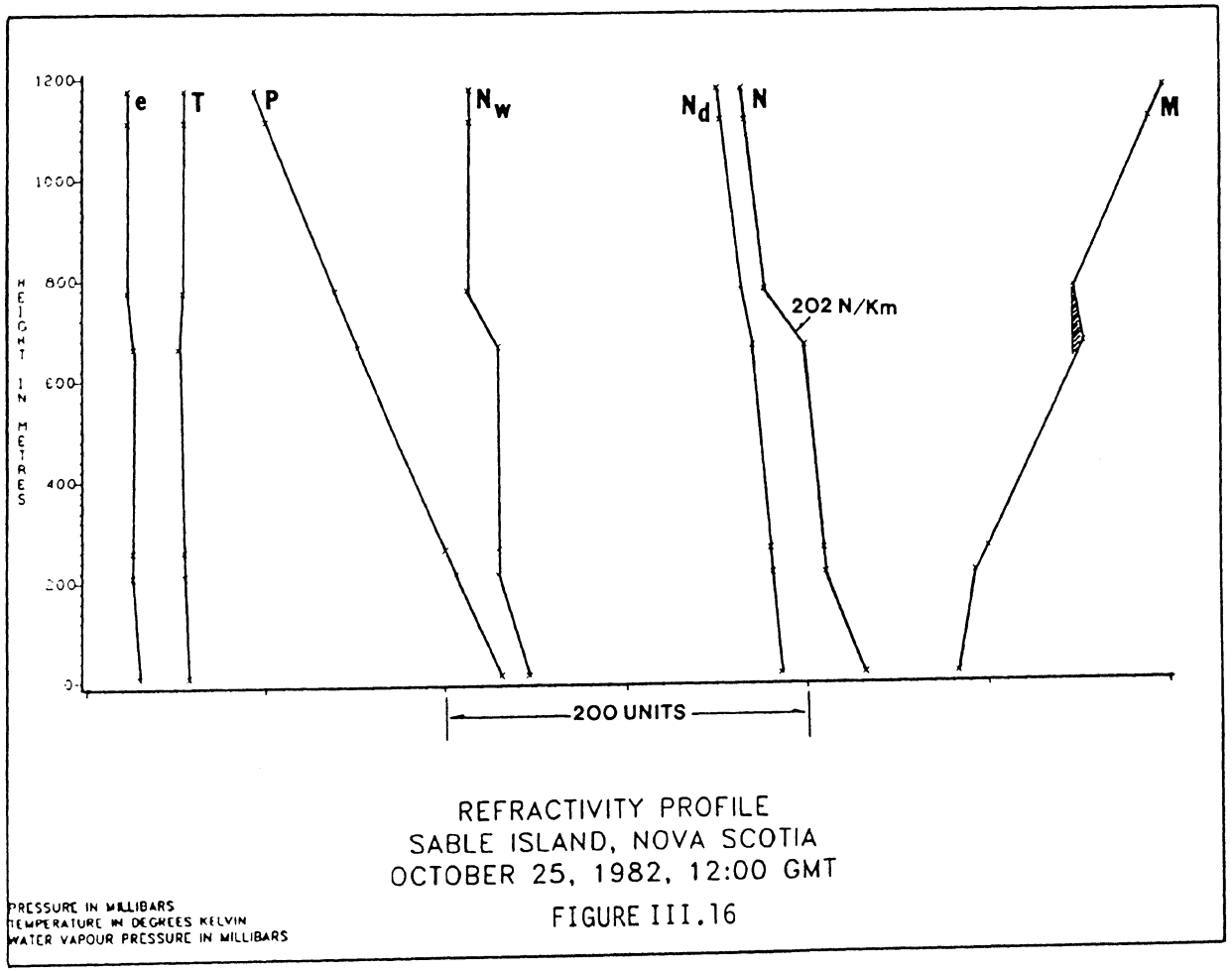

REFRACTIVITY PROFILE
SABLE ISLAND, NOVA SCOTIA
OCTOBER 25, 1982, 12:00 GMT

FIGURE III.16

APPENDIX IV

SUMMARY OF SYLEDIS RANGING DATA

MAHONE BAY, NOVA SCOTIA

JANUARY 1983

TABLE IV.1

Summary of Syledis Network Station Locations and Baseline Distances

Mahone Bay, Nova Scotia

January, 1983

Station	North Lat. (D.MS)	West Long. (D.MS)	Alt.[1] (m)	Geom. dist.[2] (m)	Radio Horiz. (m)	LOS Ratio
Prospect	44.28259	63.47380	40	---	---	---
Ovens	44.19093	64.15255	25	40708	46544	0.9
Springfield	44.37421	64.51068	215	85806	86258	1.0
Mersey	44.00294	64.41206	45	88265	53565	1.7
West. Head	43.59219	64.39446	25	87819	46544	1.9

1) Approximate, includes 15m tower.

2) $D_r = 4.11[\sqrt{h_T}+\sqrt{h_R}]$ (eqn 2.60)

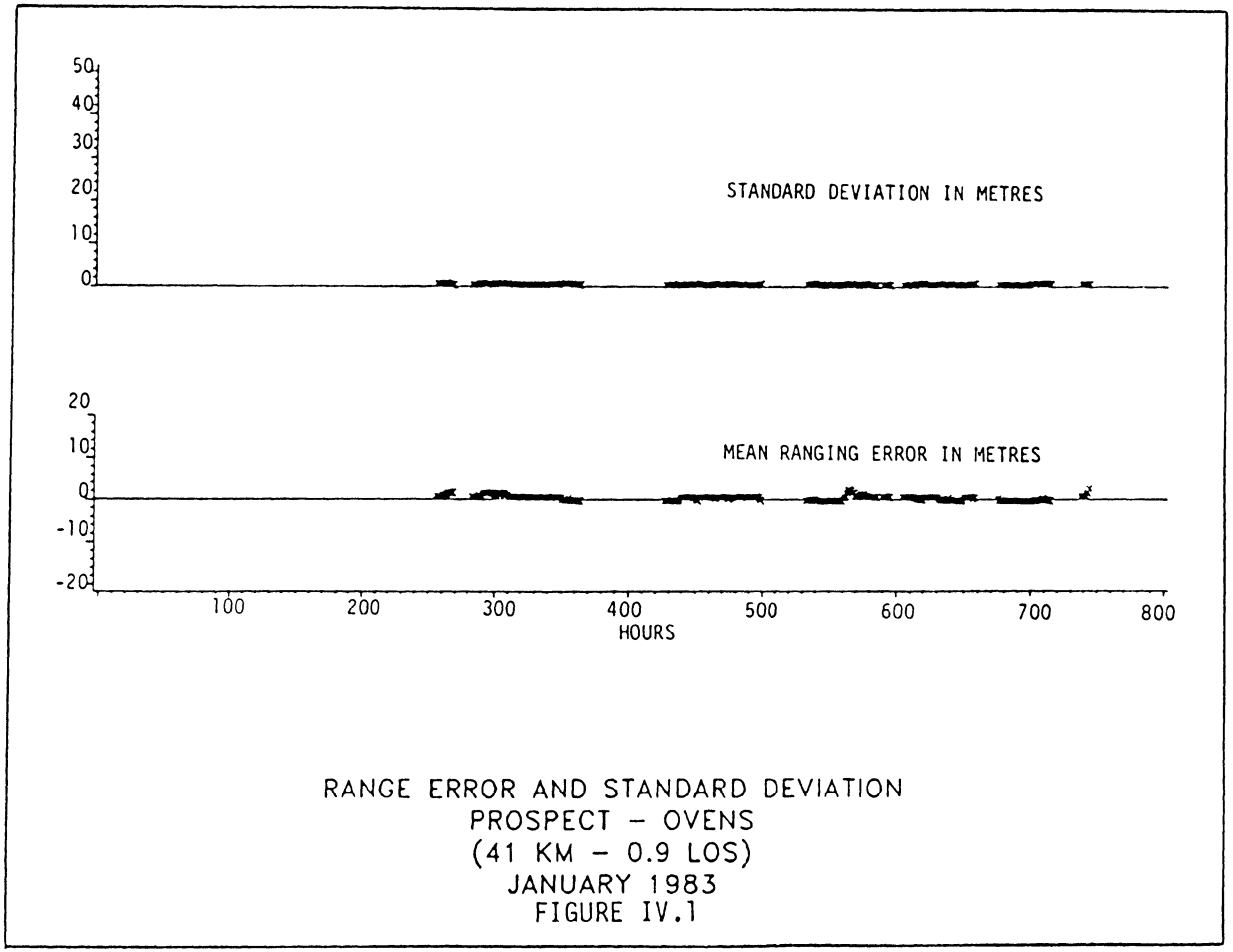

RANGE ERROR AND STANDARD DEVIATION
PROSPECT - OVENS
(41 KM - 0.9 LOS)
JANUARY 1983
FIGURE IV.1

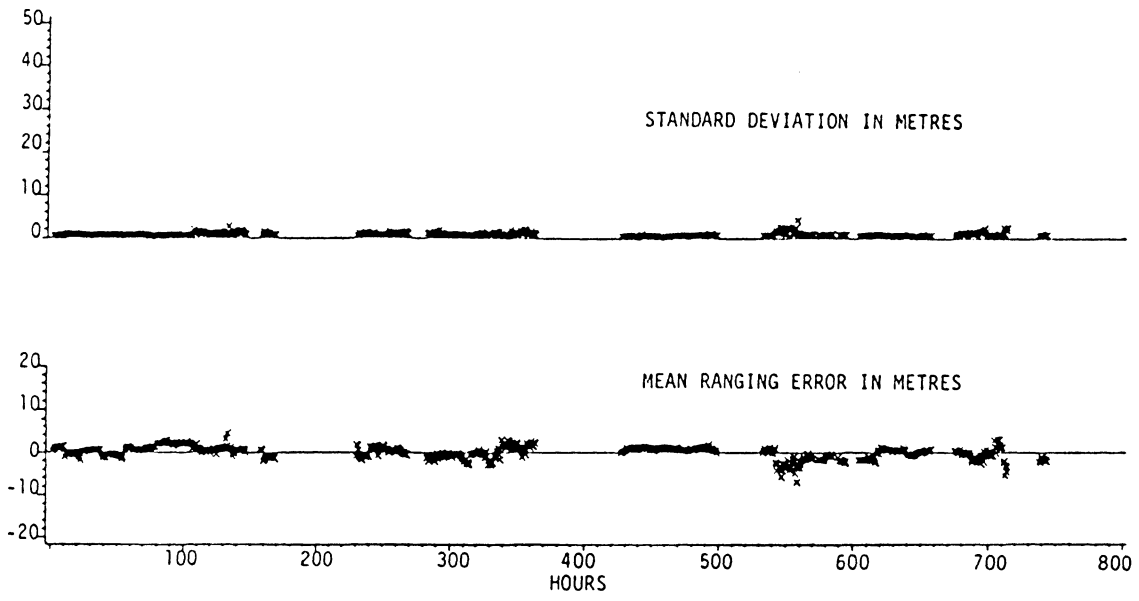

RANGE ERROR AND STANDARD DEVIATION
PROSPECT – SPRINGFIELD
(86 KM – 1.0 LOS)
JANUARY 1983
FIGURE IV.2

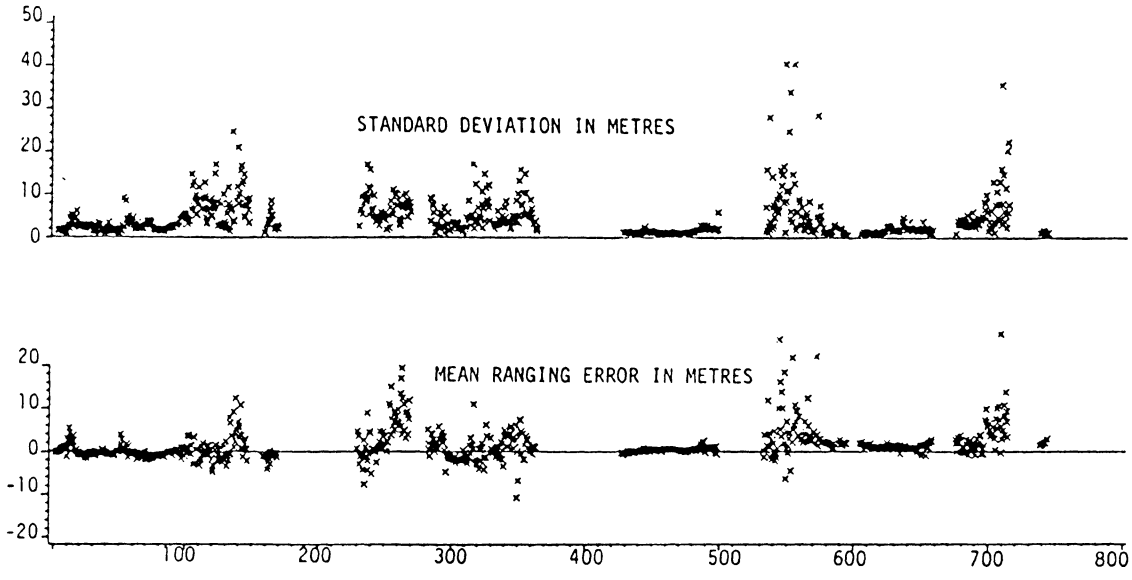

RANGE ERROR AND STANDARD DEVIATION
PROSPECT – WESTERN HEAD/MERSEY
(88 KM – 1.8 LOS)
JANUARY 1983
FIGURE IV.3

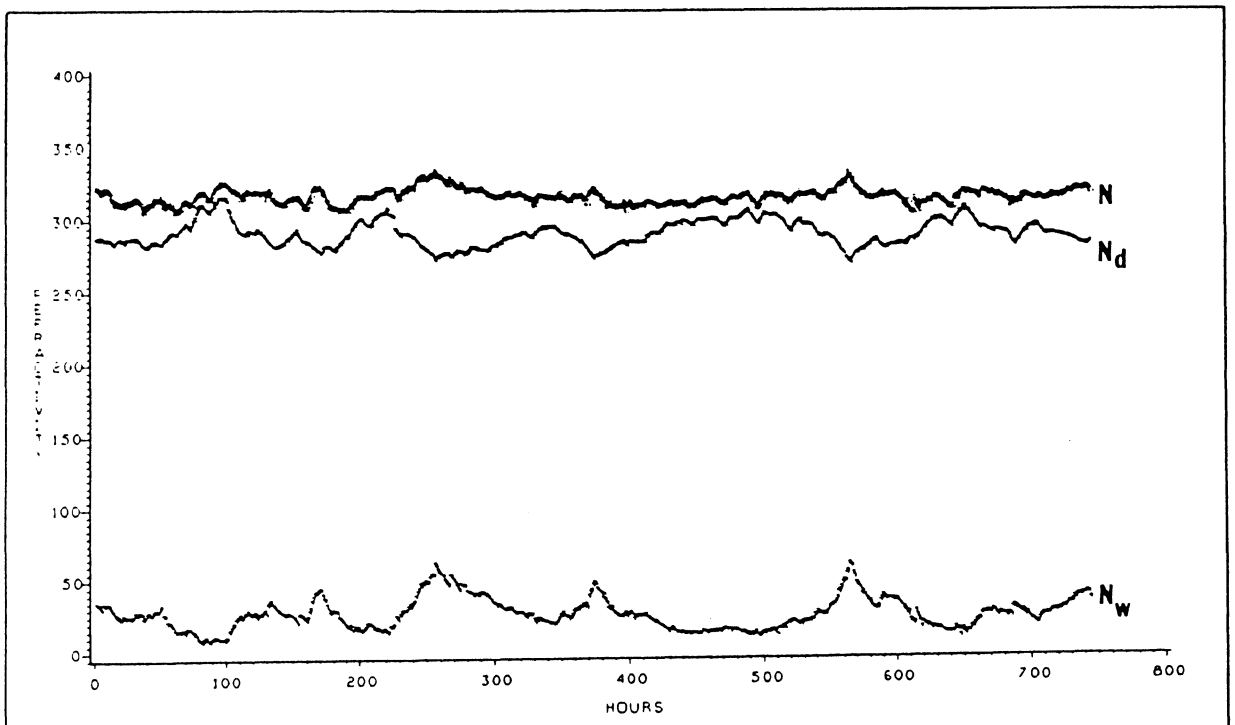

HOURLY SURFACE REFRACTIVITY
SHELBURNE, NOVA SCOTIA
JANUARY 1983

FIGURE IV.4

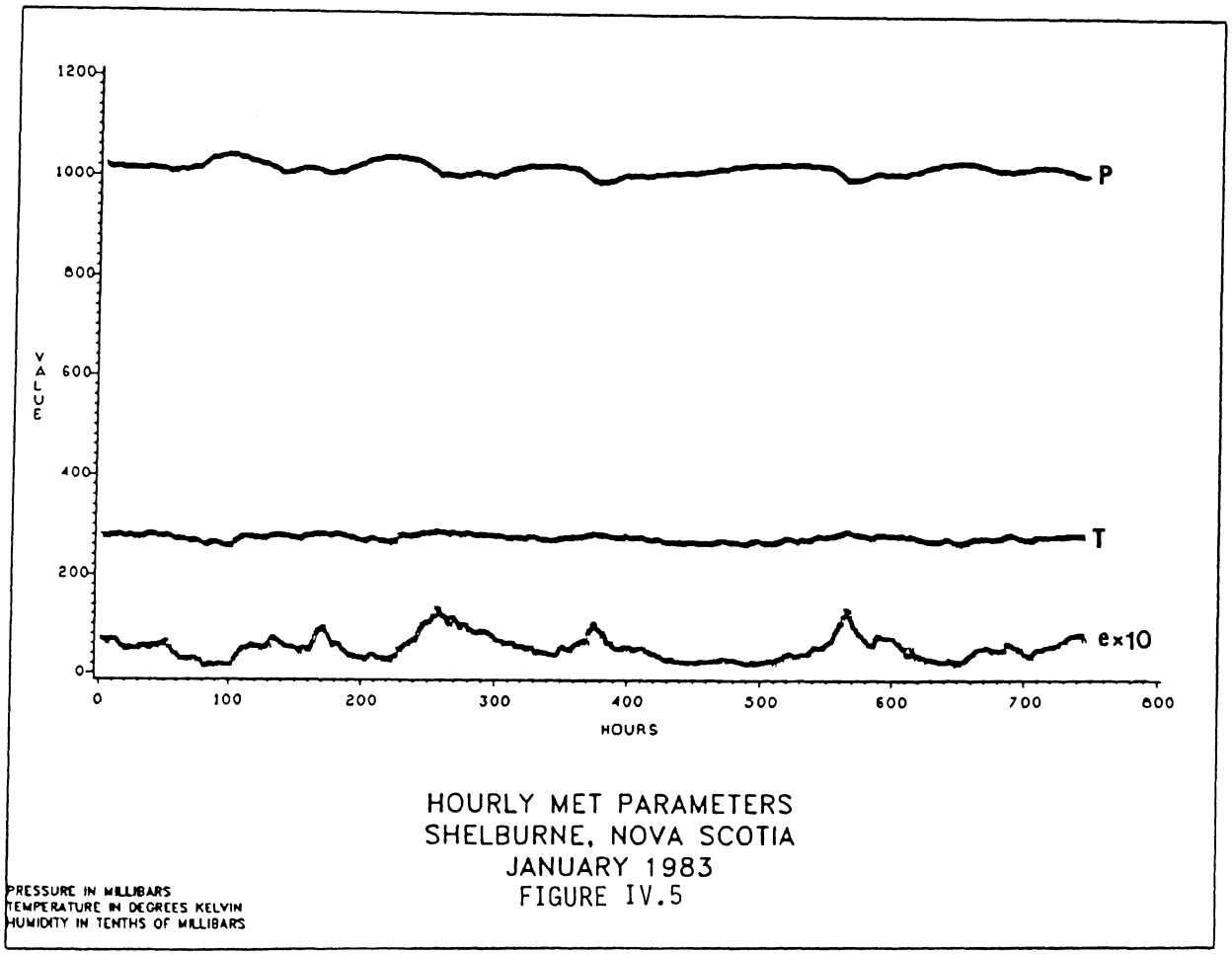

HOURLY MET PARAMETERS
SHELBURNE, NOVA SCOTIA
JANUARY 1983
FIGURE IV.5

PRESSURE IN MILLIBARS
TEMPERATURE IN DEGREES KELVIN
HUMIDITY IN TENTHS OF MILLIBARS

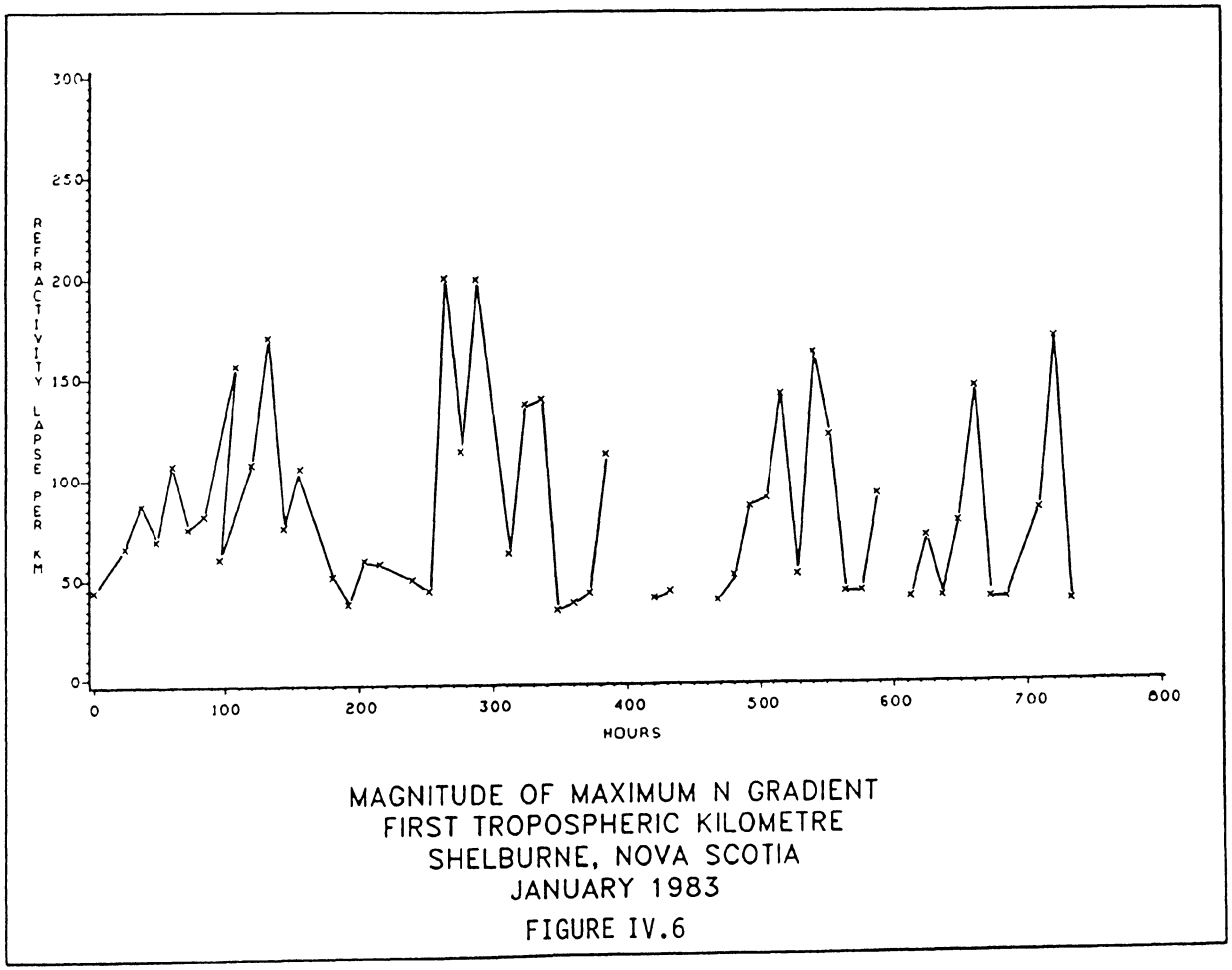

MAGNITUDE OF MAXIMUM N GRADIENT
FIRST TROPOSPHERIC KILOMETRE
SHELBURNE, NOVA SCOTIA
JANUARY 1983

FIGURE IV.6